Zirconium dioxide supported Copper Catalysts for the Methanol Steam Reforming

vorgelegt von
Diplom-Mineralogin
Alexandra Szizybalski
aus Potsdam

Fakultät II – Mathematik und Naturwissenschaften
der Technischen Universität Berlin
zur Erlangung des akademischen Grades
Doktor der Naturwissenschaften
-Dr. rer. nat.-

genehmigte Dissertation

Promotionsausschuss

Vorsitzender:	Prof. Dr. rer. nat. P. Hildebrandt
Berichter/Gutachter:	Prof. Dr. rer. nat. M. Lerch
Berichter/Gutachter:	Priv.-Doz. Dr. T. Ressler

Tag der wissenschaftlichen Aussprache: 25. April 2005

Berlin 2005
D 83

Table of Contents

„Zirkoniumdioxid geträgerte Kupferkatalysatoren für die Dampfreformierung von Methanol“
Dissertation vorgelegt von Alexandra Szizybalski

Zusammenfassung

In der vorliegenden Arbeit werden Untersuchungen zur Dampfreformierung von Methanol (MSR) mit verbesserten Cu/ZrO_2 Katalysatoren vorgestellt. Unter Verwendung verschiedener Ausgangsmaterialien und Templaten, wurden nanostrukturierte, mesoporöse und makroporöse Katalysatoren präpariert und mittels in situ Röntgenabsorptionsspektroskopie (XAS), in situ Röntgenpulverdiffraktometrie (XRD), jeweils kombiniert mit simultaner Gasphasenanalyse, unter MSR-Bedingungen untersucht. Ex situ XAS Messungen der Präkursoren identifizierten sehr kleine oder stark fehlgeordnete CuO Teilchen als die vorranginge Kupferphase. XRD Untersuchungen der Präkursoren zeigten, dass tetragonales ZrO_2 die Hauptphase des Zirkoniumdioxides ist, wobei variierende Anteile an monoklinem ZrO_2 in Abhängigkeit von der Präparation und dem Kupfergehalt detektiert wurden. Die CuO Kluster in nahezu allen Proben wurden durch 2 vol-% H_2 oder das Methanol-Wasser-Gemisch nicht vollständig reduziert. Als Grund für dieses Verhalten wird eine charakteristische Wechselwirkung zwischen dem Kupfermetall und dem ZrO_2-Träger angenommen.
Alle untersuchten Katalysatoren waren aktiv für die Dampfreformierung von Methanol. Die anfänglich niedrige Aktivität konnte durch eine temporäre Zugabe von Sauerstoff signifikant verbessert werden. Die Mikrostruktur der Kupferphase im aktivierten Katalysator weicht stark von idealem Kupfer ab. EXAFS-Analysen zeigten, dass die Zunahme der MSR-Aktivität mit einer Zunahme der Sauerstoffmenge in den Kupfermetallklustern korreliert. Weiterhin konnte gezeigt werden, dass nach längerer Reaktionszeit und einer Hochtemperaturreduktion (673 K, 2 vol-% H_2/He), die Katalysatoren immer noch aktiv waren oder wieder aktiviert (mit einer O_2 Zugabe) werden konnten.

Bezüglich des Einflusses der Präparation auf die Katalyse hat sich herausgestellt, dass die sequentielle Bildung der Katalysatorbestandteile (ZrO_2 und CuO), sowie die Imprägnierung eines kalzinierten ZrO_2-Materials zu stärkeren Metal-Träger-Wechselwirkungen und somit zu besseren MSR-Aktivitäten führen. Die Kupferkonzentration spielt ebenfalls eine entscheidende Rolle, da bei niedrigen Konzentrationen (weniger als ~ 15 %) bessere Wechselwirkungen erzielt werden können.

„Zirconium dioxide supported Copper Catalysts for the Methanol Steam Reforming“
dissertation by Alexandra Szizybalski

Abstract

In the present work improved Cu/ZrO_2 catalysts for the steam reforming of methanol (MSR) were investigated. Using various starting materials, templates and synthesis routes, nanostructured, mesoporous, and macroporous Cu/ZrO_2 catalysts were prepared and subsequently investigated under methanol steam reforming (MSR) conditions. XRD (X-ray diffraction) and XAS (X-ray absorption spectroscopy) combined with mass spectrometry were used to monitor structural changes, stability and catalytic activity under reaction conditions. Ex situ XAS measurements of the precursors identified very small or highly disordered CuO particles as the main copper phase. XRD measurements of the precursors showed that tetragonal ZrO_2 is the major zirconia phase, while various amounts of monoclinic ZrO_2 were also detectable depending on preparation and copper content. The copper oxide clusters in nearly all samples were reduced incompletely during heating in 2 vol-% H_2/He probably because of characteristic Cu metal support interactions in the Cu/ZrO_2 catalysts.

All catalysts studied were active for MSR. The initial low activity could be significantly improved by a temporary addition of oxygen to the feed. The microstructure of the copper phase in the activated catalysts strongly deviates from ideal copper metal. EXAFS analysis showed, that an increased amount of oxygen in the copper metal clusters correlates with an increasing activity for MSR. Furthermore, it was found that after extended times in the MSR feed at elevated temperatures (673 K, 2 vol-% H_2/He), the catalysts were still active or could be activated (via O_2 addition).

With regard to the influence of the preparation on the catalytic performance it was found, that the sequential formation of the ZrO_2 and CuO precursors, as well as the impregnation of a pre-formed (calcined) ZrO_2 support lead to stronger metal-support-interactions, and hence to improved MSR-activities. The copper concentration also plays a significant role, as with lower concentrations (less than ~ 15 %) better interactions are achieved.

Danksagung

Die vorliegende Dissertation wurde im Zeitraum November 2001 bis April 2005 am Fritz – Haber - Institut der Max – Planck - Gesellschaft in Berlin angefertigt.

Ich bedanke mich herzlich bei Prof. Dr. R. Schlögl für die interessante und aktuelle Themenstellung und Herrn Prof. Dr. Lerch für die Übernahme des Korreferates.

Meinem wissenschaftlichen Betreuer Dr. Thorsten Ressler möchte ich für die Erschließung der Röntgenabsorptionsspektroskopie und insbesondere derer trickreiche Auswertung danken. Durch viele Diskussionen und Anregungen gelang es, sich Stück um Stück an die ´innerste Schale´ heranzuarbeiten.

Dr. Rolf Jentoft und Dr. Frank Girgsdies sei ganz herzlich gedankt für die Geduld und ständige Bereitschaft zum Lehren vieler technischer und wissenschaftlicher Aspekte; sei es auf Messzeit oder im Labor.

Desweiteren gilt mein Dank all denjenigen, die im Rahmen des "Zeitstiftung – Projektes" zum Gelingen dieser Arbeit beigetragen haben; allen voran natürlich den Präparatoren des Max-Planck-Institutes für Kolloide und Grenzflächen in Golm: Dr. Jan-Hendrik Schattka, Dr. Yanqin Wang, Dr. Rachel Caruso, Dr. Markus Niederberger und dem Leiter der Abteilung Prof. Dr. M. Antonietti. Desweiteren der Arbeitgruppe von Prof. Dr. F. Steglich - Dr. Annegrit Rabis und Dr. M. Baenitz vom Max-Planck-Institut Chemischer Physik fester Stoffe in Dresden. Und nicht zuletzt möchte ich Dr. H. Purnama, H. Soerijanto, Dr. A. Mastalir und Prof. Dr. R. Schomäcker von der Technischen Universität Berlin danken für ihre Beiträge zum Verständnis des Systems.

Jutta Krönert sei gedankt für die vielen Arbeitsstunden am IR Spektrometer. In den Diskussionen zusammen mit ihr und Dr. Friederike Jentoft sind wir ein gutes Stück vorangekommen.

Igor Kasatkin sei gedankt für seine Arbeit am TEM und den vielen aufschlussreichen Bildern und Ergebnissen.

Besonders möchte ich auch meinem Kollegen Benjamin Louis danken. Stets bereit, einer interessanten Sache zu verfallen, haben die Diskussionen oft viel länger gedauert als geplant und nur mit Hilfe der Versorgungen Olgas und der "Westkekse" konnte der knurrende Magen dann noch besänftigt werden.

Weiterhin danke ich den ´geometrischen Strukturlern´ und allen anderen Mitarbeitern des Fritz - Haber – Institutes für die herzliche Arbeitsatmosphäre und die vielen kleinen und großen Hilfen.

Und wären da nicht meine Eltern, meine Schwester Nadine und vor allem mein Mann Lars gewesen, säße ich heute nicht hier. Ich danke besonders Lars für seine Unterstützung, sei es beim Anhören von Fachchinesisch, beim Kampf mit Word oder für das Verständnis, wenn es mal wieder spät wurde.

1 Introduction

1.1 Motivation and Strategy

The rapid advance of technical and social developments is a blessing and a curse of our times. Two important tasks of todays society are the responsible and efficient use of natural resources and the minimization of air and water pollution. For instance, attention has been directed to the continuously growing transportation sector, which is responsible for a large fraction of emitted carbon dioxide. To minimize air pollution end-of-pipe technologies such as catalytic converters and particle filters were recently implemented. A different basic approach is the use of fuel cell technologies, to further decrease or avoid emission of noxious fumes and soot particles. Hydrogen powered fuel cells for example appear to be promising to generate electrical power for mobile applications in the transportation sector. To circumvent the problems concerning the storage and handling of H_2[1] (e.g. high weight involved with the size of the storage cylinder), liquid fuels with high energy densities (high molar ratio of hydrogen to carbon) could be used for on board production of hydrogen. One promising candidate for this application is methanol and the steam reforming of methanol reaction (MSR), respectively.

$$CH_3OH(g) + H_2O(g) \rightarrow CO_2(g) + 3\ H_2(g) \qquad \Delta H^0 = 131\ kJ/mol \qquad (1)$$

The advantages of using methanol have been discussed by Lindström et al.[1], and although the MSR is an endothermic reaction, it yields a high content of hydrogen (75 vol-%) and the conversion can be achieved at relatively low temperatures. Moreover, methanol fulfils some important criteria concerning availability and handling, such as low hazardous level, inexpensive, liquefiable at a moderate pressure, easy distribution (sale). Very advantageous is the low concentration of CO (CO poisons the fuel cell performance) produced via the MSR, the absence of other harmful gases like NO_x or SO_x and soot. De Wild et al.[2] already presented promising results, where they tested an integrated reformer/combustor with a commercial copper-based catalyst.

Methanol itself can be produced from various sources, such as natural gas, oil, coal and municipal waste (e.g. trapped methane from landfills as precursor for methanol), but most important, can be extracted from renewable feedstocks (“wood alcohol”) and in this case, will therefore not add any anthropogenic carbon dioxide to the atmosphere.

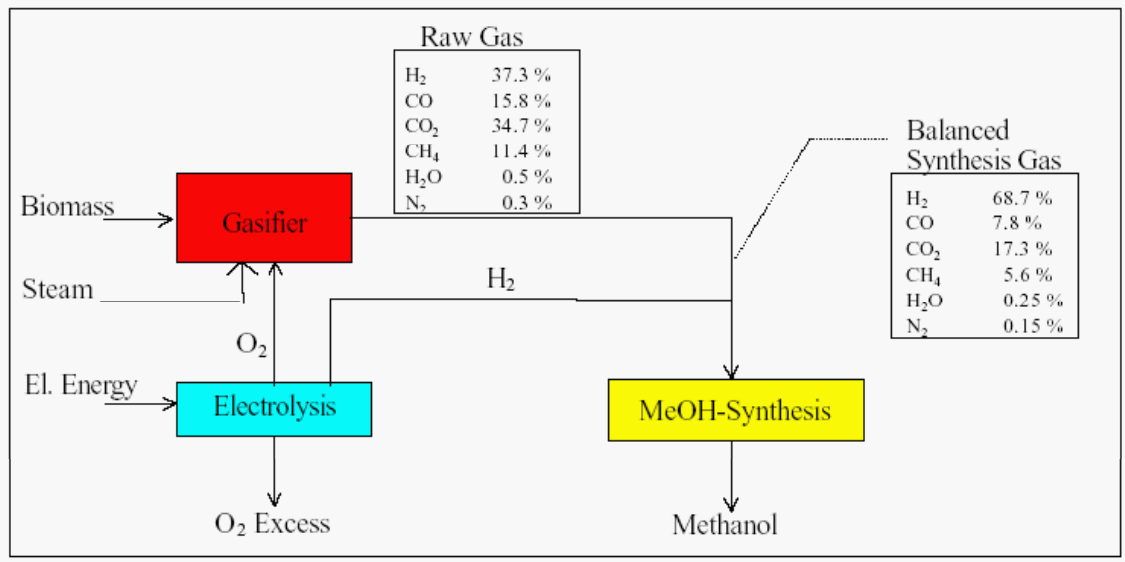

Figure 1-1 Flow diagram for a methanol synthesis plant with electrolytic hydrogen/oxygen supply and no CO_2 separation[3]

Figure 1-1 presents a flow diagram of such a methanol synthesis process. Economic calculations revealed, that depending on the spot market price, methanol from renewable resources is at least 2 - 3 times more expensive than fossil based methanol. On the other hand, comparing the untaxed renewable methanol costs with taxed gasoline, the costs difference may be rather small. If electrolytic hydrogen were to be used for the methanol generation, biomass is more cost effective than the CO_2/H_2 vectors.[3]
Worldwide many projects already picked up these ideas and for example in Germany, a refuse reprocessing plant is receiving one to 1.5 tons--up to 100 million marks of shredded notes per day from the Berlin office of the central bank, and turning them into methanol.

The efficient on board production of hydrogen from methanol for mobile applications with fuel cell technologies requires a material to catalyze the respective reaction at moderate temperatures and pressures and, furthermore, that is stable over a long time on stream. The catalysts should also favor the conversion to hydrogen and carbon dioxide, as larger amounts of carbon monoxide lead to a decrease of the voltage produced by the fuel cell (e.g. PEMFC).[4]

The commercial $CuO/ZnO/Al_2O_3$ catalysts do not fulfill the requirements satisfactorily, especially with respect to the long-term stability and low CO formation. The development of economical and ecological catalysts is therefore one of the most crucial tasks of the current research in heterogeneous catalysis. In order to achieve this a comprehensive knowledge about

the functionality of the catalyst is decisive.[5] As reactions proceed mainly on the surface of an active catalyst it is important to obtain information via surface sensitive techniques, for example with Infrared spectroscopy (e.g. CO adsorption) and Reactive Frontal Chromatography. On the other hand it was shown, that the underlying bulk structure can have a decisive influence on the surface properties of the catalyst and hence on the activity/selectivity. Therefore, it is indispensable to investigate the bulk structure under reaction conditions[6,7], too. Techniques that enable the insight into the long and short-range order are provided for example by X-ray diffraction (XRD) and X-ray absorption spectroscopy (XAS), respectively. With these complementary methods it is possible to directly investigate both, well-crystallized solids (XRD) and amorphous materials that exhibit no crystallographic long-range order. Suitable reaction cells, that allow the penetration of the x-rays, as well as the connection to mass spectrometry (MS) to simultaneously monitor changes in the gas product composition are thereby prerequisites to perform in situ experiments.

To develop an enhanced catalyst for the hydrogen production from methanol in situ investigations to the structure-activity correlations for many different materials have been performed, whereby different metals, various synthesis routes or promoters were tested. Once, the role of structural parameters for the catalytic performance has been identified, the way leads back to the question, how the synthesis method (e.g. co-precipitation, impregnation), the choice of the precursor material and the numerous preparation steps (e.g. aging, washing, calcination) influence the final active catalyst. Based on our results about the structure-activity relationships of binary Cu/ZnO catalysts[6,7,8] for the methanol synthesis and MSR reaction a copper based material supported on ZrO_2 was developed. Zirconia was chosen to reveal better long-term stability compared to zinc supported materials.

The objective of this work is the investigation of these novel Cu/ZrO_2 catalysts for the steam reforming of methanol reaction. Thereby, different techniques (e.g. impregnation, precipitation), copper precursors (copper nitrate-, acetate, acetylacetonate), templates (as structure-directing agents) and copper concentrations were used to produce porous materials with high surface areas. Furthermore, the preparation sequences and aging times were varied. All syntheses based on sol-gel chemistry and zirconium tetrapropylate served as the zirconia precursor. The influence of these various preparation parameters on the catalyst properties (morphology, modifications, crystallinity, surface- and bulk property) and on the catalytic performance will be investigated in detail.

Both, surface and structure sensitive methods were applied. To establish a correlation between preparation, bulk structural parameters and catalytic performance in situ investigations with X-ray absorption spectroscopy (XAS) and X-ray diffraction (XRD) were performed. Further details, also with respect to the thermal stability, were revealed with SEM/HRTEM. Additionally, Infrared spectroscopy and Reactive Frontal Chromatography were applied for information about surface properties of the catalysts. TG/DSC experiments in combination with mass spectrometry helped to investigate reduction/oxidation processes (e.g. degree of reduction, intermediates, particles size distribution). Kinetic studies, catalytic properties (e.g. CO selectivity) and long term stability test were performed in a different work.[9,10]

References

[1] B. Lindström, L.J. Pettersson, Inter. Jour. of Hydrogen Energy **26**, 923 (2001)

[2] P.J. de Wild, M.J.F.M. Verhaak, Cat. Today **60**, 3 (2000)

[3] M. Specht; A. Bandi, F. Baumgart, C.N. Murray, J. Gretz, Synthesis of Methanol from Biomass/CO_2 Resources, in: "Greenhouse Gas Control Technologies", B. Eliasson, P.W.F. Riemer, A. Wokaun (Eds.), Pergamon, Amsterdam 1999, p. 723

[4] H.-F. Oetjen, W.M. Schmidt, U. Stimming, F. Trila, J. Electrochem. Soc. **143** (1996) 3838

[5] R. Schlögl, Angew. Chemie **105**, 402 (1993)

[6] M.M. Günter, T. Ressler, R.E. Jentoft, B. Bems, J. Cat. **203**, 133 (2001)

[7] B.L. Kniep, T. Ressler, A. Rabis, F. Girgsdies, M. Baenitz, F. Steglich, R. Schlögl, Angew. Chem. **116**, 114 (2004)

[8] M.M Günter, T. Ressler, B. Bems, C. Buscher, T. Genger, O. Hinrichsen, M. Muhler, Schlögl, R., Cat. Lett. **71**, 37 (2001)

[9] H. Purnama, F. Girgsdies, T. Ressler, J.H. Schattka, R. A. Caruso, R. Schomäcker, R. Schlögl, Catal. Lett. **94** (2004) 61

[10] H. Purnama, Catalytic Study of Copper based Catalysts for Steam Reforming of Methanol, Thesis 2003

1.2 Hydrogen production from methanol

Copper based materials have been extensively studied under MSR and methanol synthesis reaction conditions. However, reaction mechanisms, as well as active phases and structural changes of the catalysts are still under debate, and dependent on the catalyst composition and reaction conditions.

1.2.1 Comparison of possible reactions in terms of the suitability for fuel cell applications

Among other fuels, methanol is regarded as one of the most promising candidates for the on-board reforming to hydrogen. Four processes are conceivable:

Decomposition: $CH_3OH \rightarrow 2H_2 + CO$ $\Delta H^0 = 128$ kJ mol^{-1}

Steam reforming: $CH_3OH + H_2O \rightarrow 3H_2 + CO_2$ $\Delta H^0 = 131$ kJ mol^{-1}

Partial oxidation: $CH_3OH + 1/2O_2 \rightarrow 2H_2 + CO_2$ $\Delta H^0 = -155$ kJ mol^{-1}

Combined reforming: $(s + p)\ CH_3OH + 1/2pO_2 + sH_2O \rightarrow (2p + 3p)\ H_2 + (s + p)\ CO_2$[1]

where s and p are stoichiometric coefficients for steam reforming and partial oxidation, respectively.

In contrast to the decomposition and the steam reforming (MSR), the partial oxidation is an exothermic reaction, but the evolution of heat could cause sintering of the particles and hence the deactivation of the catalyst. This must be taken into account when designing a reactor. In addition, a maximum yield of hydrogen (66 %) can only be achieved by using pure oxygen for the reaction. As for the automobile fuel cell technology preferentially air would be used, only 41 % of hydrogen could be produced, because the product stream will be diluted with nitrogen. Additionally, deactivation of the catalyst must be considered when using air as a reactant, because sulfur and chlorine compounds could lead to a poisoning of the material.[2]

The decomposition as well as the steam reforming are endothermic reactions and therefore additional energy supply is necessary.[3] One idea to solve this problem is the use of the heat of the exhaust gas. Although the decomposition reaction is a simple reaction by using solely methanol as a starting feedstock, the production of carbon monoxide makes it very unsuitable for fuel cell technologies.

By combining partial oxidation and MSR a system is generated, which is dynamic, forms a relatively high hydrogen concentration and avoids critical hot spots in the reactor. The heat for

the MSR could be provided by the partial oxidation reaction. Already Huang et al.[4] investigated the effect of adding oxygen to methanol and water. They found that the hydrogen production, but also the carbon monoxide outflow rate increased by increasing the oxygen/methanol ratio for Cu/ZnO co-precipitated catalysts. Lindström et al. presented measurements on different copper based catalysts and compared the conversion and carbon monoxide concentration of MSR and combined reforming. Dependent on the catalyst composition the one or the other reaction turned out to be more effective.[5] Velu et al.[6,7] also showed, that for a certain methanol/water ratio CO-free hydrogen can be produced with CuZnAl-oxide catalysts. Nevertheless, for this kind of process similar problems occur as for the partial oxidation, concerning oxygen supply and product composition.

The high concentration of hydrogen (75 %), and the high selectivity to carbon dioxide make the MSR to a very favourable process for the automobile application. Additionally it was recently shown, that the in contrast to previous studies[8,9,10,11] detectable carbon monoxide is a product of a consecutive reverse water gas shift (RWGS) reaction[12], and therefore chemical engineering processes to minimize the CO formation can be applied (e.g. use of membrane reactor).

1.2.2 Catalysts for the methanol synthesis and steam reforming of methanol

In the early stages of the methanol production from synthesis gas (mixture of H_2 and CO/CO_2) ZnO/chromia catalysts were used. These catalysts were not particularly active, but they could operate with relatively high levels of poison (mainly sulfur compounds) in the synthesis gas produced from coal. With the development of the steam reforming of hydrocarbons, cleaner synthesis gas enabled the more efficient exertion of copper based catalysts. With the subsequent large-scale production, methanol itself became a feedstock for the production of formaldehyde and of hydrogen in electronic industry, for example.

According to the stability of the metals proposed by Hughes,[13] copper is very susceptible to thermal sintering. Therefore, copper based catalysts typically contain one or more oxides, that enhance the stability mainly by physically separating the copper crystallites. Many different catalyst compositions are discussed in the literature. For industrial applications mainly Al_2O_3 and/or Cr_2O_3 in addition to CuO and ZnO are used for the methanol synthesis. Nevertheless, slow deactivation occurs due to sintering effects and can limit the technical time on stream to 2 – 8 years.[14] The catalytic behavior of copper based catalysts with silica, magnesia and zirconia supports, ternary and quaternary mixtures with copper have also been investigated. Denise et al.[15] reported on the influence of various supports on the catalytic performance for the methanol

synthesis form different mixtures of CO/CO_2 and hydrogen. The methanol productivities of Cu/MgO and Cu/ZrO_2 systems turned out to be superior to those of $Cu/ZnO/Al_2O_3$ in terms of titratable copper for the conversion of carbon monoxide. On the other hand, if carbon dioxide is used for the feedstock, the ternary system produced more methanol.

Nitta et al.[16] investigated the methanol synthesis reaction from CO_2/H_2 and found that Cu/ZrO_2 is more effective than Cu/ZnO (both prepared by coprecipitation method) at higher temperatures (> 473 K) and they also showed that ZnO affects the Cu dispersion, whereas ZrO_2 has a positive influence on the methanol selectivity and diminishes the production of CO.

As the stability of the catalyst is important, Kurtz et al.[17] investigated $Cu/ZnO/Al_2O_3$, Cu/ZnO, and Cu/Al_2O_3 catalysts under methanol synthesis conditions and found that the ZnO-containing catalysts deactivated rapidly at 473 K within the first days due to sintering of the copper crystallites. Al_2O_3 was found to inhibit the thermal sintering and moreover, to enhance the catalytic activity. Nevertheless, a linear correlation between the activity and the copper surface area was only found in a first approximation and it was proposed to group the catalysts in different classes to find systematic correlations.

Hence, the catalytic performance of a catalysts depends on the feedstock composition, on the support, and partly on the resulting copper surface area.

Since the demand of hydrogen increased, catalysts are also under investigation for the reverse reaction, namely the production of hydrogen from methanol.

However, the partial pressure of the reactants and the products in the methanol synthesis differ from those in the steam reforming of methanol and hence, different by-products and intermediates can be present in significant amounts. Therefore it must be considered, that optimum catalysts for the methanol synthesis do not necessarily perform the hydrogen production to the same extent. This might explain, that numerous studies report on catalysts for the steam reforming of methanol, methanol decomposition and partial oxidation.

In the 1980s the group around Takezawa[18] and Takahashi[19] reported on studies about Cu/SiO_2 catalysts. They investigated the effect of copper loading and calcinations temperature on the reaction and tried to understand the reaction pathway by comparison with a Pt/SiO_2 catalyst. It was suggested that, dependent on the catalyst material, the steam reforming of methanol proceeds via different intermediate reactions of formaldehyde, resulting in better MSR selectivities with the Cu/SiO_2 system. Cu/SiO_2 catalysts with higher copper loadings

(≥ 10 wt-%) or calcined at higher temperatures turned out to be highly active and selective due to the presence of CuO clusters and bulk CuO, which readily transformed into metallic copper during reaction.

Later they compared the MSR performance over copper and group VIII metals supported on SiO_2, but also on Pd with different supports (alumina, zirconia, ZnO, La_2O_3 and others). They assigned the high performance of copper based and Pd/ZnO catalysts to these differences in the reactivity of formalehyde and proposed that the modification of the Pd upon the formation of PdZn alloys similarly influenced the structure of adsorbed HCOH as it was suggested for Cu/SiO_2.[20] For all the other tested Pd, Ni and Pt catalysts (supported on various oxides) inferior hydrogen production rates and selectivities were observed.

Breen and Ross[21] performed a study to investigate the influence of the preparation method and the zirconia addition to copper-based catalysts on the steam reforming of methanol. Various types of catalysts were tested, i.e. binary materials with Cu supported on ZnO or ZrO_2, as well as ternary and quaternary systems with additional alumina (sequential and co-precipitation with the metal nitrate salts). Most of the catalysts were prepared by sequential precipitation, whereas the Cu-Zr material was coprecipitated. The activity of the Cu/ZrO_2 catalysts increased with increasing copper content under MSR conditions (H_2O/CH_3OH 1.3:1). Moreover, no significant amounts of CO were detected for all catalysts up to temperatures of 553 K. Despite, the low hydrogen production of the Cu-Zr systems, they show higher TOF than the Cu-Zn catalysts. The addition of zinc oxide to Cu-Zr materials, and to a lesser extent also the addition of alumina to Cu-Zn-Zr catalysts increased the copper dispersion, as well as the activity. The best performance was found for the Cu-Zn-Zr-Al catalysts.

The role of ZnO in Cu/ZnO based catalysts is discussed by Chinchen et al.[22] as to enhance the dispersion of copper at the surface. Other authors have proposed that the activity of the catalyst is influenced by the morphology and the structural disorder of the copper particles, or by incorporation of copper into ZnO.[23, 24, 25]

Lindström et al.[3] compared copper-based catalysts (where nitrates of Cu, Zn, Cr, and Zr were impregnated on alumina pellets, followed by drying and calcination) in the MSR reaction (molar ratio CH_3OH/H_2O of 1). For temperatures above 513 K the activity of Cu/ZrO_2 catalysts was comparable to copper-chromia and Cu/ZnO catalyst, while their selectivity towards CO_2 was higher. This group also investigated the performance of copper-based monoliths (MSR with 30 % excess of water) and observed a superior selectivity towards CO_2 for zirconia doped Cu-Zn catalysts over the entire investigated temperature interval and for all copper loadings.[26]

Concerning the stability of copper based catalysts, Cu/ZrO_2 was compared with a commercial $Cu/ZnO/Al_2O_3$ catalyst under methanol steam reforming conditions for 250 h. For both systems an initial period, where the conversion is decreasing exponentially, is followed by a linear behaviour. However, after 150 h time on stream the conversion appears to be constant for the binary catalyst, while it continues to decrease for the ternary system.[12]

In summary, main aspects in the research of heterogeneous catalysis concern the influence of the preparation methods and conditions,[27, 28] as well as the support/promoter material on the reaction kinetics, the relationship between structure and activity, the active sites and the role of the catalyst surface.

1.3 Temperature programmed reduction of CuO/ZrO_2 in comparison with bulk CuO and Cu/ZnO

Copper metal is widely considered as the active state of copper catalysts in the methanol chemistry. Therefore, one important step, after preparation and calcination of the precursor material and prior to catalysis, is the reduction of the copper oxide.

The reduction behaviour of copper oxide is thereby dependent on the precursor phases, loading and dispersion, the calcinations temperature, the interaction of copper oxide with the support, the copper oxide particle size and morphology.[29] Moreover, the reducing agent, its concentration and flow rate, but also heating rates, reactor design and the properties of the catalyst bed play a decisive role. All these parameters influence the reduction temperature and the formation of intermediates; that is the reduction kinetics. Some of these aspects will be discussed briefly in the next paragraph.

The influence of the support on the reduction of copper oxide can be estimated by first investigating the behaviour of pure copper oxide.[30 and ref. therein]

Many of the detailed analysis on this subject were done isothermally.[31] For example the group of Rodriguez et al.[32,33] looked at the isothermal reduction of commercial CuO in hydrogen with in situ time-resolved XRD. No intermediate phases were observed until they drastically decreased the flow conditions of 5 vol-% H_2/He from 20 cm^3/min to 1 cm^3/min and increased the temperature to 300 °C. Under these extreme conditions they observed an increasing amount of intermediate Cu_2O. From those results they conclude the existence of a sequential reduction at low H_2 pressure, otherwise a direct reduction. They further confirmed their theory with the

detailed analysis of the lattice parameters (XRD pattern) and XAS measurements at the Cu K-edge. From the results they propose the embedding of hydrogen instead of oxygen vacancy formation leading to the restructuring and oxygen release during the transformation from CuO to Cu metal.

Fierro et al.[34] used a temperature programmed technique to investigate the reduction of CuO prepared from gerhadtite and malachite. Only one major peak of H_2 uptake was detected in both cases, whereas the material prepared from gerhadtite needed a wider temperature window, than this from malachite. They partly assign this behavior to particle size differences. However, little information is given on the formation of intermediates, as the investigations were done without structural analysis.

It was shown by several authors[21,35,34] that the usage of a support, for example zirconia, drastically decreases the reduction temperature of CuO during temperature programmed experiments in diluted hydrogen. This result indicates a copper/support interaction, which facilitates the reducibility of copper (II) oxide. The nature of this relationship is however still under debate. Moreover, it was observed, that the usage of a support leads to the formation of multiple TPR peaks. Some authors ascribe this phenomenon to the existence of different kinds of copper oxide species,[36, 37] i.e. highly dispersed CuO and/or copper (II) ions in an octahedral environment (reducing at lower temperatures) and bulky CuO (reducing at higher temperatures). In the case of CuO/ZnO catalysts they were classified as (a) bulk copper oxide (b) three-dimensional copper clusters partially interacting with the support and (c) two-dimensional copper metal in intimate contact to the support (epitaxial growth) according to the reducibility.[34]

For example, Zhou et al.[38] applied temperature-programmed reduction to examine the reduction behavior of copper oxide supported on zirconia. Their catalysts were prepared via impregnation of ZrO_2 with an aqueous $Cu(NO)_3$ solution. They assigned the occurrence of various TPR peaks (hydrogen consumption) to the existence of highly dispersed copper species that reduce at lower temperatures and on the other hand, bulk CuO that needs higher temperatures. XRD measurements revealed, that upon impregnation the tetragonal ZrO_2 modification became the dominant crystal phase.

Whether the zirconia modification has a direct influence on the reducibility of copper oxide is unclear. Some authors propose an interaction between the low coordinated O^{2-} of monoclinic ZrO_2 and Cu^{2+}, that makes the reduction of CuO more difficult.[39] At least the existence of an interaction between the support and the copper oxide, was indicated repeatedly by the fact, that

upon decreasing the copper loading, the monoclinic zirconia modification becomes more prominent.[38, 40]

1.4 Relationship between bulk structure and activity of supported copper catalysts

In the last years various methods have been applied to answer the questions concerning the active site or state in a catalyst. In this respect, scientists investigated for example changes in the crystallite morphology, micro structure, and oxidation state of copper under methanol synthesis and MSR conditions.

For Cu/ZnO catalysts (5 % Cu) changes of the copper crystallite morphology have been concluded from in situ EXAFS investigation and were confirmed later on with in situ TEM.[25,41,23] It was found, that dependent on the oxygen partial pressure copper particles tend to change their morphology from a disc-like to a more spherical shape and, therefore the total copper surface area will be affected. If for example water is added to the gas atmosphere, the adsorption of these molecules on the different Cu facets is believed to be the driving force for the surface reconstruction. The transfer of these observation to other systems was only partly shown for Cu/SiO_2. In principle, the ability of the support to form oxygen vacancies was suggested to be an important prerequisite.

Additional to the observation above, modifications of the Cu lattice have been reported for Cu supported on ZnO.[42] From the comparison of experimental and calculated EEL spectra (Electron Energy Loss) it was concluded, that dependant on the gas environment (diluted H_2 or H_2/CO) strain and even alloy formation occur and thus alter the metal-support interaction. These phenomenons are believed to originate from the epitaxial mismatch between Cu and the ZnO support. The results also indicate an increased tendency to form Cu-Zn alloy under more severe conditions (CO/H_2). For Cu/ZnO catalysts with higher copper concentrations, Günter et al.[43] found, that the observed microstructural changes of copper and zinc oxide correlate with the MSR activity. In the proposed model the increase in activity after oxygen addition (to methanol and water) cycles is explained with the depletion of Zn in the Cu lattice and the resulting larger domains of structural disorder (e.g. strain).

It has been reported for Cu/Al_2O_3 and Cu/ZnO catalysts, that after a certain activation time the catalysts became active for MSR[44,45] and that the activity resulted from a partial re-oxidation of

previously reduced copper metal to Cu_2O. Depending on the methanol : water ratio the amount of Cu_2O formed was different. Chinchen et al.[46] observed similar results for $CuO/ZnO/Al_2O_3$ catalysts in the methanol synthesis reaction. Cheng et al.[47] showed that MSR activity of a copper catalyst on an oxygen ion conducting yttria-ceria-alumina support, provides sites for the adsorption of mobile oxygen and therefore enhances the oxidation of Cu to Cu^+. For the catalyst investigated here such an interaction is not evident, nevertheless it is possible that oxygen is stored at the surface of the ZrO_2 support and helps in stabilizing partially oxidized copper clusters.

1.5 Relationship between surface structure and activity of supported copper catalysts

Besides bulk structural properties, the surface of a catalyst is important in facilitating and promoting chemical reactions. Thereby, the surface area of the active material plays an important role. In a first order approximation it was shown, that the larger the surface area of copper, the higher the activity for methanol synthesis.[22] Nevertheless, it is still a much debated question as to whether all copper catalysts can be grouped in one single class. Kurtz et al.[17] for example investigated the deactivation behavior of co-precipitated Cu/ZnO, Cu/Al_2O_3 and $Cu/ZnO/Al_2O_3$ catalysts under methanol synthesis conditions. Although the observed deactivation during long time on stream could be attributed to the thermal sintering of the Cu crystallites (resulting in a decrease in the Cu surface area), the three catalysts did not show an overall linear correlation between specific cu metal area and methanol synthesis activity. One explanation to this could be different morphologies of the copper surface,[48] originating from the variation of the preparation method.[49] Other approaches consider the direct influence of bulk structural effects on the activity for methanol synthesis and MSR, as it was discussed in the former paragraph.

1.6 Outline of the work

Reliable structure-activity relationships for copper catalysts in methanol chemistry that are prerequisites for a knowledge-based design of improved catalytic materials remain rare. In this thesis the complementary techniques in situ X-ray absorption spectroscopy (XAS) and X-ray diffraction (XRD) were employed to elucidate correlations between activity, stability, and

structural changes of differently prepared Cu/ZrO_2 catalyst obtained under methanol steam reforming conditions.

As the precursor is very frequently an oxide, the material must be activated by reduction. After the calcination, this is the next step to form a final catalyst. The activation, that means the transformation of the precursor solid to the active phase, determines or influences to a large part the properties of catalysts: activity, selectivity, and resistance to ageing.[29] For copper catalysts several studies discussed, that the preparation[28,43,49,50] already determines these properties and is also reflected in the reduction behavior. For the nanostructured Cu/ZrO_2 catalysts in this work, prepared by various precipitation and templating techniques and with different copper contents, the phase evolution and reduction temperatures are investigated in situ under different reduction atmospheres in more detail.

Due to low copper loadings and/or small copper crystallite sizes, XRD was found unsuitable to describe the microstructural parameters of the copper particles. However, in order to obtain information on this field, XAS and Nuclear Magnetic Resonance (NMR) was employed. Additionally high resolution Transmission Electron Microscopy (HRTEM) revealed insight into the morphology and structure of the crystallites, and into the distribution/interaction of the metal and the support. Furthermore, the relationship between the catalyst surface and activity was estimated using Infrared (IR) spectroscopy and Reactive Frontal Chromatography (RFC). RFC is a method to determine the specific copper surface area apart from the estimation based on the copper metal particle size. On the basis of the specific copper surface area, it is possible to evaluate structural effects besides the Cu metal surface area on the catalytic activity.

In the chapter 4 the in situ investigations of one nanostructured binary Cu/ZrO_2 catalyst under MSR conditions are presented. Besides TG-DSC/MS, XAS is employed to obtain information on the phase evolution during reduction. Subsequent, a detailed analysis of the microstructural changes during methanol steam reforming, and high temperature treatment is performed applying in situ XAS, and NMR. Furthermore, oxidation/reduction cycles are performed (temporary addition of oxygen to the feed of methanol and water), in order to investigate changes in the microstructure of copper and zirconia, and the corresponding MSR activity. The gained information are summarized and combined to describe the correlation between bulk structure and activity.

Binary Cu/ZrO_2 catalysts were prepared with three major preparation routes. To obtain nanostructured, mesoporous and macroporous materials, the different precursors were precipitated or impregnated onto different templates. Additionally, the sequence of precursor formation was changed. In chapter 5, all the investigated catalysts are compared with respect to their reduction behavior, their surface and bulk structural properties, and the corresponding catalytic performance. The observed differences and similarities are discussed, taking into account the influences of the various preparation techniques.

In order to analyze the influence of the copper content in more detail, materials with different copper loadings were prepared based on the technique for nanostructured catalysts. To establish a correlation between copper content, bulk structure and activity again, the reducibility as well as the behavior under MSR conditions were analyzed.

Finally the obtained results were used to prepare ternary ceria-zirconia systems with varying copper contents. For these catalysts activity, selectivity, long term stability, and activation energies are presented. Furthermore, the specific copper surface area helps to estimate the influence of the copper particle size on the catalytic performance.

1.7 References

[1] J. Agrell, B. Lindström, L.J. Pettersson, S.G. Järas, Catalysis: specialist periodical reports, **16** (2002) 67

[2] M.V. Twigg, M.S. Spencer, Top. Catal. **22** (2003) 191

[3] B. Lindström, L.J. Pettersson, Int. J. Hydrogen Energy **26** (2001) 923

[4] T.-J. Huang, S.-W. Wang, Appl. Catal. **24** (1986) 287

[5] B. Lindström, L.J. Pettersson, P. Govind Menon, Appl. Catal. A: **234** (2002) 111

[6] S. Velu, K. Suzuki, T. Osaki, Chem. Commun., **23** (1999) 2341

[7] S. Velu, K. Suzuki, M Okazaki, M.P. Kapoor, T. Osaki, F. Ohashi, J. Catal. **194** (2000) 373

[8] B.A. Peppley, J.C. Amphlett, L.M. Kearns, R.F.Mann, Appl. Catal. A: **179** (1999) 21

[9] B.A. Peppley, J.C. Amphlett, L.M. Kearns, R.F.Mann, Appl. Catal. A: **179** (1999) 31

[10] J.C. Amphlett, M.J. Evans, R.F. Mann, R.F. Weir, Can. J. Chem. Eng., **63** (1985) 605

[11] J.C. Amphlett, K.A.M. Creber, J.M. Davis, R.F. Mann, B.A. Peppley, D.M. Stokes, Int. J. Hydrogen Energy, **19** (1994) 131

[12] H. Purnama, T. Ressler, R.E. Jentoft, H. Soerijanto, R. Schlögl, R. Schomacker, Appl. Catal. A – General, **259** (2004) 83

[13] R. Hughes, Deactivation of Catalysts, Academic Press, New York, 1994

[14] P.J. Denny, M.V. Twigg, in: Catalyst Deactivation, eds. B. Delmon and G.F. Froment, Elsevier Amsterdam, 1980, p. 577

[15] B. Denise, R.P.A. Sneeden, B. Beguin, O. Cherifi, Appl. Catal. **30** (1987) 353

[16] Y. Nitta, O. Suwata, Y. Ikeda, Y. Okamoto,T. Imanaka, Cat. Lett. **26** (1994) 345

[17] M. Kurtz, H. Wilmer, T. Genger, O. Hinrichsen, M. Muhler, Cat. Lett. **86** (2003) 77

[18] N. Takezawa, H. Kobayashi, A. Hirose, M. Shimokawabe, K. Takahashi, Appl. Catal. **4** (1982) 127

[19] K. Takahashi, H. Kobayashi, N. Takezawa, Chem. Lett. **6** (1985) 759

[20] N. Takezawa, N. Iwasa, Catal. Today, **36** (1997) 45

[21] J.P. Breen, J.R.H. Ross, Catal. Today, **51** (1999) 521

[22] G.C. Chinchen, K.C. Waugh, D.A. Whan, Appl. Cat. **25** (1986) 101

[23] P.L. Hansen, J.B. Wagner, S. Helveg, J.R. Rostrup-Nielsen, B.S. Clausen, H. Topsøe, Science **295** (2002) 2053

[24] J.B. Bulko, R.G. Herman, K. Klier, G.W. Simmons, J. Phys. Chem. **83** (1979) 3118

[25] B.S. Clausen, J. Schiøtz, L. Gråbæk, C.V. Ovesen, K.W. Jacobsen, J.K. Nørskov, H. Topsøe, Top. Catal. **1** (1994) 367

[26] B. Lindström, L.J. Pettersson, Journ. of Power Sources, **106** (2002) 264

[27] B. Bems, M. Schur, A. Dassenoy, H. Junkes, D. Herein, R. Schlögl, Chem. Eur. Journ. **9** (2003) 2039

[28] M.M Günter, PhD Thesis, Berlin, Technical University (2001)

[29] G. Ertl, H. Knözinger, J. Weitkamp, Handbook of heterogeneous catalysis, VCH-Wiley, New York (1997) 264

[30] N.W. Hurst, S.J. Gentry, A. Jones, Catal. Rev.-Sci. Eng. **24** (1982 233)

[31] W.D. Bond, J. Phys. Chem. **66** (1962) 1573

[32] J.A. Rodriguez, J.Y. Kim, J.C. Hanson, M. Pérez, A.I. Frenkel, Catal. Lett. **85** (2003) 247

[33] J.Y. Kim, J.A. Rodriguez, J.C. Hanson, A.I. Frenkel, P.L. Lee, J. Am. Chem. Soc. **125** (2003) 10684

[34] G. Fierro, M. Lo Jacono, M. Inversi, P. Porta, F. Cioci, R. Lavecchia, Appl. Catal. **137** (1996) 327

[35]P.H. Matter, D.J. Braden, U.S. Ozkan, J. Catal. **223** (2004) 340

[36] M. Shimokawabe, H. Asakawa, N. Takezawa, Appl. Catal. 59 (1990) 45

[37] J.P. Breen, J.R.H. Ross, Catal. Today **51** (1999) 521

[38] R-x. Zhou, T-m. Yu, X-y. Jiang, F. Chen, X-m. Zheng, Appl. Surf. Sci. **148** (1999) 263

[39] Y. Zhao, K. Tao, H.L. Wan, Catal. Comm. **5** (2004) 249

[40] Y. Wang, R.A. Caruso, J. Mater. Chem. **12** (2002) 1442

[41] B.S. Clausen, H. Topsøe, R. Frahm, Adv. Catal. **42** (1998) 315

[42] J.B. Wagner, P.L. Hansen, A.M. Molenbroek, H. Topsøe, B.S. Clausen, S. Helveg, J. Phys. Chem. B, **107** (2003) 7753

[43] M.M. Günter, T. Ressler, R.E. Jentoft, B. Bems, J. Catal. **203** (2001) 133

[44] Y. Okamoto, K. Fukino, T. Imanaka, S. Teranishi, J. Phys. Chem. **87** (1983) 1747

[45] K. Klier, V. Chatikavanij, R.G. Herman, G.W. Simmons, J. Catal. **74** (1982) 343

[46] G.C. Chinchen, K.C. Waugh, J. Catal. **97** (1986) 280

[47] W-H. Cheng, I. Chen, J-s. Liou, S.-S. Lin, Top. Catal. **22** (2003) 225

[48] K.C. Waugh, Catal. Lett. **58** (1999) 163

[49] R.A. Hadden, P.J. Lambert, C. Ranson, Appl. Catal. A: **122** (1995) L1

[50] B. Kniep, T. Ressler, A. Rabis, F. Girgsdies, M. Baenitz, F. Steglich, R. Schlögl, Angew. Chem. **116** (2004) 114

2 Materials

Copper based catalysts are widely used in methanol chemistry. The commercial catalyst for the methanol synthesis is a $Cu/ZnO/Al_2O_3$ material. The usage of a support has shown to increase the stability against sintering by spatially separating the copper particles. Further synergetic effects have been observed, e.g. alloy formation, and morphology changes or the induction of strain in the crystallite lattice of copper metal in the case of Cu supported on ZnO. To obtain these promoting effects various preparation techniques have been tested. For copper supported on zinc oxide, mostly co-precipitation is applied.[1,2,3]

An approach to prepare catalysts with high surface areas is based on the usage of templates (organic compounds, amphiphilic block copolymers or preformed objects) for the structuring of inorganic networks or the formation of nanometric building blocks (NBB)[4 and references therein]. In the later synthesis, the controlled precipitation of these NBB is a very important point. All of these strategies base on transcription, synergic assembly and morphosynthesis. However, for non-silica mesostructured materials several difficulties have to be overcome, for example the high reactivity of Zr toward hydrolysis and condensation, the relatively rigid linkage between metal-oxo coordination polyhedra (restricting the adaptation to a variety of shapes) and finally, instability of the network toward template removal. Besides the choice of the reagents and their concentration, the individual preparation steps influence the texture, structure and stability of the material. For example the aging process in solution was shown to determine the surface area of zirconia prepared from aerogels.[5,6 and references therein] In accordance with the knowledge of many studies[4] tetramethylammonium hydroxide or acetyl acetone were used to slow down hydrolysis and condensation during the preparation of the CuO/ZrO_2 materials of this work.[7,8] Furthermore, an amphiphilic block copolymer (Pluronic P 123) and a macroporous gel template were used to tailor the inorganic network. Especially the usage of the copolymer has shown to reduce the problem of insufficient stability (e.g. due to poor condensation or crystallization).[9,10]

Porous materials are very attractive, for example for catalytic reactions. On the one hand pores (provided they are large enough) reduce diffusion limitations of reactants and products and on the other hand, large surface areas of active components promote the catalytic reaction.

2.1 Preparation and characterization of CuO/Zr0$_2$

The samples were prepared at the MPI for Colloids and Interfaces in Golm (Potsdam) by Dr. Jan-Hendrik Schattka, Dr. Yanqin Wang, Dr. Atul Desphande and Dr. Markus Niederberger. We also thank Dr. Rachel Anne Caruso for her scientific support.

The investigated Cu/ZrO_2 catalysts can be divided into three groups.

First, Cu/ZrO_2 nanopowders were synthesized via a precipitation method described in detail in Ref. [11]. The sample denoted as *Nano-SA* was prepared by a *short-aging* method (addition of copper nitrate to the mixture of zirconium tetrapropylate and tetramethylammoniumhydroxide (TMAOH) after 1 h stirring, corresponds to *in situ* method in Ref. 11).

First, 5 ml zirconium tetrapropylate (10 mmol) [$Zr(OC_3H_7)_4$, 70 % in1-propanol] solution were added dropwise to 43 mL of an aqueous solution of TMAOH (2.5 mmol) [$N(CH_3)_4OH$), 25 % in methanol]. Subsequently, the solution was heated for 1 h at 353 K. This was followed by the addition of a 2.2 ml of aqueous copper nitrate solution (0.5 M). The resulting white suspension was stirred at room temperature for 1 h and finally heated at 353 K for 20 h. After centrifugation and washing, the sample was calcined at 773 K under air for 12 h (ramp 2 K/min).

The samples denoted as *Nano-LA-1* and *Nano-LA-2* were prepared by *long-aging* preparation method (addition of the copper nitrate after 20 h stirring, corresponds to the *step-by-step* method in Ref. 11). 5 mL zirconium tetrapropylate (10 mmol) [$Zr(OC_3H_7)_4$, 70 % in 1-propanol] solution were added dropwise to 43 mL (*Nano-LA-1*) or 25 mL (*Nano-LA-2*) of an aqueous solution of TMAOH (2.5 mmol) [$N(CH_3)_4OH$), 25 % in methanol]. Subsequently, the solution was heated for 20 h at 353 K. During this step hydrolysis and condensation lead to the formation and agglomeration of zirconium oxyhydroxides. Afterwards 2.2 mL (*Nano-LA-1*) or 25 mL (*Nano-LA-2*) copper nitrate solution (0.5 M) were added to the suspension. Heating at 353 K continued for another 6 h (meanwhile copper-oxyhydroxy species formed), and finally the sample was collected by centrifugation. Afterwards the samples were calcined at 773 K for 12 h in air. In contrast to the "*short-aging*" route, this should lead to a structure, where the support is mainly located in the center and the copper covers the surface of the particles (Figure 2-1).

The amount of Cu and Zr were adjusted to yield catalysts with 10 mol-% Cu and 90 mol-% Zr (*Nano-SA and Nano-LA-1*) and 30 mol-% Cu and 70 mol-% Zr, respectively for *Nano-LA-2* (with respect to the metal content). X-ray fluorescence analysis was performed on a Seiko Instrument (SEA 2010) a yielded 8.9 mol-% and 9.3 mol-% Cu in the *Nano-SA* and *Nano-LA-1* samples, respectively, and 20.6 mol-% copper in the *Nano-LA-2* sample. Independently we used

the height of the Hf L_3 edge (XAS; Hf is a natural impurity of zirconia) to estimate the copper content and got similar results.

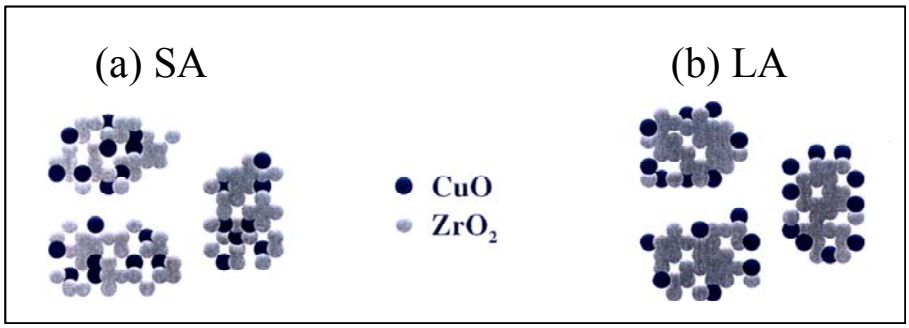

Figure 2-1 Schematic representation of the catalyst material (a) short-aging (SA) or (b) long-aging (LA) method

In the second preparation procedure employed, mesoporous zirconia was synthesized by a templating procedure. The zirconium alkoxide precursor ($Zr(OC_3H_7)_4$) was modified with acetyl acetone to slow down hydrolysis. After obtaining a stable solution, the solution of the copolymer $EO_{20}PO_{70}EO_{20}$ (Polyethyleneglycol-Polypropyleneglycol, Pluronic P123, Aldrich) was slowly added and the mixture obtained was heated at 353 K for 90 h, resulting in a transparent gel. This gel was dried at 333 K over 3 days and then calcined at 723 K for 12h. The introduction of the copper precursor into the mesoporous ZrO_2 network was achieved via two methods. (i) By a *post-support formation* method: 1 g of the calcined ZrO_2 sample was soaked in an aqueous solution of $[Cu(NH_3)_4(H_2O)_2]^{2+}$ (0.45 M, prepared by mixing copper nitrate with excess ammonia) for 5 h, then diluted with cooled deionised water (273 K), washed three times with deionised water and ethanol, and dried at 333 K overnight. Finally the material was calcined at 723 K for 2 h in air (sample *Meso-post*). (ii) By a *post-support formation* method: $Cu(CH_3COO)_2$ was dissolved in the solution of the block copolymer and then reacted with the zirconium precursor solution ($Zr(OC_3H_7)_4$ plus acetyl acetone). This material (sample *Meso-pre*) heated and calcined as described above. Prior to the first calcination the material was treated with hexamethyldisilazane (HMDS, $(CH_3)_3$-Si-NH-Si-$(CH_3)_3$) to prevent particle growth. The amount of Cu and Zr were adjusted to yield catalysts with 10 mol-% Cu and 90 mol-% Zr (*Meso-pre*) and 18 mol-% Cu and 82 mol-% Zr (*Meso-post*) (with respect to the metal content). XFA revealed that the materials obtained contained 9.6 and 5.8 mol-% Cu, respectively.

In the third preparation procedure employed, macroporous ZrO_2 was prepared from a polymer gel template.[12] The template was impregnated with a solution containing $Zr(OC_3H_7)_4$ [20.0 g, 70 % in 1-propanol], copper acetylacetonate (2.0 g, 7.6 mmol) and left standing for several hours. For hydrolysis and condensation reactions the soaked gels were transferred to a water/1-propanol (1:1 vol) solution. In order to avoid leaching of the copper acetylacetonate, the hydrolysis solution was saturated with the copper salt. Calcination in oxygen for 10 h at 773 K resulted in the macroporous ZrO_2 (denoted as *Macro*). The amount of Cu and Zr were adjusted to yield catalysts with 15 mol-% Cu and 85 mol-% Zr (with respect to the metal content). XFA yielded a copper concentration of 15.5 mol-%. All reagents for the preparation were obtained from Aldrich and used without further purification. The water employed was doubly deionised.

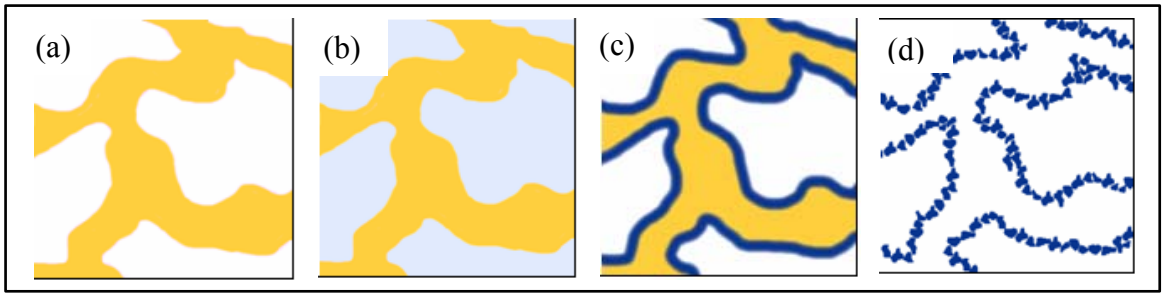

Figure 2-2 Schematic representation of the preparation of the macroporous catalyst via impregnation of an organic template, (a) polymer template, (b) template soaked with precursor solution, (c) amorphous metal oxide layer on the wall of template, (d) after calcination

The nomenclature of all CuO/ZrO_2 catalysts and the characterization of the calcined precursor (S_{BET}) and reduced material (XRD copper metal crystallite size) are given in Table 2-1.

Table 2-1 Chemical composition and characterization of calcined CuO/ZrO_2 precursor*, and reduced material#

Sample name	Calcination Temperature [K]	Cu content (XFA) (atom-%)	ZrO_2 crystallite size (Å)	copper metal# crystallite size (Å)	S_{BET} (m^2/g)
Nano-SA	773	8.9	-	20 (XRD)	72
Nano-LA-1	353[1], 773	9	-	-	110
Nano-LA-2	353[1], 773	20.6	-	50-100 (TEM)	168
Meso-pre	723	9.6	45-60/100** (TEM)	(400)/≤ 70# (TEM)	157
Meso-post	353[1], 723	5.8	-	-	226
Macro	773	15.5	60-80 (TEM)	55/150 *(TEM)	67

[1] Temperature corresponds to formation of zirconia precursor, * for metal/ oxidized particles, ** round/elongated ZrO_2 particles, # after feed reduction / after 2nd O_2 addition (all Cu_xO_y)

2.2 Structural Chemistry

2.2.1 Copper metal: Cu

Copper metal has a face centered cubic structure (fcc), belongs to the space group Fm3m and has a lattice constant a = 3.61 Å (see also ICSD[1] 64699). Each copper atom has 12 next nearest neighbors. This generates a cluster with 14 faces (Figure 2-3). Along the axes of the cubic lattice, the polyhedron share one face, whereas along a face diagonal, four polyhedrons share one copper atom (the face-centered atom).

[1] Inorganic Crystal Structure Database (maintained by the FIZ Karlsruhe)

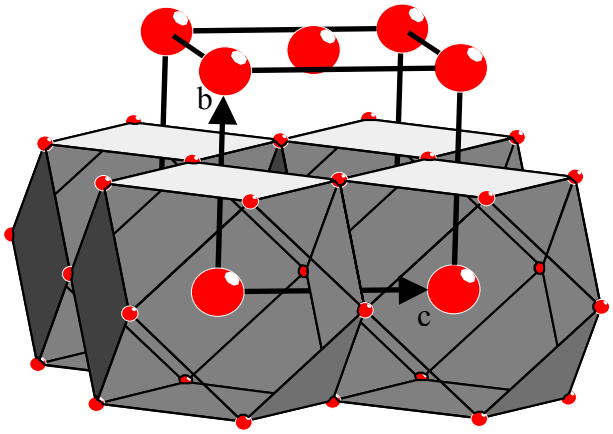

Figure 2-3 Detail from the structure of copper metal

According to the structure typically used for X-ray absorption spectroscopy, Figure 2-4a-d shows the coordination geometry around a central atom. Figure 2-4a represents the first 12 next nearest face-centered atoms. At a distance of 3.61 Å, which is equal to the lattice constant a, 6 atoms are located at the corners of a cube (Figure 2-4b). The 24 neighbors at a distance of 4.4213 Å are face-centered atoms that are not on the faces near the central atom (Figure 2-4c). 5.1053 Å equals the length of the face diagonal and in this distance 12 atoms are located around the central absorber (Figure 2-4d).

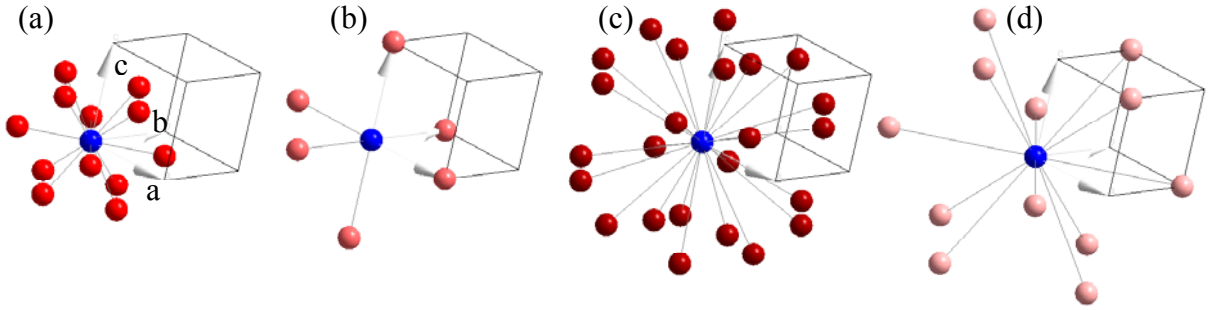

Figure 2-4 Copper metal structure around a central Cu atom (a) 12 next nearest neighbours at distance of 2.5527 Å, (b) 6 neighbours at distance of 3.6100 Å, (c) 24 neighbours at distance of 4.4213 Å, (d) 12 neighbours at distance of 5.1053 Å

2.2.2 Copper (II) oxide (tenorite): CuO

CuO has a monoclinic structure and belongs to the space group C12/c1. The corresponding unit cell data were taken from the IDSD data file 16025. This structure has three different axes lengths.

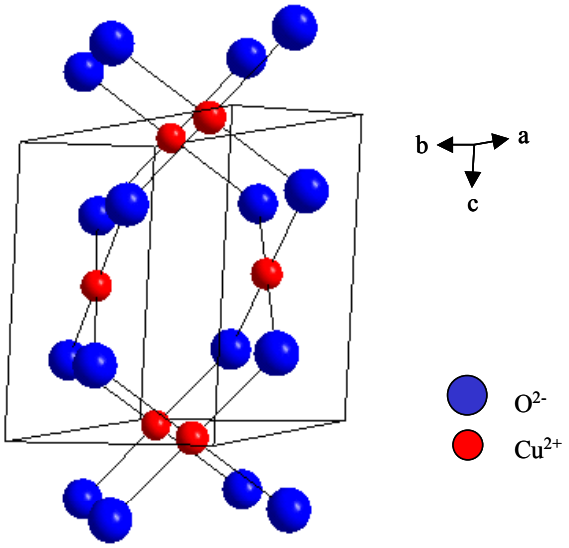

Figure 2-5 Detail from the structure of copper (II) oxide

A copper atom is surrounded by four oxygen atoms in a quadratic-planar coordination (Figure 2-5). Thereby, two opposing oxygen atoms have the same distances from the central copper atom, namely 1.9509 Å or 1.961 Å. The nearest copper atom is located at a distance of 2.9007 Å.

2.2.3 Copper (I) oxide (cuprite): Cu_2O

Cu_2O crystallizes also in a cubic structure with a lattice constant of 4.2696 Å and belongs to the space group Pn3m (PDF[1] data file 5-667). In this case oxygen atoms cover the corners of the unit cell (Figure 2-6) and the center. This central oxygen atom is tetrahedrally coordinated by four copper ions. The structure can be derived from the cristobalite structure, where four of such units build up the unit cell.

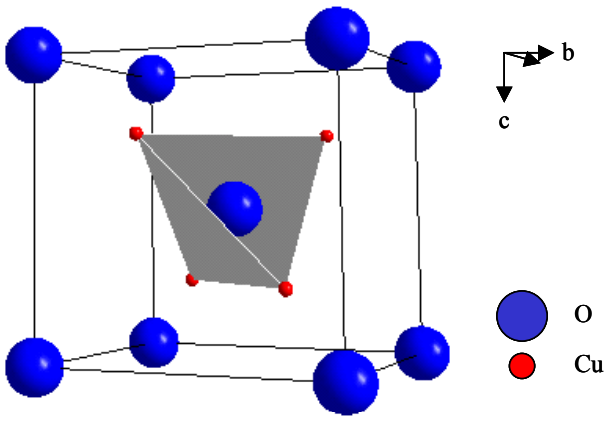

Figure 2-6 Unit cell of Cu_2O

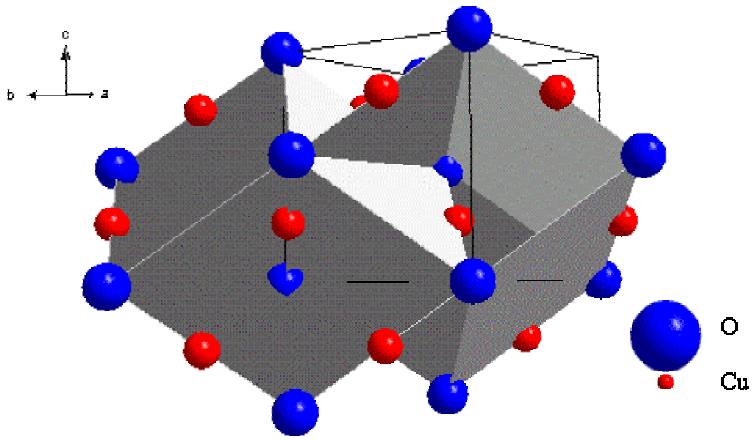

Figure 2-7 Detail from the structure of copper (I) oxide

Two oxygen atoms at a distance of 1.8488 Å and 6 oxygen atoms at 3.5402 Å built up a distorted cube around a copper atom. The copper atoms lie on the edges of the distorted cubes. The smallest Cu-Cu distance is 3.0191 Å (Figure 2-8). These distorted cubes penetrate each other (Figure 2-7).

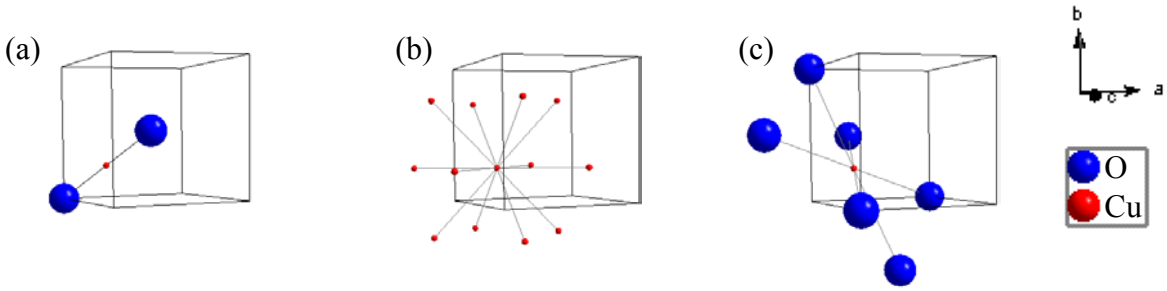

Figure 2-8 Cuprite structure around a central atom (a) 2 oxygen atoms at distance 1.8488 Å, (b) 12 copper atoms at distance 3.0191 Å, (c) 6 oxygen atoms at 3.5402 Å

[1] Powder Diffraction File™

Table 2-2 Near neighbors around an absorbing Cu atom in copper metal and Cu_2O

Neighboring atoms for copper metal	Distance (Å)	Neighboring atoms for Cu_2O	Distance (Å)
1 Cu-Cu	2.5527	1 Cu-O	1.8488
2 Cu-Cu	3.6100	2 Cu-Cu	3.0191
3 Cu-Cu	4.4213	3 Cu-O	3.5402
4 Cu-Cu	5.1053	4 Cu-Cu	4.2692

2.2.4 Zirconium dioxide: ZrO_2

At ambient pressure zirconium dioxide exists in three modifications (Figure 2-9). At room temperature only the monoclinic form is stable (besides the high pressure orthorhombic I and II structure). Tetragonal and cubic structures are found at higher temperatures (1373 K and 2573 K, respectively), although both can be quenched to ambient conditions.

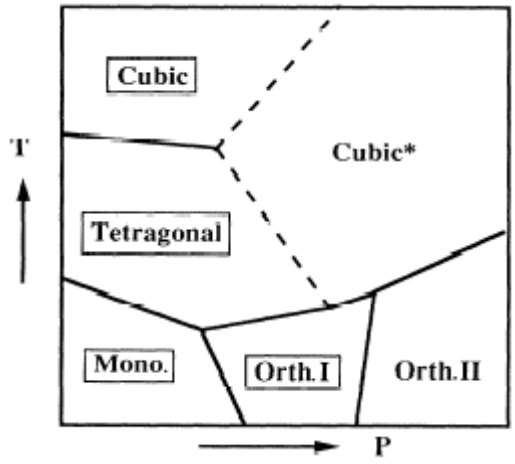

Figure 2-9 Schematic P-T phase diagram of ZrO_2.[13]

The three polymorphs are closely related to the cubic fluorite-type structure (Figure 2-10a-c). Cubic ZrO_2 crystallizes in a fcc structure with Zr surrounded by 8 oxygen atoms. In principle, the same coordination number, but a longer c-axis is found for t-ZrO_2. In the monoclinic phase (baddeleyite) one Zr (IV) is surrounded by seven oxygen atoms (CN = 7).

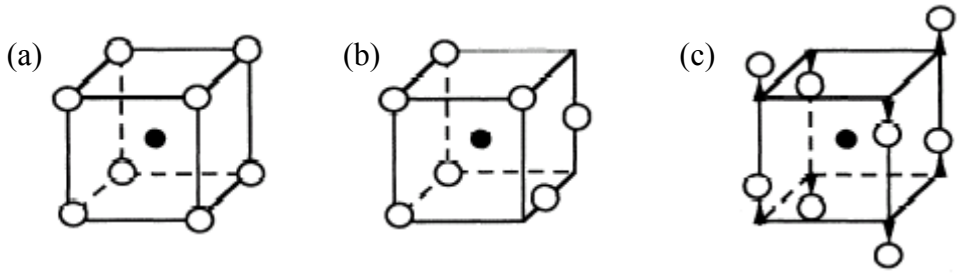

Figure 2-10 Schematic fluorite-type structure (a) idealized c-ZrO_2, (b) m-ZrO_2, (c) t-ZrO_2[13]

In the following the monoclinic and tetragonal modifications are introduced in more detail.

Baddeleyite (monoclinic ZrO_2)

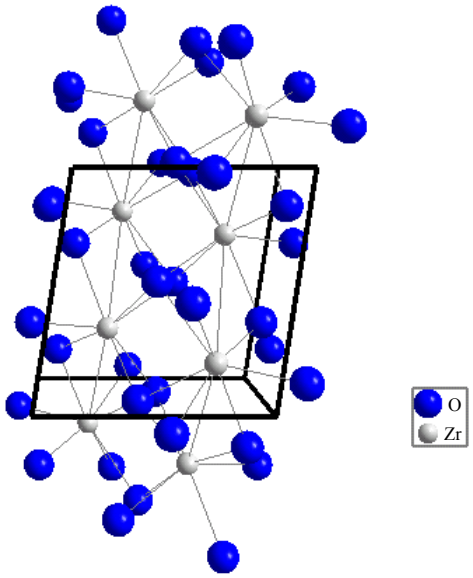

Figure 2-11 Projection of the crystal structure of baddeleyite along c axis

The baddeleyite structure has been describe among others, in 1959 by McCullough and Trueblood.[14] The Zr atom exists in a sevenfold coordination, whereas the oxygen atoms exist either in tetrahedral or triangular coordination (Figure 2-11). Thus the structure is an alternation of fluorite-like layers.

Tetragonal ZrO_2

The eightfold coordination of Zr^{4+}-ions is shown in (Figure 2-12). The lowest Zr-Zr distance is 3.5953 Å, whereas the second nearest Zr neighbor is located at a distance of 3.60110 Å.

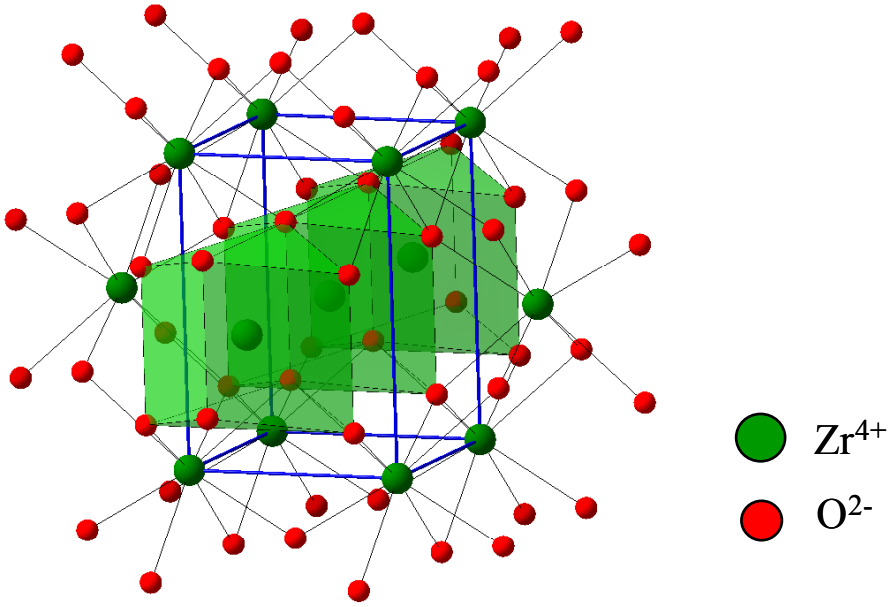

Figure 2-12 Projection of the crystallite structure of tetragonal ZrO_2.

2.3 SEM (Secondary Electron Microscopy)

The morphologies of the various catalyst materials are shown in Figure 2-13. For the nanostructured (Figure 2-13) and macroporous (Figure 2-14) samples sponge-like structures are typical, whereas the mesoporous material appears very compact with a rather smooth surface.

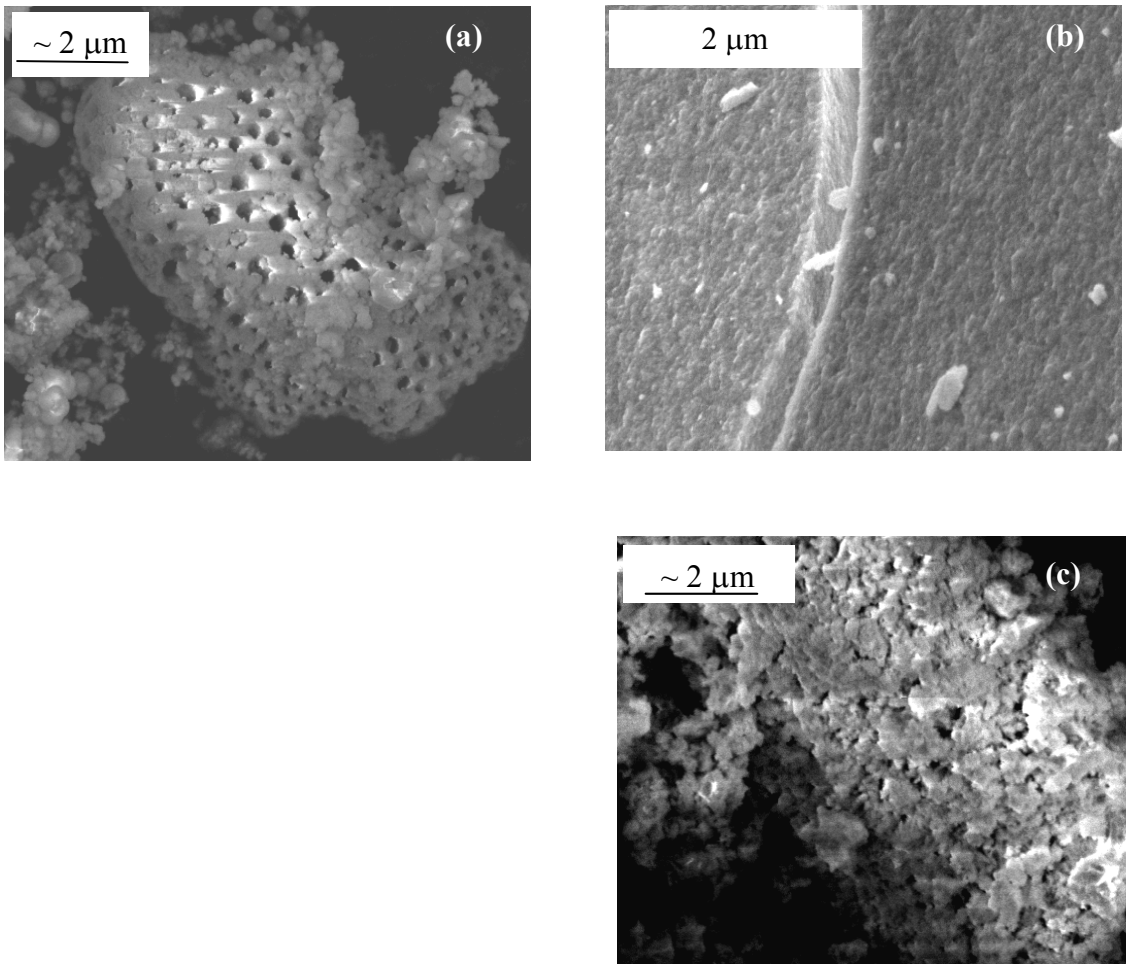

Figure 2-13 SEM-micrograph of (a) Macro, (b) Meso-post and (c) Nano-INS; as prepared

2.4 References

[1] B. Bems, M. Schur, A. Dassenoy, H. Junkes, D. Herein, R. Schlögl, Chem. Eur. Journ. **9** (2003) 2039

[2] M.M. Günter, T. Ressler, R.E. Jentoft, B. Bems, J. Catal. 203 (2001) 133

[3] K. Klier, V. Chatikavanij, R.G. Herman, G.W. Simmons, J. Catal. 74 (1982) 343

[4] G.J. de A.A. Soler-Illia, C. Sanchez, B. Lebeau, J. Patarin, Chem. Rev. **102** (2002) 4093

[5] A.F. Bedilo, K.J. Klabunde, Nanostructured Materials 8 (1997) 119

[6] Handbook of porous solids, F. Schüth, edited by F. Schüth, K.S.W. Sing, J. Weitkamp, Volume 1, Wiley Weinheim 2002, 619

[7] A. Chemseddine, T. Moritz, Eur. J. Inorg. Chem. 1999 (1999) 235

[8] Y.-Y. Huang, T. J. McCarthy, W. M.H. Sachtler, Appl. Cat. **148** (1996) 135

[9] P. Yang, D. Zhao, D.I. Margolese, B.F. Chmelka, G.D. Stucky, Nature **396** (1998) 152

[10] P. Yang, D. Zhao, D.I. Margolese, B.F. Chmelka, G.D. Stucky, Chem. Mater. **11** (1999) 2813

[11] Wang, Y., Caruso, R.A., J. Mater. Chem. **12**, 1442 (2002)

[12] Schattka, J.H., Shchukin, D.G., Jia, J., Antonietti, M., Caruso, R.A., Chem. Mater. **14**, 5103 (2002)

[13] P. Li, I-W. Chen, J.E. Penner-Hahn, Phys. Rev. B: **48** (1993) 10063

[14] J.D. McCullough and K.N. Trueblood, Acta Cryst. **12** (1959) 507

3 Experimental and Theoretical Details

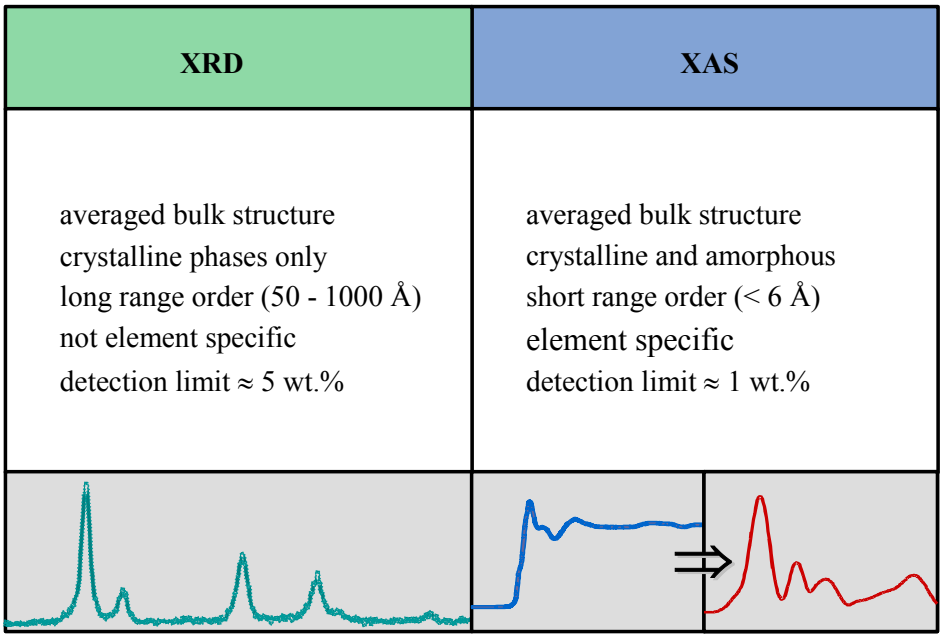

Figure 3-1 Comparison of XRD and XAS

X-ray diffraction (XRD) and X-ray absorption spectroscopy (XAS) have been applied successfully in the past, in order to investigate the bulk crystallite structure of catalyst materials.[1,2,3] Both methods can be used under in situ conditions and therefore provide information about the active phase under working conditions. Oftentimes the gas phase evolution is monitored simultaneously and hence, allows the correlation of structural changes with the catalytic performance. Both, information about the unit cell and d-spacings, and about the coordination sphere (around an absorbing central atom, < 6 Å) are given by the complementary techniques XRD and XAS, respectively (Figure 3-1).

3.1 X-ray diffraction

3.1.1 Theory

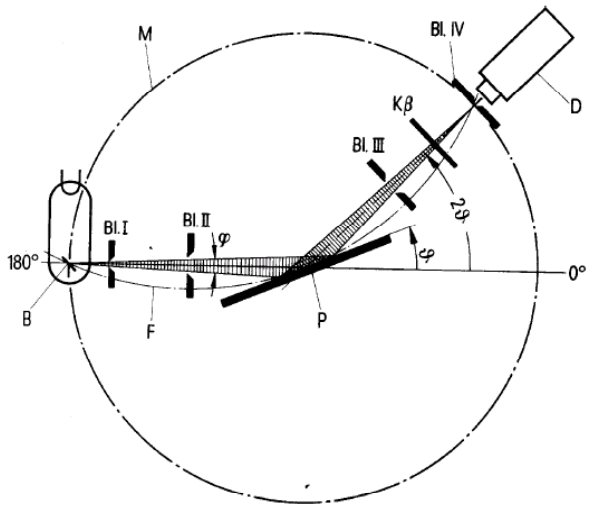

Figure 3-2 Arrangement of x-ray tube, sample and detector in Bragg-Brentano geometry; B focal spot of the x-ray tube, B1.I to B1.IV aperture, D detector, P sample, M goniometer circle, F circle of focus (ϑ=θ)

The arrangement of a typical Bragg-Brentano geometry is given in Figure 3-2. With this setup it is possible to measure in reflection geometry. The incident beam and the sample enclose the Bragg angle θ (theta). After the incident beam is diffracted at the sample, the detector measures the intensity of the scattered beam. Scattered and incident beam enclose the angle 2θ. The occurrence of a peak in a X-ray pattern is coupled to the requirements of Bragg´s equation (equation 1).[4]

$$n\lambda = 2\, d_{hkl} \sin\theta \qquad (1)$$

λ = wavelength, d_{hkl} = distance between lattice planes (hkl), θ = diffraction angle, hkl = Millerindices

Only if the incident beam impinges the lattice planes under the angle theta, diffraction can occur (

Figure 3-3a). The corresponding pattern is the presentation of the diffraction lines at certain angles 2 θ, with their intensity. The position of the peaks contains information about the lattice parameters.

In order to measure powder samples, it is important, that the crystallites in the sample are randomly oriented.

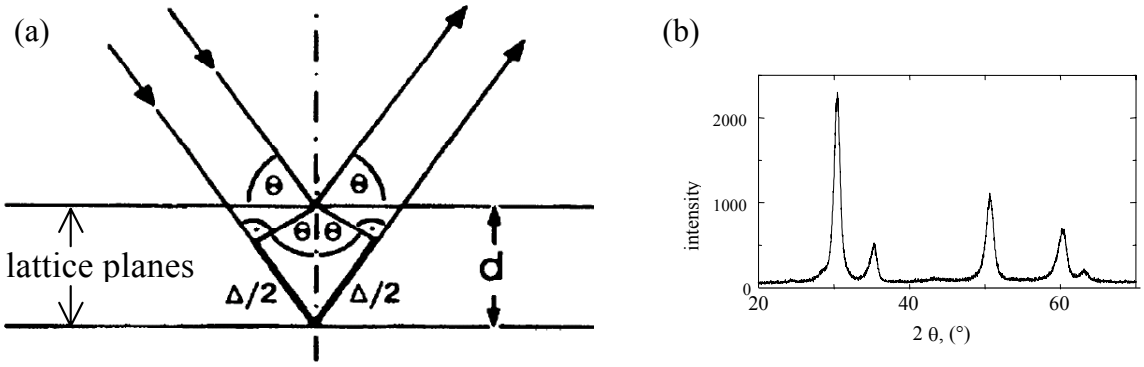

Figure 3-3 Bragg diffraction at family of lattice planes (a), example of a powder x-ray pattern (b)

The breadths of the diffraction lines (for example
Figure 3-3b) are usually described by the full width at half maximum (FWHM). Together with the intensity, these parameters define the sharpness of the diffraction lines. Line broadening occurs, when many small crystallites with fewer lattice planes are present in the powder. The Scherrer formula[5] (2) estimates the crystallite size, by relating the peak width of a broadened peak to the thickness of the crystal.

$$\beta = \frac{\lambda * K}{L * \cos\theta} \qquad (2)$$

β = FWHM, λ = wavelength, K = formfactor: 0.89 for cubic and 0.94 for spherical crystallites, L = crystallite thickness, θ = Bragg angle

The intensity of a peak is dependant on the electron density distribution, which in turn is determined by the spatial arrangement of the atoms; the crystale structure. The structure itself is defined by the crystal lattice, the symmetry and the sort of atoms and their position. The peak intensity can therefore be an indicator for the crystallinity of the sample.
With the help of all these information and additional parameters (e.g. contribution of instrumental broadening to the FWHM) it is possible to simulate a diffraction pattern and to obtain information about the lattice parameters and crystallite sizes.

3.1.2 Ex- and in situ set-up and instrumentation

Combined in situ XRD/MS experiments were performed on a STOE Theta/theta diffractometer with secondary Si (111) monochromator (Cu Kα1 and Kα2 radiation) in reflection geometry. The diffractometer was equipped with a XRK 900 high temperature cell for in situ measurements. Approximately, 30 - 40 mg (particle size ≤ 200 μm) of the samples was put on the top of the sample holder and the gas entered the cell over three inlets; one from the front side, the second from the backside and the third from the bottom of the sample holder. The bottom of the sample holder was made from a sieve that allows the gas to flow through the sample. The bottom with its holes was covered with glass microfibre filter to prevent the sample from blocking the gas flow. This construction provided that the entire sample was in close contact with the chosen gas atmosphere.

The gases (He, O_2, H_2), and 3.0 vol-% MeOH and and 1.5 vol-% H_2O (total flow 100 ml/min) were introduced into the chamber similarly as described in more detail in (6). The composition of the gas phase was monitored with a Balzers quadrupole mass spectrometer (QMS 200, Pfeiffer).

The treatment of the catalyst started either with a reduction in 2 vol-% H_2 in He or directly with methanol and water. A total gas flow of 150 ml/min was used. At 523 K the sample was held for about 1.5 h. During this time XRD patterns were recorded with a range from 25-65° 2θ, a counting rate of 3 sec/step, and a step width of 0.04° 2θ. For studies under MSR reaction conditions two helium streams were saturated with methanol or water at room temperature and atmospheric pressure. A volume ratio of 2:1 (methanol:water) was adjusted by changing the corresponding flow conditions. After the reduction in hydrogen and cooling down to room temperature the gases were changed to MSR conditions and the sample was again heated to 523 K at a rate of 6 K/min. Similar to the XAS experiments 10 mol-% of oxygen were temporarily added to the feed mixture of methanol/water. After the oxygen was switched off again, the correlating changes in the activity and the crystallite structure/size were detected.

An overview over the various reaction treatments is given in Table 3-1. First results revealed no detectable changes for the zirconium dioxide during the reaction and therefore the measuring range was shortened to 41-46° 2θ and only the Cu 111 peak was measured during catalysis. Crystallite size calculations were based on the Scherrer equation.[6] The $K\alpha_2$ contribution was removed from the pattern with the help of the software package STOE Win XPOW 1.06. Subsequently, the full width at half-maximum (FWHM) was determined by fitting a pseudo-Voigt profile function to the Cu 111 and the ZrO_2 111 peak.

Based on the crystallite size (XRD) and assuming spherical particles, the volume (ρ_{Cu} = 8.92 g/cm^3) of all copper particles, the corresponding specific copper surface area $S_{Cu(XRD)}$ was also determined.

Table 3-1 Reaction scheme for (I) reduction in 2 vol-% H_2/He, (II) methanol steam reforming (feed), (b, f) feed + 10 vol-% O_2 for ~ 30 min, afterwards MSR again.

		Treatment	Temperature, [K]
I		Reduction in 2 % H_2	523
II	a	Reduction in feed	523
	b	MSR after 1st temporary addition of O_2	523
	c	2 % H_2	673
	d	In 2 % H_2 after treatment (c)	523
	e	In feed after treatment (c)	523
	f	MSR after 2nd temporary addition of O_2	523

3.2 X-ray absorption spectroscopy (XAS)

3.2.1 Theory of EXAFS and XANES

X-ray absorption spectroscopy provides element specific structural information for crystalline and amorphous materials. With these high energy X-rays it is possible to probe the short range order (coordination sphere of about 6 Å) of crystallites, e.g. local disorder or strain in the solids. XAS with hard X-rays (> 5 keV) is insensitive to gas phase absorption and can therefore be used as an in situ technique. With these advantages it is very suitable to investigate heterogeneous catalysis under working conditions.

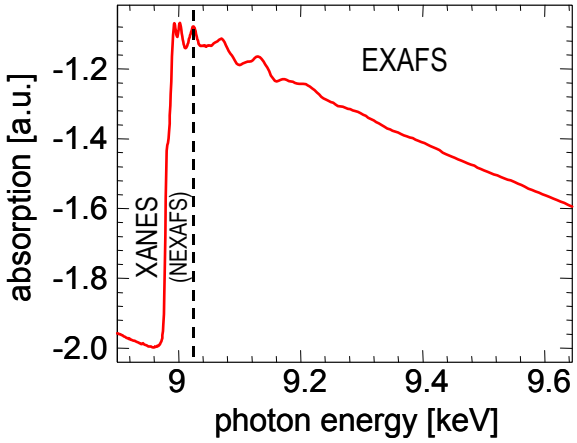

Figure 3-4 X-ray absorption spectra of copper metal at the Cu K-edge

Absorption of the X-ray photon occurs, when its energy is tuned to the binding energy of the core level electron of a specific element. In this case, the electron will be excited to an unoccupied state. Figure 3-4 shows a copper metal spectra recorded at the Cu K-edge. The position of the absorption edge is related to a specific atomic number and hence, to a certain quantum-mechanical transition that excites a particular atomic core-orbital electron to the free or unoccupied continuum levels. The nomenclature for X-ray absorption is related to this origin, for example K edges refer to transitions that excite the innermost 1s electron. The edge position can therefore, give information about valence states.[7,8] The more oxidized the element, the higher lies the absorption edge and vice versa.

Generally, two regions can be distinguished in the spectrum. The region near the absorption edge ["Near edge X-ray absorption fine structure" (NEXAFS, soft X-ray regime) or "X-ray absorption near edge structure" (XANES, hard X-ray regime)] is dominated by local atomic resonance and strong multiple scattering.[9] This region typically lies within the first 30 eV of the edge position.

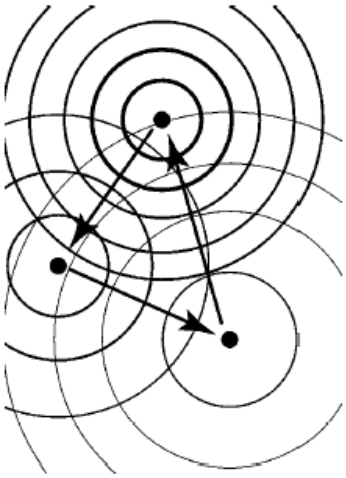

Figure 3-5 Pictorial view of the multiple scattering of an outgoing wave off a neighboring atom. The topmost atom is the original source of the wave, which diffracts first off the atom at the lower left and finally off the atom at the lower right. Each successive outgoing spherical wave is weaker, which is reflected in the thickness of the spherical wave fronts. This type of path is called a triangular path.[9]

As the energy of the x-ray photon increases, excitation above the Fermi-edge occurs and the corresponding photoelectron behaves like a "free" electron and can be represented by as an outgoing wave.[10] If the absorbing atom is surrounded by neighbors (e.g. in solids), the outgoing spherical wave will be scattered back by them. Figure 3-5 gives an example of such a process (multiple scattering). The interference of the outgoing and successive backscattered waves leads to a modulation of the absorption coefficient. Depending on the wavelength (i.e. the energy) of the electron, the distance between neighboring atoms and the phase shift caused by scattering events, outgoing and backscattered waves enhance or destroy each other. For example, maxima in the cross section for X-ray absorption occur at energies, where constructive interference takes place. Therefore, the wiggly structure has embedded within it information about near-neighbor distances, coordination numbers, and fluctuations in bond distances.

The following equations will be shortly introduced to describe EXAFS mathematically.
EXAFS $\chi(k)$ can be calculated from the measured absorption using equation (3).

$$\chi(k) = \mu(k) - \mu_0(k)/ \mu_0(k) \quad (3)$$

$\mu(k)$ = measured absorption, $\mu_0(k)$ = atomic absorption

Taking the structural parameters into account (e.g. interatomic distance R, coordination number N) the EXAFS equation was formulated and the common description[9] is given in equation (4).

$$\chi(k) = \sum S_0^{\,2} N_R * \frac{|f(k)|}{kR^2} \times \sin(2kR + 2\delta_c) e^{\frac{-2R}{\lambda(k)}} e^{-2\sigma^2 k^2} \qquad (4)$$

S_0 = amplitude reduction factor, N_R = amount of backscattering atoms in the distance R, f(k) = backscattering amplitude , $\lambda(k)$ = mean free path of the photoelectron, σ^2 = relative mean square disorder between the absorber and an atom (Debye-Waller factor), δ_c = phase shift due to the atomic potentials, k = photoelectron wave number

In order to allow for thermal and static disorder in the material, the Debye-Waller factor σ has been included in the EXAFS equation. Thermal disorder is attributed to the thermal lattice vibrations at higher temperatures, whereas static disorder is encountered if the distance of atoms of the same coordination shell differs slightly. The Debye-Waler factor σ characterizes a Gaussian pair distribution. If the distribution deviates from a Gaussian shape, the cumulant expansion approach has been introduced by Bunker et al.[11] and see also Ref.12.

The Fourier transform of the $\chi(k)$ (with respect to the photoelectron wavenumber) leads to the radial distribution function (RDF). The envelope peaks at distances corresponding to the nearest-neighbor coordination shell of atoms.
The conventional analysis procedure of the EXAFS spectrum was described in detail by Koningsberger in 1988.[13]

3.2.2 XAS experiments, instrumentation and data processing

3.2.2.1 Experiments and instrumentation

XAS investigations were performed at the beamlines X1 and E4 (HASYLAB at DESY, Hamburg, Germany). The calcined precursor material (CuO/ZrO_2) was measured at the Cu K edge (E = 8.979 keV) at room temperature. For the ex situ measurements 68 mg of the material were mixed with 200 mg polyethylene and pressed at a force of 1 t into a 13 mm in diameter pellet. A copper reference foil between the second and third detector was used for energy calibration. The useable energy range was limited to 8900-9699 eV because of the Hf L_3 edge at 9561 eV.

In situ XAS investigations of the catalyst under reaction conditions were also performed at the Cu K edge in the transmission mode. 10 mg of the catalyst (max 200 µm grain size) together with 30 mg boron nitride (BN) were pressed at a force of 1 t into a 5 mm in diameter pellet. The total flow through the in situ cell[14] was set to 40 ml/min at a cell volume of 4 ml and, hence, satisfying the conditions of differential conversion. Helium was used as a carrier gas at 293 K and a volume ratio of 2:1 methanol/water (3 % : 1.5 %) was adjusted taking into account the different partial pressures (methanol (p_{MeOH} = 12496.1 Pa, 1,13 ml/min)/water (p_{H2O} = 2337.8 Pa, 0,57 ml/min)). The He flows necessary for the right ratio at 293 K were 8 ml/min for MeOH and for H_2O 24 ml/min (plus extra He 4 ml/min). A photograph and schematic representation is given in Figure 3-6.

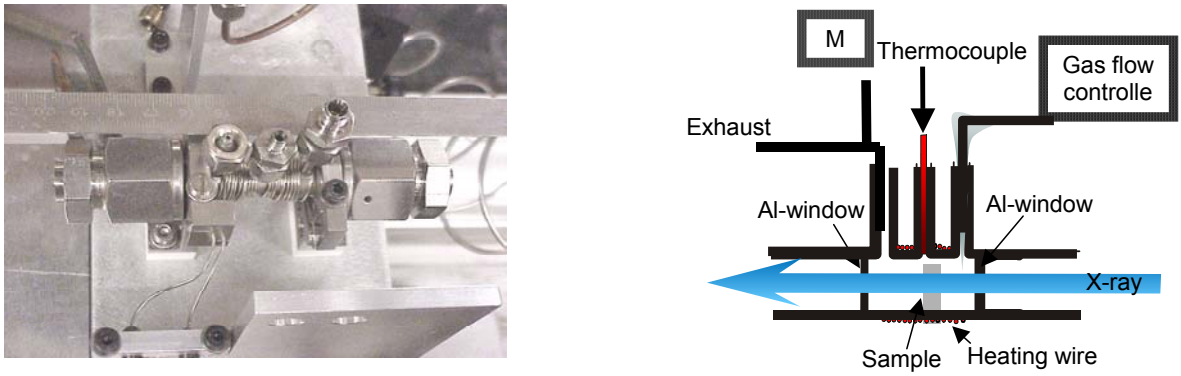

Figure 3-6 (a) Photograph of the in situ EXAFS cell, (b) schematic setup of the in situ EXAFS cell operated in transmission geometry

Two different reaction procedures were applied (see also Table 3-1). In the first procedure the catalyst was heated with 6 K/min to 523 K in 2 vol-% H_2/He until no further changes in the XANES spectra could be observed. The reactor was rapidly cooled down to room temperature and an EXAFS spectrum was measured for detailed structural analysis. Subsequently, the feed of water and methanol for the steam reforming reaction (methanol:water, 2:1) was introduced into the reactor and the catalyst was heated to 523 K at 6 K/min. In order to reveal the structural and catalytic effect of a temporary oxidative treatment,[5,3] after 1 to 5 h time on stream 10 vol-% O_2 were added to the feed for about 30 min.

In the second procedure the catalyst was reduced directly in a mixture of methanol and water (ratio 2:1). The material was heated to 523 K in the feed at a rate of 6 K/min. Already after 1 h time on stream 10 vol-% O_2 were temporarily added to the feed, because the catalyst was already in an active state after thermal treatment. Both procedures are illustrated in Table 1. After

reduction in the MSR feed and a short oxygen addition (Table 1) the catalyst was treated at 673 K in 2 vol-% H_2/He for 30 min in order to test the stability of the material under higher temperatures. After cooling down to 523 K the gas atmosphere was changed back to MSR conditions, followed by an addition of oxygen, and continuing methanol steam reforming.

3.2.2.2 Data processing

Analysis of the XAS spectra was performed with the software WinXAS 3.1.[15] The data were energy calibrated according to the copper reference foil measured. After background correction, normalization, and transformation into the k-space, an atomic background μ_0 (k) was determined, using a cubic spline function. The radial distribution function FT(χ(k)*k^3) was obtained by Fourier transforming the k^3 – weighted experimental χ(k) function (k = 2.3 - 10 $Å^{-1}$, restricted by Hf L_{III} edge at 9.561 keV), multiplied by a Bessel window, into the R space. It has been shown recently, that the analysis of coordination shells above the first shell, should take into account multiple scattering processes.[7] Therefore, theoretical backscattering phases and amplitudes for single and multiple scattering paths were calculated using
FEFF 7[16] up to 6 Å for Cu metal and Cu_2O. Refinements using the standard EXAFS equation were carried out in R space using the Cu-Cu coordination shells for copper metal and, when necessary, the first Cu-O shell of Cu_2O. One E_0 shift and one 3rd cumulant for all scattering paths, the Debye-Waller factors (DWF) for the single scattering paths, and the single shell distances were determined by a least-squares fit to the experimental data. Coordination numbers and S_0^2 (0.9) were kept invariant. In addition DWFs of two multiple scattering paths (MSP) were also allowed to vary in the refinement. Both describe scattering of the photoelectron by the copper atoms in the second shell amplified by forward scattering by the atoms in the first shell ("focusing effect").

For the quantification of the contribution of Cu-O scatterers to the EXAFS FT(χ(k)*k^3) a refinement of the experimental spectra was performed as described above taking copper metal (first Cu-Cu shell at R = 2.56 Å) and the first Cu-O shell of Cu_2O (R = 1.84 Å) into account and varying the ratio of the two phases. The DWF of the Cu-O distance was set to 0.0037 $Å^2$ and kept invariant. This value was determined by a refinement to an experimental spectrum of bulk Cu_2O and, therefore, is based on the static and dynamic disorder of bulk Cu_2O.

3.2.2.3 Principle Component Analysis (PCA)

A PC analysis of the experimental XANES spectra recorded during the reduction of the catalyst was performed to obtain the number of chemical phases present and to identify suitable references to describe the set of spectra. The identification of suitable references (real factors) is performed by PCA in combination with target transformation.[17] For the nanostructured catalyst studied here, it was found that the spectra of common references like Cu foil or CuO were not able to sufficiently describe the experimental spectra. This is probably because of the small crystallite size and the disorder in the Cu/ZrO_2 catalyst material. However, to describe the changes occurring during reduction, the "abstract concentrations" resulting from the PC analysis are compared. They indicate the evolution of the different spectra in the experimental data, but must not be mistaken for absolute concentrations.

3.3 N_2O decomposition (refers to Reactive Frontal Chromatography (RFC)) and N_2 adsorption (BET)

3.3.1 Fundamentals and experiment

Adsorption and desorption isotherms were measured on a Quantachrome Autosorb instrument after outgassing at 423 K for 6 hours. The total surface area was calculated from a 5-point BET plot ($1/[W((p_0/p)-1)]$ versus relative pressure p/p_0).

N_2O decomposition was used to determine the copper surface area after activation in methanol and water and after temporary oxygen addition at 523 K. RFC was first introduced and described by Chinchen et al.[18,19] The technique is based on the assumption, that N_2O decomposes at the copper surface to N_2 via oxidation of two Cu atoms to Cu_2O. The following procedure was employed here. After activation in the feed (second procedure in the XAS section) the sample was purged for 1 h in He at 523 K with a flow of 50 ml/min to diminish the amount of adsorbed molecules. Afterwards, the sample was cooled down to 313 K. RFC measurements were performed at 313 K with a mixture of 0.5 vol-% N_2O/He at a flow of 15 ml/min with the sample placed on a quartz frit in a quartz tube reactor. The sample was diluted with boron nitride to provide a bed height of about 15 mm with a thermocouple directly positioned in the powder bed (Figure 3-7).

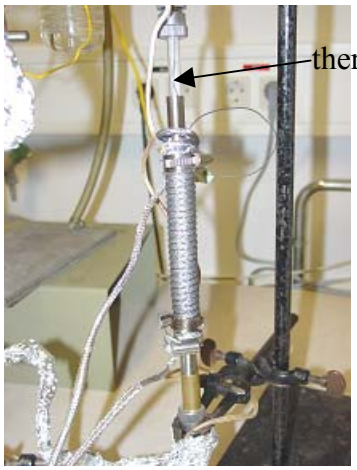

Figure 3-7 Photograph of the glass reactor wrapped with heating wire and thermocouple positioned directly in the reactor

3.3.2 Evaluation of the experimental results

In the RFC method described by Chinchen et al.[18], the area under the ion current trace m/e = 28 of N_2 is directly used to determine the copper surface area. Because N_2O also gives a signal for m/e = 28 in the MS used, we chose to monitor the amount of m/e = 44 (representing N_2O) consumed during the "reactive frontal chromatography". For a blank measurement, the reactor was filled with an appropriate amount of boron nitride. N_2O/He was passed through the sample bed and the evolution of the MS ion currents of N_2O (m/e = 44), N_2 (m/e = 28), and He (m/e = 4) was monitored. For measurements of the catalyst, detection of the m/e = 44 current (N_2O) occurs later compared to the boron nitride blank experiment, because N_2O reacts with the surface of the copper particles to yield nitrogen.

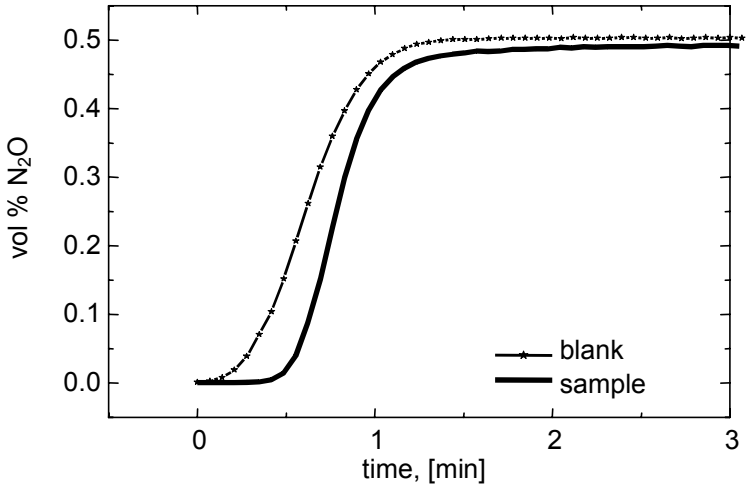

Figure 3-8 N_2O decomposition experiment: evolution of vol-% N_2O for sample and blank, areas under both curves are determined for calculation of the S_{Cu},

For calculating the Cu surface area, first the inflection point of the N_2O ion current trace (m/e = 44) from the measurement of the catalyst was determined as the endpoint of the titration (Figure 3-8). Second, the areas under the N_2O ion current traces of the catalyst and the blank measurement were calculated up to the endpoint determined. Third, the difference between the areas under the N_2O ion current trace from the catalyst and the blank measurement was used to calculate the corresponding volume of N_2 produced by the decomposition of N_2O. The copper surface area was calculated assuming $1.47*10^{19}$ copper atoms per m^2.[18,20] In addition to measuring Cu/ZrO_2 samples, N_2O decomposition on Cu/ZnO samples was performed, where the copper surface areas have been previously presented.[27] Although these former measurements[21,27] were done at 333 K instead of 313 K, comparable results were obtained by

the procedure employed here. The experimental error of individual measurements was estimated to be about 15 %.

3.4 Thermal Analysis (TG and DSC) combined with mass spectrometry

3.4.1 Fundamentals and Apparatus

Decomposition processes, dehydration, corrosion/oxidation, and reduction processes are generally characterized by changes of the weight and heat effects. Thermo analysis can quantify these effects and hence give information about the thermal stability, purity, or conversion of reaction mixtures. For thermal analysis the samples are exposed to a controlled temperature program and their behavior is monitored in dependence of temperature or time. The Thermogravimetry (TG) measures sample specific weight changes; whereas the Differential Calorimetry (DSC) samples specific heat effects. Therefore, the heat flow of the sample is compared with the heat flow of a reference material. If the gas atmosphere is monitored simultaneously, the steps in the weight change can be correlated to products of the reaction/decomposition. Figure 3-9a shows a classical example for thermal analysis. With increasing temperature the transition from the solid to the liquid state was measured. Figure 3-9b represents mass loss and heat evolution of the dehydration process of $CuSO_4$ during temperature programmed heating to 623 K.

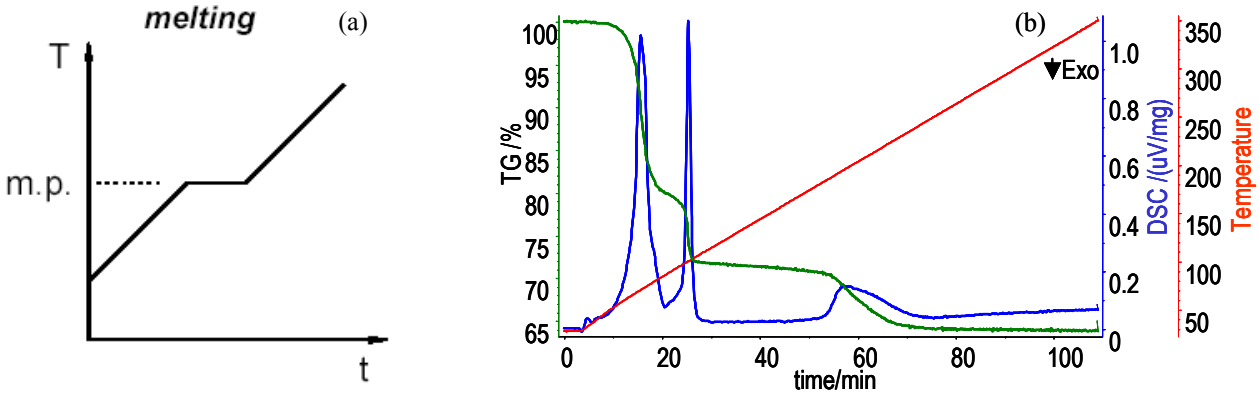

Figure 3-9 Thermal analysis of a solid to liquid transition (a), TG/DSC measurement of the dehydration of $CuSO_4$ (b)

The measurements of this thesis were performed on a Netzsch STA 449C. The evolution of the corresponding gas phase was monitored with an Omnistar mass spectrometer (Pfeiffer).

3.4.2 Experimental details

Usually approximately 26 mg of the catalyst material were put into an Al_2O_3 crucible and positioned onto the TG/DSC sample holder. An empty Al_2O_3 crucible was used for the reference. The temperature evolution of the sample during reaction and simultaneously of an empty reference crucible were measured with thermocouples (at the bottom of the crucibles) and converted into the DSC signal.

Prior to TG-DSC measurements, the CuO/ZrO_2 sample was heated twice to 523 K in He and held at that temperature for 1 h to remove adsorbed water and CO_2. Subsequently, the catalyst was heated in 2 vol-% H_2/He from 300 K to 523 K at a heating rate of 6 K/min.

3.5 Nuclear Magnetic Resonance (NMR)

3.5.1 Motivation

Analysis of the width and the profile of ^{63}Cu NMR lines of reduced copper particles permit qualitative conclusions concerning crystallite size and amount of disorder (e.g. microstrain). Similar to X-ray diffraction line broadening, a symmetric and narrow line profile indicates large and ordered crystallites. A decrease in the copper crystallite size results in a symmetric NMR line broadening, while an increase in strain or disorder causes an asymmetric line profile and/or the occurrence of additional NMR lines.[22] This was previously confirmed by results on Cu/ZnO catalysts, where the existence of microstrain in the copper particles was additionally verified with XRD and XAS.[23]

3.5.2 Fundamentals and Apparatus

Nuclear magnetic resonance is a phenomenon, which occurs when the nuclei of certain atoms are immersed in a static magnetic field and exposed to a second oscillating magnetic field.

In nuclear magnetic resonance, it is unpaired nuclear spins that are of importance. Furthermore, when an atom is placed in a magnetic field, its electrons circulate about the direction of the applied magnetic field. This circulation causes a small magnetic field at the nucleus which opposes the externally applied field. The electron density around each nucleus in a molecule varies according to the types of nuclei and bonds in the molecule. The opposing field and therefore the effective field at each nucleus will vary. This is called the chemical shift phenomenon. The chemical shift of a nucleus is the difference between the resonance frequency

of the nucleus and a standard, relative to the standard. This quantity is reported in ppm and given the symbol delta,.[24]

$\delta = (\nu - \nu_{REF}) \times 10^6 / \nu_{REF}$

Cu NMR spectra of the Cu/ZrO_2 catalysts were measured at the MPI for Solid State Physics in Dresden by Dr. Annegrit Rabis with a Bruker MSL 300 spectrometer at 79.618 MHz for ^{63}Cu and 85.288 MHz for ^{65}Cu at 4.2 K in an Oxford cryostat. Spin-echo experiments (90°-tau-180°) were performed with a 90° pulse of 5.5 μs, a "recycling delay" of 2 s, and a tau value of 25 μs. The ^{63}Cu-NMR spectra shown are calibrated against $CuBr_{(s)}$ at - 381 ppm.

3.5.3 Experimental details

For NMR investigations, various samples were collected from a fixed bed reactor after different reaction steps (see also Table 3-1): a. after direct reduction in the feed at 523 K,
b. after the 1st oxygen addition, d. after heating in 2 vol-% H_2/He to 673 K and cooled down to 523 K, e. after the heating treatment at 673 K and switching back to MSR conditions, and f. after the 2nd oxygen addition; and transferred into NMR tubes without contacting air.

3.6 Transmission Electron Microscopy (TEM) and Scanning Electron Microscopy (SEM)

Microscopy can be a useful tool, to obtain information of the catalyst material in the active state. High resolution TEM and in situ TEM studies on copper supported on ZnO (copper content ≈ 5 %) have been presented in the last decades.[25,26] For well-ordered Cu particles on a large ZnO support a strong dependence of the copper crystallite morphology on the reduction potential of the gas phase was shown. The influence of the preparation of copper supported catalysts on the copper surfrace area, particle size, microstructure, and finally the catalytic performance, has been presented for Cu/ZnO catalysts, too.[1,27]

3.6.1 Fundamentals and Apparatus

3.6.1.1 TEM

Using TEM, we look through a piece of material with electron "waves," usually at high magnification. The intensity distribution of the electron waves leaving the specimen can be magnified by an electron optical system and resolutions of ≈ 0,1 nm are attainable. The electrons interact with the material in two ways: inelastic and elastic scattering. Inelastic scattering (leading eventually to absorption) must be avoided since it contains no local information. The electron beam then will be only elastically scattered, i.e. diffracted; the lattice and the present defects modulate amplitude and phase of the primary beam and the diffracted beams locally. The energy of the monochromatic electron beam is somewhere between (100 - 400) keV. The resolution depends on the specimen thickness; high-resolution TEM (HRTEM) demands specimens thickness in the nm region.[29,28]

Here, Transmission electron microscopy was conducted on differently treated catalysts on a Phillips CM 200 FEG TEM with an electron beam of 135 - 470 kV. The first samples were collected directly after the reduction in the feed, while the other times the reaction was stopped after the high temperature treatment (673 K, 2 vol-% H_2) at 523 K, after switching back to MSR conditions and finally after the 2nd O_2 addition (see also Table 3-1). After the reaction the samples were transferred into a glove box to avoid air contact. Prior to the investigation the samples were deposited on holey-carbon films supported on gold grids.

3.6.1.2 SEM

Secondary electrons are produced when an incident electron excites an electron in the sample. The excited electron moves towards the surface of the sample undergoing elastic and inelastic collisions until it reaches the surface, where it can escape if it still has sufficient energy. Their energies are a function of E_o and the surface work function, E_w, which defines the amount of energy needed to remove electrons from the surface of a material. One of the major reasons for coating a non-conductive specimen with a conductive material is to increase the number of secondary electrons that will be emitted from the sample (decrease E_w). The mean free path length of secondary electrons in many materials is approximately 10 Å. Thus, although electrons are generated throughout the region excited by the incident beam, only those electrons that

originate less than 10 Å deep in the sample escape to be detected as secondary electrons. The shallow depth of production makes them very sensitive to topography and, hence they produce a picture of the material surface.[29]

Here, Scanning electron microscopy (SEM) was conducted on an S 4000 FEG microscope (Hitachi). The acceleration voltage was set at 5 kV.

3.7 Infrared Spectroscopy (IR)

IR spectroscopy is a useful tool to investigate the state of solid catalysts, either with probe molecules (e.g. CO, NO) or directly under in situ conditions. The adsorption bands of e.g. CO probe molecules, depend on the substrate metal, its surface structure, and the coverage. Accurate analysis of the band position can for example reveal information on ligand effects between two metals or the surface coverage of the active material.[29] Furthermore, statements about oxidation states are possible.[30] On the other hand, in situ investigations help to understand and locate the chemical reaction, e.g. formation of intermediates.[31,32,33]

3.7.1 Fundamentals and Aparatus

Vibrations in molecules or in solid lattices (e.g. bond stretching, bending of bond angles, torsion vibrations etc.) are excited by the absorption of photons with wavelengths between 1000 and 2.5 μm. Absorption of a photon only occurs if a dipole moment changes (i.e. the distance between the atoms or the charges) during the vibration.[29]

There are several ways to use infrared radiation for analytical applications. Mostly, the experiments are performed in the transmission mode for weakly absorbing bulk materials or by measuring the diffuse reflected radiation (DRIFTS, Diffuse Reflectance Infrared Spectroscopy).

The IR experiments were carried out on a Perkin Elmer S 2000 equipped with a DTGS detector at a spectral resolution of 4 cm^{-1} and accumulation of 32 scans. The samples were pressed into infrared transparent, self-supporting wafers (typically 15 mg/cm^2), which were placed in an in situ infrared cell with CaF_2 windows. The cell was connected to a vacuum system. The activation was performed in situ in the heating zone of the IR cell via two procedures:

(i) For reduction the samples were heated in 2 vol-% H_2 in He (50 ml/min) to 523 K at 6 K/min. The samples were hold at this temperature for 1h. Afterwards the samples were cooled down to RT under vacuum.
(ii) For oxidation the samples were heated in 20 vol-% O_2 in He (50 ml/min) to 523 K at 6 K/min. The samples were hold at this temperature for 30 min. Afterwards the samples were cooled down to RT under vacuum.
For adsorption measurements CO 4.7 (Messer Griesheim) was used. The spectra were recorded at RT while the equilibrium pressure of the probe molecule was increased stepwise. All IR spectra were obtained after subtraction of the background and gas-phase absorption and were normalized to the mass of the sample. Difference spectra represent the difference between spectra of the sample recorded in presence and in absence of CO.
Alternatively, Diffuse reflectance IR (DRIFTS) experiments were performed. Therefore, a Graseby Specac "Selector" attachment with an environmental chamber placed in a Bruker IFS 66 was used. CO was diluted with He to achieve the desired partial pressure and then admitted to the cell for 15 min. Spectra were recorded after purging gas phase CO species from the cell.

3.8 References

1 M.M. Günter, T. Ressler, R.E. Jentoft, B. Bems, J. Catal. **203** (2001) 133

2 B.S. Clausen, L. Gråbæk, H. Topsøe, L.B. Hansen, P. Stoltze, J.K. Nørskov, O.H. Nielsen Top. Catal. **1** (1994) 367

3 B.S. Clausen, H. Topsøe, R. Frahm, Adv. Catal. **42** (1998) 315

4 Manual of Mineralogy, ed. C. Klein, C.S. Hurlbut, Wiley, 1993

5 R. Allmann, Röntgen-Pulverdiffraktometrie, publisher Sven von Loga, 1994

6 Young, The Rietveld Method, Oxford University Press, New York, 1993

7 T. Ressler, S.L. Brock, J. Wong, S.L. Suib, J. Phys. Chem, B **103** (1999) 6407

8 T. Ressler, J. Wong, J. Roos, I.L. Smith, Environ, Sci. Technol. **34** (2000) 950

9 J.J. Rehr, R.C. Albers, Rev. Mod. Phys. **72** (2000) 621

[10] E.A. Stern, in *X-ray absorption*, edited by D.C Koningsberger and R. Prins, Chemical Analysis **92**, editor J.D. Winefordner, I.M. Kolthoff, John Wiley & Sons, New York 1988

[11] G. Bunker, Nucl. Instrum, Methods **207** (1983) 437

[12] B.S. Clausen, J.K. Nørskov, Top. Catal. **10** (2000) 221

[13] D.E. Sayers and B.A. Bunker, in *X-ray absorption*, edited by D.C Koningsberger and R. Prins, Chemical Analysis **92**, editor J.D. Winefordner, I.M. Kolthoff, John Wiley & Sons, New York 1988

[14] Designed by M. Hagelstein, T. Neisius, et al., ESRF, France in a collaborative effort with the Fritz-Haber-Institute, Berlin, Germany

[15] T. Ressler, J. Synch. Radiat. **5** (1998) 118

[16] S.I. Zabinsky, J.J. Rehr, A. Ankudinov, R.C. Albers, M.J. Eller, Phys. Rev. B: Condens. Matter **52** (1995) 2995

[17] T. Ressler, J. Wong, J. Roos, I.L. Smith, Environ. Sci. Technol. **34** (2000) 950

[18] J.J.F. Scholten, J.A. Konvalinka, Trans. Faraday Soc. **65** (1969) 2465

[19] G.C. Chinchen, C.M. Hay, H.D. Vandervell, K.C. Waugh, J. Catal. **103** (1987) 79

[20] J.W. Evans, M.S. Wainwright, A.J. Bridgewater, D.J. Young

[21] O. Hinrichsen, T. Genger, M. Muhler, Chem. Eng.Technol. **23** (2000) 11

[22] A.V. Chadwick, I.J.F. Poplett, D.T.S. Maitland, M.E. Smith, Chem. Mater. **1**0 (1998) 864

[23] B.L. Kniep, T. Ressler, A. Rabis, F. Girgsdies, M. Baenitz, F. Steglich, R. Schlögl, Angew. Chem. **116** (2004) 114

[24] J.P. Hornak, Ph.D., The basics of MRI, 1996-2004, http://www.cis.rit.edu/htbooks/nmr/inside.htm

[25] Clausen, B.S., Schiøtz, J., Gråbæk, L., Ovesen, C.V., Jacobsen, K.W., Nørskov, J. K. Topsøe, H., Top. in Catal. **1**, 367 (1994)

[26] P.L. Hansen, J.B. Wagner, S.Helveg, J.R. Postrup-Nielsen, B.S. Clausen, H. Topsøe, Science **295** (2002) 2053

[27] M.M. Günter, T. Ressler, B. Bems, C. Büscher, T. Genger, O. Hinrichsen, M. Muhler, R. Schlögl, Catal. Lett. **71** (2001) 37

[28] L. Reimer, Transmission Electron Microscopy, Springer Verlag, Berlin Heidelberg 1984

[29] J.W. Niemansverdriet, Spectroscopy in Catalysis, Wiley-VCH, Weinheim 2000

[30] A.N. Pestryakov, A.A. Davydov, Kin. Catal. **37** (1996) 859

[31] K.-D. Jung, A.T. Bell, Journ. Catal. **193** (2000) 207

[32] J. Weigel, C. Fröhlich, A. Baiker, A. Wokaun, Appl. Catal. A: **140** (1996) 29

[33] S. Bailey, G.F. Froment, J.W. Snoeck, K.C. Waugh, Catal. Lett. **30** (1995) 99

4 In situ investigation of structure-activity relationships

4.1 Introduction

The development of an economical and ecological catalyst for the steam reforming of methanol has caused large interest in the research of heterogeneous catalysis and a comprehensive knowledge about the functionality of the catalyst (i.e. structure-activity relationships and surface properties) is an important step to a knowledge based rational catalyst design.

Copper based materials have been extensively studied under MSR and methanol synthesis reaction conditions. However, reaction mechanisms, as well as active phases and structural changes of the catalysts are still under debate, and dependent on the catalyst composition and reaction conditions. In this respect, the positive effect of a large specific copper surface area has been established and confirmed oftentimes. We have previously reported, that the turn-over frequency (TOF) for the methanol synthesis reaction and the methanol steam reforming is correlated to the microstrain in copper in the Cu/ZnO system.[1,2] The microstrain in the copper nanoparticles originates at the Cu-ZnO interface and emphasizes the role of ZnO to disperse and influence the microstructure of the active copper phase. For the MSR reaction we could also show that the increase in activity after a temporary addition of oxygen to methanol and water is correlated with an increase of the disorder in the copper particles.[3]

Reliable structure-activity relationships for copper catalysts in methanol chemistry that are prerequisites for a knowledge-based design of improved catalytic materials remain rare. Here, we report studies on a nanostructured catalyst (*Nano-SA*) prepared by simultaneous precipitation of zirconium dioxide and copper oxide. The complementary bulk techniques in situ X-ray diffraction (XRD) and X-ray absorption spectroscopy (XAS) were employed to elucidate correlations between activity, stability, and structural changes of the Cu/ZrO_2 catalyst obtained under MSR reaction conditions.

4.2 Results

4.2.1 XRD investigation of the precursor and the reduced Cu/ZrO_2 catalyst

The XRD pattern of the calcined CuO/ZrO_2 shows tetragonal ZrO_2 (Figure 4-1a) as the major crystalline phase with a minor contribution of monoclinic ZrO_2 (5 - 8 %). The pattern exhibits no peaks corresponding to a copper oxide phase.

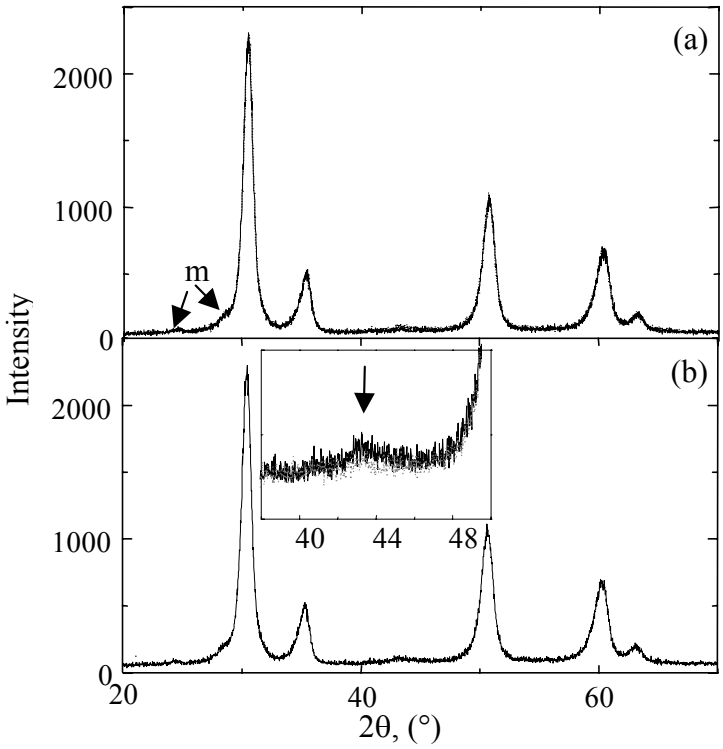

Figure 4-1 XRD patterns of (a) CuO/ZrO_2 precursor and (b) after reduction in 2 vol-% H_2/He. Arrows indicate small peaks of monoclinic zirconium dioxide (m) and copper metal. Inset: precursor (dotted line), reduced Cu/ZrO_2 (solid line).

Measurements with Al_2O_3 as an internal standard yielded a good crystallinity of the sample (> 95 %). The crystallite size of the tetragonal ZrO_2 is about 70 Å as calculated on the basis of the FWHM of the ZrO_2 111 peak. After the reduction of the precursor material (inset in Figure 4-1b) in 2 vol-% H_2/He a small Cu 111 peak is observed (copper crystallite size ~ 20 Å). Exposure to the steam reforming feed or oxygen addition cycles have no significant influence on the diffraction patterns of Cu or CuO, and the zirconia phases.

4.2.2 N_2O decomposition

The specific copper surface area was determined by N_2O decomposition (A) after reduction of the CuO/ZrO_2 material in a quartz glas tube reactor in methanol and water, (B) after temporary addition of oxygen to the feed, (E) after treatment at 673 K in hydrogen, and (F) after a second addition of oxygen to the feed (see also Table 3-1). Although the first oxygen addition yielded a slight decrease in Cu surface area of the Cu/ZrO_2 catalyst, the resulting Cu surface exhibited a higher activity in the steam reforming of methanol. Figure 4-2 shows the corresponding turnover frequencies (TOF). Those were calculated on the basis of the specific copper surface area S_{Cu} (m^2/g_{Cu}) and the corresponding hydrogen production rate (µmol/sec*g_{Cu}) (Table 4-1). The hydrogen production rate and the specific copper surface are were determined after ~ 30 min time on stream when the activity of the Cu/ZrO_2 catalyst had reached a constant level.

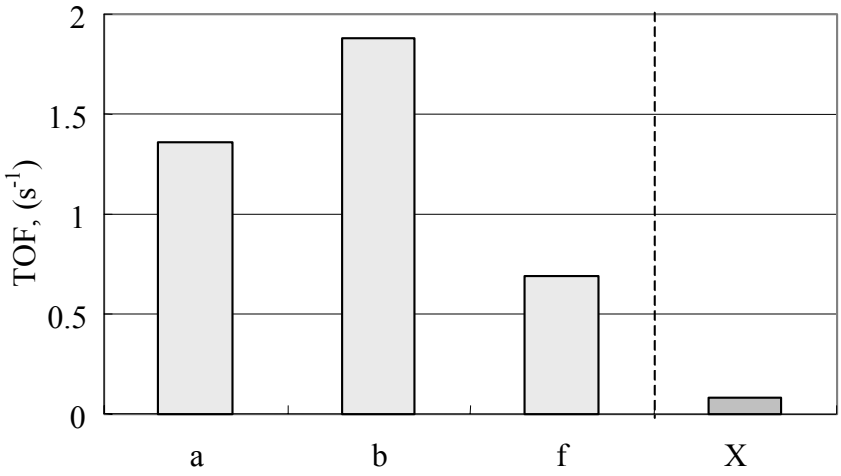

Figure 4-2 Turnover frequencies (based on specific copper surface area per gram copper) for various treatments of the Cu/ZrO_2 catalyst. (a) After initial reduction in methanol and water (feed), (c) after first oxygen addition, and (g) after heating to 673 K in 2 vol-% H_2, switching back to feed at 523 K, and the second addition of oxygen and (X) for comparison, the TOF of the industrial $Cu/ZnO/Al_2O_3$

While the MSR activity exhibited a constant increase after the first addition of oxygen, a spiked increased followed by deactivation was observed after the high temperature treatment and the second addition of oxygen. Based on the crystallite size (XRD) and assuming spherical particles, the volume (ρ_{Cu} = 8.92 g/cm^3) of all copper particles and the corresponding surface area was also determined. Except for the copper surface area after treatment at 673 K and oxygen addition to

the feed, the surface areas based on the XRD crystallite size compare well to those obtained by N_2O decomposition (Table 4-1). For comparison with the results obtained for the Cu/ZrO_2 material, the catalytic performance and the copper surface area of an industrial $Cu/Al_2O_3/ZnO$ catalyst with about 50 weight-% copper were determined under identical conditions. Although this catalyst possesses a higher surface area (32.4 m^2/g_{Cu}) than the Cu/ZrO_2 catalyst (13.2 m^2/g_{Cu}) it exhibits an inferior turnover frequency (Table 4-1).

Table 4-1 Specific copper surface areas calculated on basis of N_2O decomposition measurements or crystallite sizes from in situ XRD investigation and hydrogen production rates (industrial $Cu/ZnO/Al_2O_3$ catalyst, S_{Cu} = 32.4 m^2/g_{Cu}, R_{H2} = 67 µmol/g_{Cu} * s, TOF = 5.1 min^{-1})

Treatment	S_{Cu} (m^2/g_{Cu}) [N_2O]	H_2 production rate (µmol/g_{Cu} * s)	TOF (min^{-1})	S_{Cu} (m^2/g_{Cu}) [XRD]
After reduction in feed at 523 K	13.2	440	82	9.2
After first addition of O_2 after reduction in feed	10.4	480	113	11.5
After high temperature treatment in hydrogen	15.7	42	7	6.7
After second addition of O_2 after high temperature treatment in hydrogen	30.7	470	41	10.6

4.2.3 X-ray absorption spectroscopy

Local structure of the CuO/ZrO_2 precursor

Figure 4-3a shows the Cu K-edge XANES spectra of the CuO/ZrO_2 precursor material and the CuO reference (obtained by calcination of malachite) measured at room temperature.

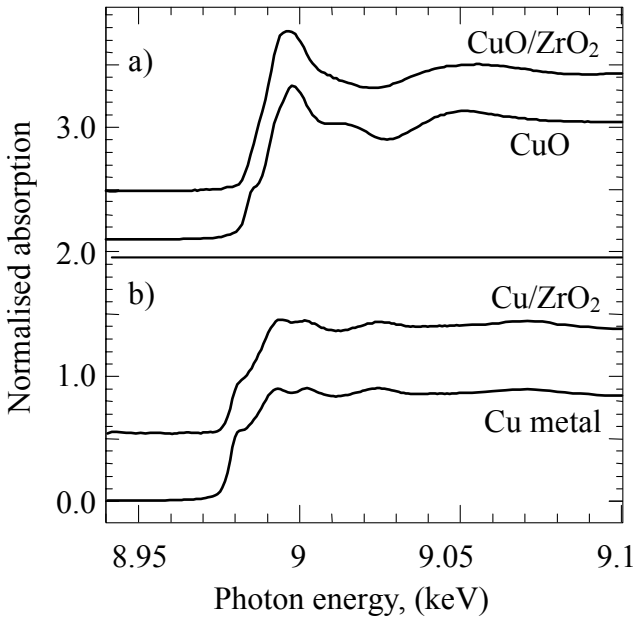

Figure 4-3 Cu K edge XANES spectra of (a) CuO/ZrO_2 precursor together with CuO, (b) Cu/ZrO_2 after reduction in 2 vol-% H_2/He at 523 K together with Cu metal.

Compared to the spectrum of CuO the spectrum of the CuO/ZrO_2 precursor is less structured, i.e. the characteristic pre-edge at 8984 eV and the peaks directly after the absorption edge are less pronounced, probably because of a considerable static disorder or small particle size. The differences in the $FT(\chi(k)*k^3)$ of the catalyst precursor and the CuO reference are clearly visible in Figure 4-4.

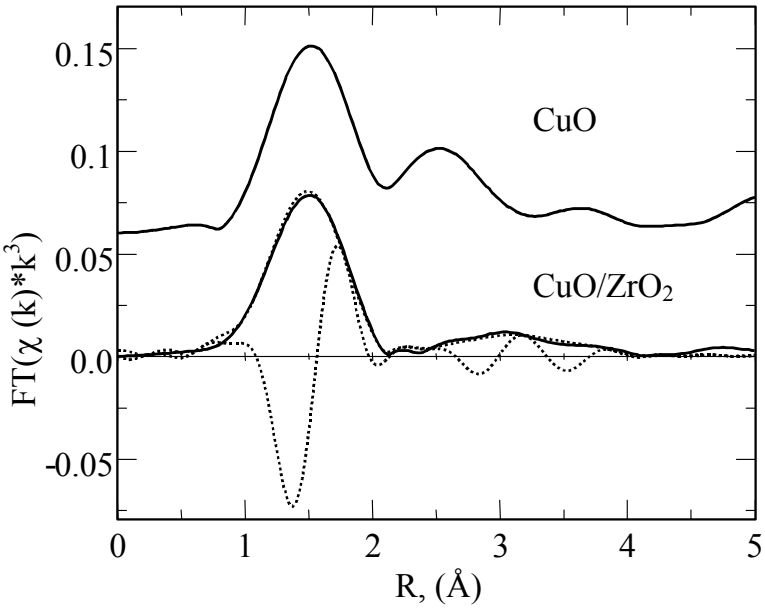

Figure 4-4 Refinement of a theoretical Cu K edge FT(χ(k)*k^3) (dotted line) of CuO to the experimental FT(χ(k)*k^3) of the CuO/ZrO_2 precursor (solid line) together with the experimental FT(χ(k)*k^3) of a CuO reference.

Instead of one high peak representing the second nearest oxygen and copper neighbors in CuO (at distances of 2.8 and 2.9 Å), the FT(χ(k)*k^3) of the CuO/ZrO_2 precursor exhibits two strongly reduced peaks at ~ 3.0 Å. Nevertheless, a theoretical XAFS function of a CuO model structure could be successfully refined to the experimental spectrum of the CuO/ZrO_2 precursor resulting in a good agreement between theory and experiment in the range from 1.0 to 4.0 Å in the FT(χ(k)*k^3) (Figure 4-4). This indicates that disordered CuO is the main copper phase present in the CuO/ZrO_2 precursors.

4.2.3.1 Reduction in 2 % H_2/He

The normalized XANES spectrum of the catalyst at 523 K after reduction in hydrogen is plotted in Figure 4-3b together with that of a reduced copper reference at 523 K (commercial CuO, Merck). The reduced Cu/ZrO_2 catalyst shows edge features similar to that of Cu obtained from the reduction of CuO.

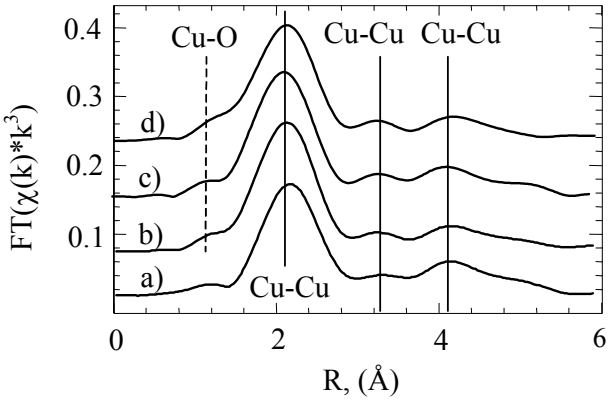

Figure 4-5 FT(χ(k)*k^3) of (a) copper metal, (b) Cu/ZrO_2 after reduction in 2 vol-% H_2/He at 523 K, (c) Cu/ZrO_2 after reduction in 2 vol-% H_2 followed by MSR, and (d) Cu/ZrO_2 after direct reduction in methanol and water (feed).

The characteristic doublet in the post-edge region (8.99 –9.0 keV) is also well resolved.
The FT(χ(k)*k^3) of the Cu/ZrO_2 catalyst (Figure 4-5b) strongly resembles that of the copper reference (Figure 4-5a). Only slight differences can be seen in the shape of the peaks and the small shoulder left of the first Cu-Cu shell of the Cu/ZrO_2 catalyst.

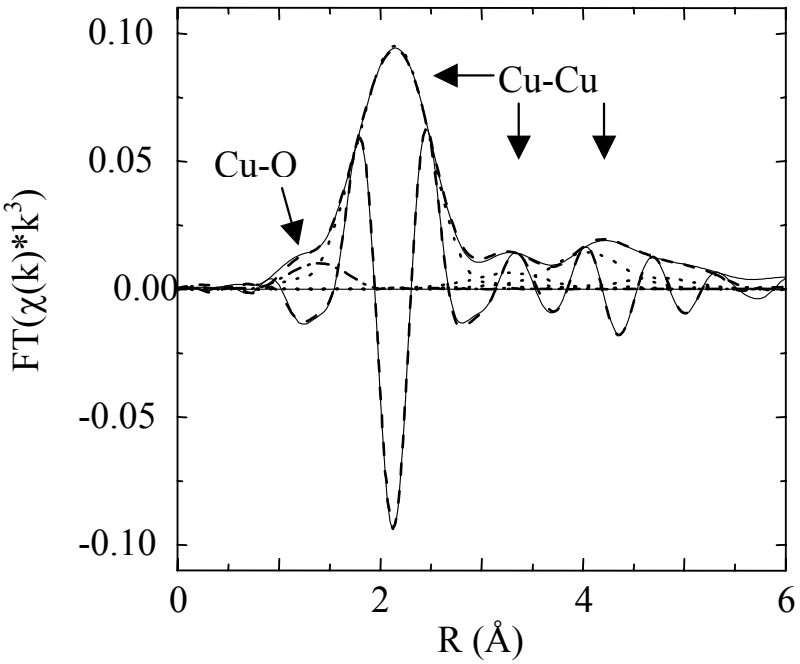

Figure 4-6 Refinement of a theoretical Cu K edge FT(χ(k)*k^3) (dotted line) of copper metal and one additional Cu-O distance to the experimental FT(χ(k)*k^3) of the Cu/ZrO_2 catalyst after reduction in 2 vol-% H_2 at 523 K (solid line).

Figure 4-6 shows the result of a XAFS refinement of a copper model structure with an additional Cu-O distance (R = 1.84 Å) to the experimental FT(χ(k)*k^3) of the Cu/ZrO_2 catalyst after reduction in 2 % H_2 at 523 K. With the addition of the Cu-O nearest neighbor it is possible to simulate the coordination shell, while contribution from higher shells of copper oxide phases are not detectable in the remaining spectrum. In order to corroborate the validity of our approach to analyze the experimental Cu K edge XAFS data of the Cu/ZrO_2 catalyst under reaction conditions, Figure 4-7 shows a simulated FT(χ(k)*k^3) for a mixture of 20 % Cu-O in Cu_2O and 80 % Cu metal at 523 K together with an experimental FT(χ(k)*k^3) of the catalyst after reduction in 2 vol-% H_2/He. The amplitude of the oxygen shoulder and the imaginary part are well reproduced by the simulation, confirming partially oxidized copper clusters as constituents of the activated Cu/ZrO_2 catalyst.

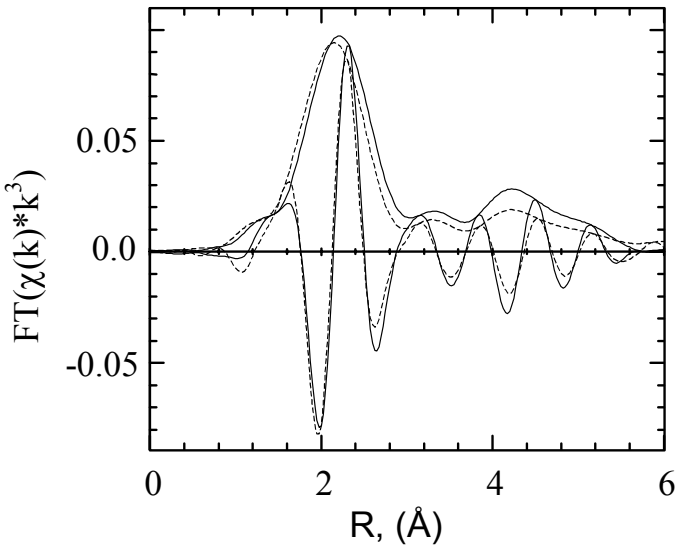

Figure 4-7 Simulated FT(χ (k)*k^3) (solid) for a mixture of 20 % Cu_2O and 80 % Cu in comparison with the experimental FT(χ (k)*k^3) (dashed) of the Cu/ZrO_2 catalyst after reduction in methanol and water at 523 K.

After the reduction in 2 % H_2/He the sample was heated to 523 K in methanol and water and the XAFS spectrum of the Cu/ZrO_2 catalyst in the feed exhibits no significant differences compared to the spectrum in hydrogen (Figure 4-5b, c).

4.2.4 Reduction kinetics

A PC analysis of the XANES spectra of CuO/ZrO_2 measured during reduction in 2 vol-% H_2 showed that three primary components are sufficient to reconstruct the experimental data. The evolution of the abstract concentrations during the reduction in 2 vol-% H_2/He indicates a third component as an intermediate phase (Figure 4-8), probably corresponding to Cu_2O.

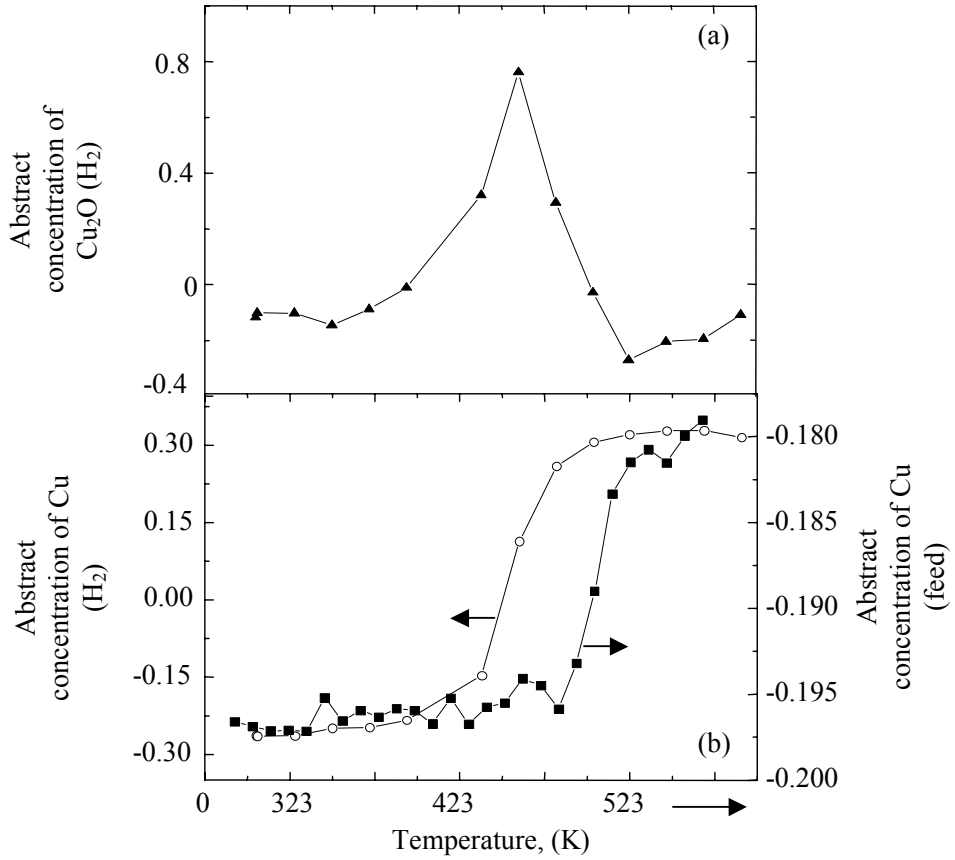

Figure 4-8 Evolution of (a) the abstract concentrations (PCA) of Cu during reduction in 2 vol-% H_2/He and during reduction in methanol and water (feed) and (b) of water and the intermediate Cu_2O phase during reduction in 2 vol-% H_2/He.

Figure 4-8b shows that the reduction in hydrogen started much earlier, than in methanol and water. Peak reduction temperatures (corresponding to the maximum reduction rate, i.e. the inflection point of the sigmoidal trace) were determined to be 461 K and 496 K, respectively.

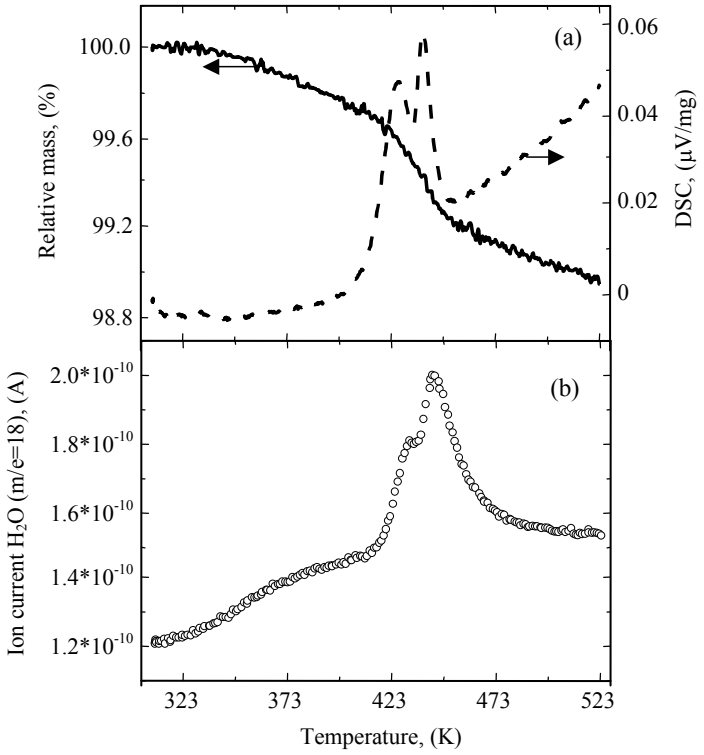

Figure 4-9 (a) Evolution of relative mass and DSC signal during reduction of the CuO/ZrO_2 precursor in 2 vol-% H_2/He to 523 K at 6 K/min and (b) evolution of the corresponding MS signal of water (m/e = 18).

Prior to TG-DSC measurements, the CuO/ZrO_2 sample was heated twice to 523 K in He and held at that temperature for 1 h to remove adsorbed water and CO_2. Subsequently, the catalyst was heated in 2 vol-% H_2/He from 300 K to 523 K at a heating rate of 6 K/min. Two exothermic DSC signals occurring between 423 and 440 K correlate with two peaks in the MS water signal (Figure 4-9). During reduction the sample exhibits a loss of ~0.9 % of its original weight. This is less than calculated for a complete reduction of CuO/ZrO_2 to Cu/ZrO_2 (1.2 %) and corroborates the incomplete reduction detected by in situ XAS.

4.2.5 Steam reforming of methanol

Figure 4-5d depicts the FT(χ(k)*k^3) of the Cu/ZrO_2 catalyst reduced in methanol and water. The position and shape of the first peak, representing the first shell of Cu-Cu nearest neighbors, are very similar to the peak of the sample reduced in hydrogen (Figure 4-5b). The main difference can be seen in the reduced amplitude of the Cu-Cu peak and the increased height of the small

Cu-O shoulder. After reduction in 2 vol-% H_2 the Cu/ZrO_2 catalyst exhibits a low initial activity in the steam reforming of methanol (Figure 4-10).

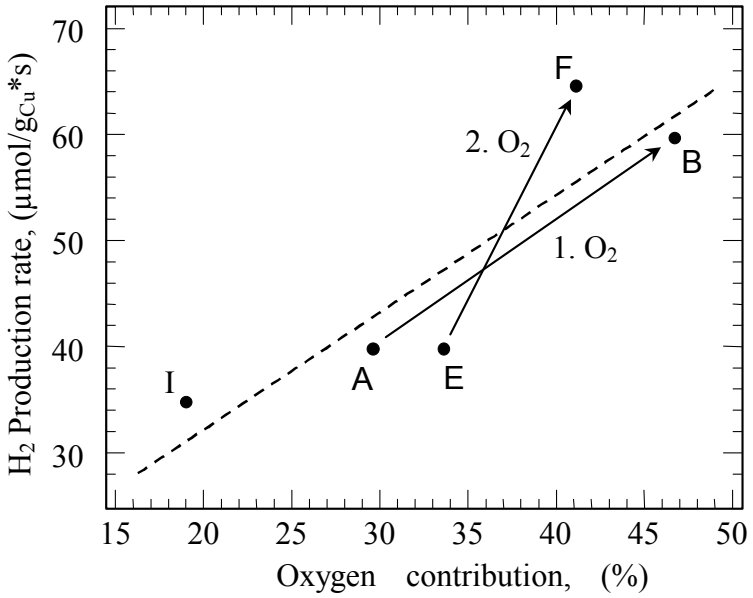

Figure 4-10 Oxygen contribution to the Cu K edge FT(χ (k)*k^3) of the Cu/ZrO_2 catalyst (I) after reduction in 2 vol-% H_2/He at 523 K followed by switching to feed (methanol and water), (A) after reduction in feed, (B) after first addition of oxygen to the feed, (E) after heating to 673 K in 2 vol-% H_2/He and switching to feed, and (F) after second addition of oxygen to the feed together with the corresponding H_2 production rates (not normalized to the specific copper surface area) measured in the XAS in situ cell (Figure 10). The arrows indicate the increase in oxygen contribution and production rate after first (1. O_2) and second (2. O_2) addition of oxygen.

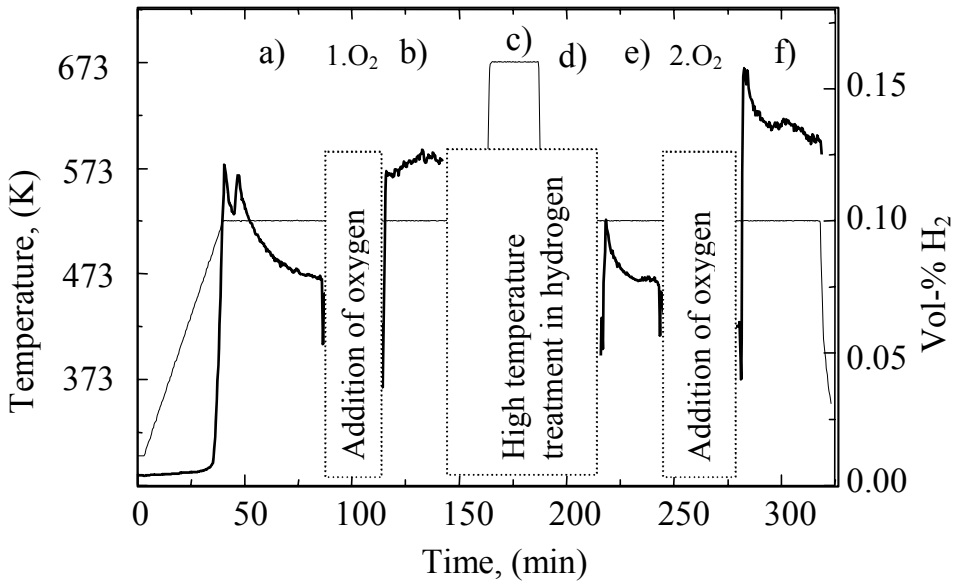

Figure 4-11 Evolution of the H_2 production rate on the Cu/ZrO_2 catalyst (a) methanol steam reforming (MSR feed), (b, f) MSR after temporary addition of 10 vol-% O_2, (c) heating to 673 K in 2 vol-% H_2/He, (e) subsequent feed.

After direct reduction in the feed, however, the Cu/ZrO_2 catalyst possesses a significantly increased activity in the MSR. The $FT(\chi(k)*k^3)$ of the catalyst reduced in the feed exhibits a shoulder (Cu-O peak, left of the first Cu-Cu peak) with a higher amplitude (~ 30 %) (Figure 4-5c, d) compared to that of the catalyst reduced in hydrogen (~ 20 %) (Figure 4-10). After reduction of the Cu/ZrO_2 catalyst in the feed at 523 K the temperature was kept constant until no further changes were observed in the XAFS spectra. After temporary addition of oxygen and partial re-reduction in the feed, the activity of the Cu/ZrO_2 catalyst increased considerably (Figure 4-11). An overview of the structural changes in the copper nanoparticles is given in Figure 4-12, where the $FT(\chi(k)*k^3)$ of the various reaction steps are depicted. It can be seen that the main changes are observable in the amplitude of the $FT(\chi(k)*k^3)$, in particular of the small shoulder (left of the first Cu-Cu peak) and the first Cu-Cu peak.

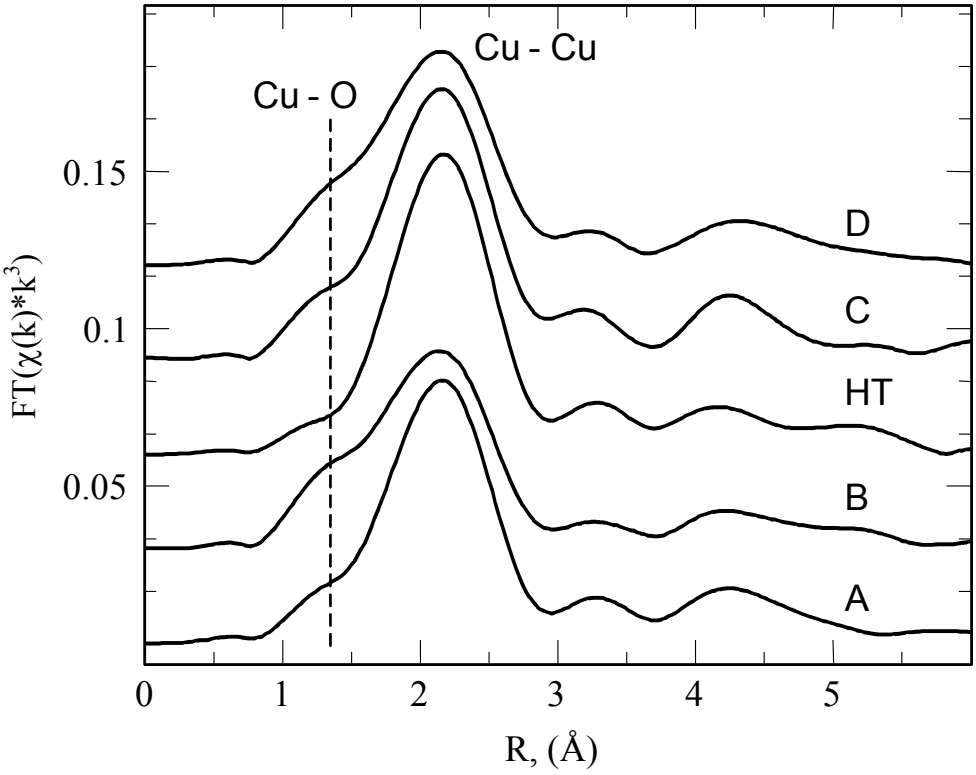

Figure 4-12 Cu K edge FT(χ(k)*k^3) of the Cu/ZrO_2 catalyst measured in situ after various treatments (Figure 10): (A) reduction in methanol and water at 523 K (feed), (B) feed after first temporary addition of oxygen (10 vol-% O_2), (HT) treatment in 2 vol-% H_2 at 673 K, (C) feed after treatment at 673 K, (D) feed after second addition of oxygen.

The corresponding oxygen contribution determined are plotted in Figure 4-10 and indicate that an increasing amount of oxygen remains in the copper particles after oxidation and re-reduction. This incomplete re-reduction is characteristic for the Cu/ZrO_2 system and is in contrast to the reduction characteristics of Cu/ZnO catalysts where no such oxygen contributions were observed.[4,5,6] Figure 4-10 shows that after the first and second addition of oxygen the increase in hydrogen production rate of the Cu/ZrO_2 catalyst (Figure 4-11) correlates with an increasing amount of oxygen.

4.2.6 High temperature treatment of Cu/ZrO_2 in H_2

In order to test the thermal stability of the Cu/ZrO_2 catalyst after MSR and addition of oxygen, the sample was heated in 2 vol-% H_2/He to 673 K (Table 3-1). After cooling down to 523 K in hydrogen, a XAFS analysis of the experimental Cu K edge FT(χ(k)*k^3) revealed complete reduction of the copper phase to copper metal clusters on ZrO_2. The only slightly increased

amplitude of the first Cu-Cu peak in the FT(χ(k)*k^3) excludes major sintering of the Cu particles during the high temperature treatment in hydrogen. Subsequent steam reforming of methanol resulted in similar activities as after initial reduction of the catalyst in the feed (Figure 4-11). The XAFS FT(χ(k)*k^3) measured under MSR reaction conditions after hydrogen treatment exhibits a pronounced contribution of an oxygen nearest neighbor. Moreover, a strong increase in activity could again be achieved by adding oxygen to the feed (Figure 4-11). This in turn resulted in an increase of the amount of oxygen in the copper particles (Figure 4-10, 4-12). The corresponding turnover frequencies (based on the specific copper surface area per gram copper) of the various reaction steps as determined in a quartz reactor are given in Table 4-1. It can also be seen from Table 4-1 that the copper surface area as determined by N_2O decomposition increased considerably after hydrogen treatment at 673 K and addition of oxygen to the feed.

Determination of the copper crystallite size from the Cu 111 XRD line revealed only small changes after the various reaction steps (reduction in the feed, first oxygen addition, heating to 673 K in hydrogen, treatment in the feed, and second oxygen addition). The sizes vary in a range of about 15 % and remain small (~ 20 Å) indicating a good thermal stability of the Cu/ZrO_2 catalyst. Changes in the copper crystallite size should also be detectable in the Debye-Waller factors of the first Cu-Cu shell. In particular, for particles smaller than 70-80 Å, the reduced average number of nearest Cu neighbors results in a decreased amplitude of the FT(χ(k)*k^3).[4] However, for the nanostructured Cu/ZrO_2 catalysts the presence of an additional Cu-O shell and the limited data range render a reliable determination of crystallite size effects from an EXAFS analysis difficult.

4.2.7 Nuclear magnetic resonance (NMR) spectroscopy

Analysis of the width and the profile of ^{63}Cu NMR lines of reduced copper particles permit qualitative conclusions concerning crystallite size and amount of disorder (e.g. microstrain). Similar to X-ray diffraction line broadening, a symmetric and narrow line profile indicates large and ordered crystallites. A decrease in the copper crystallite size results in a symmetric NMR line broadening, while an increase in strain or disorder causes an asymmetric line profile and/or the occurrence of additional NMR lines.[5] This was previously confirmed by our results on Cu/ZnO catalysts, where the existence of microstrain in the copper particles was additionally verified with XRD and XAS.[2] Figure 4-13 shows the ^{63}Cu NMR spectra of the Cu/ZrO_2 catalyst after various reaction steps. Besides differences in the amplitude it can be seen, that the width of the NMR lines varies only slightly as a function of the treatment conditions. In order to quantify

this effect, the areas under the curve left and right of the peak maximum were determined and the ratio calculated.

Table 4-2 Asymmetry of ^{63}Cu NMR lines of Cu/ZrO_2 catalyst measured after various treatment procedures and determined from calculating the ratio of the area under the curve left and right from the line maximum. (a) After direct reduction in the feed at 523 K,(b) after first addition of oxygen, (d) after heating to 673 K in 2-vol% H_2/He, (e) after heating to 673 K in 2 vol-% H_2/He and subsequent treatment in methanol and water at 573 K, and (f) after second addition of oxygen.

	Treatment	Ratio left/right
a	Reduced in feed at 523 K	1.20
b	MSR after 1st addition of O_2	1.01
d	After 2 % H_2 at 673 K	1.07
e	In feed after treatment (c)	1.33
f	MSR after 2nd addition of O_2	1.13

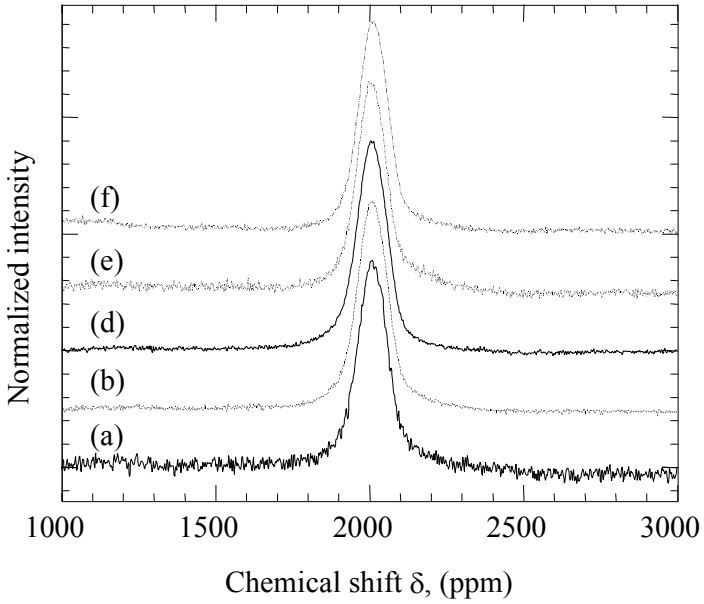

Figure 4-13 ^{63}Cu NMR spectra of the Cu/ZrO_2 catalyst after various reaction steps. (a) After direct reduction in the feed at 523 K, (b) after first addition of oxygen, (d) after heating to 673 K in 2-vol% H_2/He, (e) after heating to 673 K in 2 vol-% H_2/He and subsequent treatment in methanol and water at 573 K, and (f) after second addition of oxygen.

4.3 Discussion

The successful knowledge-based design of new catalysts exhibiting an increased activity, selectivity, and stability is the long-term goal of research in heterogeneous catalysis. Considerable improvements of conventional catalysts can already be achieved by using reliable structure-activity relationships to direct preparation of modified materials even without an all-conclusive picture of the active phase of a heterogeneous catalyst. Our previous studies on Cu/ZnO[4] catalysts revealed that the preparation and the resulting microstructure of the catalyst significantly influence the catalytic properties. It emerges that ZnO is not merely a support for copper clusters but represents an effective participant in the active phase of Cu/ZnO catalysts. ZnO prevents sintering of Cu clusters and modifies the bulk structure of the copper clusters (correlation of microstrain and activity). However, Cu/ZnO catalysts possess a poor stability and unsatisfying selectivity. Hence, new MSR catalysts consisting of nanostructured ZrO_2 as a stable support material for copper particles were investigated. This material exhibits an improved activity and selectivity as was demonstrated before.[3] Here, we present structure-activity relationships for Cu/ZrO_2 catalysts.

4.3.1 Structure of the CuO/ZrO_2 precursor

The combination of small CuO particles and low concentration of Cu in the material (8 %) accounts for the fact, that no copper oxide phases are detected in the XRD pattern of the CuO/ZrO_2 precursor (Figure 4-1). XAS measurements of the precursor material identified CuO as the main copper phase (Figure 4-4). The deviations between the FT(χ(k)*k^3) of the reference CuO and the CuO/ZrO_2 precursor in the amplitude of the higher shells (Figure 4-4) are caused by a strongly disordered structure and/or small crystallite sizes of the nanostructured precursor as indicated by the increased Debye Waller factors compared to those of ideal copper oxide. Okamoto et al. proposed highly dispersed Cu^{2+} in CuO/ZrO_2 to account for the deviations from ideal CuO in the Fourier transformed χ(k).[6] However, a calcination temperature of 973 K used by these authors may have resulted in a considerable incorporation of Cu in ZrO_2 which renders a comparison to the Cu/ZrO_2 material used here difficult. Previously, we reported on the catalytic properties of a nanostructured Cu/ZrO_2 catalyst.[10] For this material also CuO was determined to be the major copper phase exhibiting a similar degree of structural disorder.

Zhou et al. have reported on Cu/ZrO_2 catalysts ($Cu(NO_3)_2$ impregnated onto ZrO_2 calcined at 773 K in oxygen), consisting mostly of tetragonal (*t*) zirconia for copper concentration less than 10 wt-%.[7] They suggested an interaction between copper oxide and the ZrO_2 support that prevents phase transformation to monoclinic ZrO_2 according to the oxygen vacancy model of Sanchez and Gazquez.[8] However, it is not evident that at the reduction and calcinations temperatures used (773 – 1073 K), oxygen vacancies were indeed generated in the ZrO_2 support. Various cations (e.g. Y, Ce, Al, Cu) were also reported to stabilize the tetragonal zirconia phase.[9,10,11] Because no incorporation of Cu into the ZrO_2 lattice was detectable by XRD or EXAFS (complete reduction of Cu at 673 K, detection limit ~ 1 %), a significant stabilizing effect of Cu centers in ZrO_2 can be excluded in agreement with our previous results on nanostructured Cu/ZrO_2 catalysts.[3] Garvie et al.[12,13] and Chraska et al.[14] discussed the influence of the particle size on the stability of the tetragonal phase and found, that for small particles ($r_{critical} \approx$ 9 nm to 30 nm) the stability of the tetragonal phase at room temperature can be explained by the lower surface energy of t-ZrO_2 compared to m-ZrO_2. This may explain the stabilization of the tetragonal ZrO_2 particles with a diameter of about 7 nm in addition to the influence of the copper phase and the particular preparation technique on the surface termination of the ZrO_2 particles. Further support to these assumptions, is given by the fact, that the structure of pure ZrO_2, prepared by the same technique and from the same precursor, is also dominated by the tetragonal modification.[15]

4.3.2 Reduction of the CuO/ZrO_2 precursor

The reduction behavior of the CuO/ZrO_2 precursor was investigated by TG/DSC (Figure 4-9) and XAS. The two DSC signals at 423 K and 440 K may be caused by the reduction of CuO to Cu_2O and Cu_2O to Cu metal, respectively with Cu_2O as an intermediate of the reduction. The PC analysis of the in situ XAFS spectra also shows that the reduction in 2 vol-% H_2/He and methanol/water proceeds via an intermediate phase (Figure 4-8a). Hence, a bimodal particle sizes distribution like that suggested for Cu on Y-doped ZrO_2 [16] with small CuO clusters and bulk CuO that reduce at ~ 423 K and ~ 448 K, respectively, should not be the main source for the DSC/MS signals measured.

The formation of an intermediate Cu_2O phase during the reduction of CuO/ZrO_2 in both hydrogen and methanol/water (feed) is in agreement with our previous results on Cu/ZnO catalysts. The reduction temperatures determined by the PC analysis indicate that the reduction of CuO/ZrO_2 in the feed is shifted to higher temperatures probably because of the oxidizing influence of water and carbon dioxide[3,17] (Figure 4-8). The increased reduction temperature, however, does not seem to result in significantly larger Cu particles. In contrast to the reduction of Cu/ZnO under similar conditions, the reduction of the CuO/ZrO_2 precursor in 2 vol-% H_2/He at 523 K did not result in pure copper metal clusters on ZrO_2 but in a partially oxidized copper phase (Figure 4-6, 8). Similarly, significant amounts of Cu^+ were still detectable at the surface of copper chromia catalysts after reduction in 20 vol-% H_2/He at 553 K.[18] Moreover, Cu^+ species were also detected in Cu/ZnO catalysts after reduction in pure hydrogen at 523 K.[19]

4.3.3 Structure of the activated Cu/ZrO_2 catalyst

In contrast to Cu/ZnO catalysts that appear to reduce completely at 523 K in 2 % H_2, the activated Cu/ZrO_2 catalyst exhibits a lower degree of reduction with a considerable amount of oxygen still detectable in the Cu K edge XAFS data. High temperature treatment of the Cu/ZrO_2 catalyst in hydrogen resulted in a complete reduction of the copper oxide phase to copper metal. Hence, the remaining amount of oxygen in the copper particles after initial reduction in methanol and water or after re-reduction following the addition of oxygen to the feed cannot be ascribed to isolated copper centers in the ZrO_2 or copper oxide particles inaccessible to the gas phase. From the XAFS data of the Cu/ZrO_2 catalyst shown here it is difficult to distinguish between oxygen in the copper particles, a mixture of separated Cu clusters and very small Cu oxide particles, or a copper oxide interface between the Cu clusters and the ZrO_2 support. Because the experimental $FT(\chi(k)*k^3)$ of activated Cu/ZrO_2 catalysts can be well described beyond the first shell by Cu

metal alone, a considerable amount of large or well-crystalline Cu_2O particles can be excluded. Additionally, no isolated copper oxide particles were detected in TEM measurements on a Cu/ZrO_2 sample prepared and activated similarly to the one described here. This seems to corroborate the presence of either oxygen in the copper particles or a copper oxide interface layer.

4.3.4 High temperature treatment of Cu/ZrO_2 in H_2

During reduction in H_2 at 673 K, the Cu/ZrO_2 catalyst exhibited a stable Cu crystallite size with only minor sintering of the Cu particles detectable. Both XAFS measurements at 673 K and 523 K, and XRD measurements at 523K after high temperature treatment showed a similar Cu crystallite size compared to the material prior to heating to 673 K. Conversely, Cu/ZnO catalysts treated at 673 K in hydrogen exhibit strong sintering of the copper particles accompanied by loss of surface area and catalytic activity. This process appears to be irreversible for Cu/ZnO materials, whereas the fully reduced Cu/ZrO_2 catalyst could be re-activated by an oxidation/re-reduction treatment. Hence, the Cu/ZrO_2 catalyst described here possess a considerable stability towards temporarily increasing temperatures which may make it more suitable than the conventional Cu/ZnO materials for use in mobile applications under changing reaction conditions.

4.3.5 Methanol steam reforming on a Cu/ZrO2 catalyst

A linear correlation between the specific copper surface area of a catalyst and methanol synthesis activity has already been proposed by Chinchen et al.[22] However, it has been realized recently, that additional factors influence the activity of copper catalysts and deviations in the microstructure of the catalysts may result in differently active copper surfaces. Kurtz et al.[17], for instance, tested various groups of copper catalysts in methanol synthesis. They found that the methanol production increases only in a first-order approximation with an increasing copper surface area requiring additional parameters to describe the activity correlations obtained.

Similar to our results on Cu/ZnO catalysts,[1,2,3] the MSR activity of the Cu/ZrO_2 catalyst described here (Table 1) exhibits no simple linear correlation with the specific Cu surface area. A sufficient copper surface area is a prerequisite for an active methanol catalyst, however, it cannot account for the differences observed after the various oxidation/reduction treatments (Table 4-1). While after the first addition of oxygen to the MSR feed the detectable Cu surface

area decreased, the corresponding H_2 production rate increased indicating a more active specific copper surface (i.e. higher TOF). Conversely, after high temperature reduction and addition of oxygen to the feed the Cu surface area increased considerably accompanied by a constant H_2 production rate. This corresponds to a less active specific Cu surface (i.e. a lower TOF) after the second addition of oxygen possibly because of a deteriorated interaction between the Cu metal and ZrO_2 support, and an increased amount of smaller but less active copper particles. It seems that also in the Cu/ZrO_2 systems additional microstructural parameters need to be considered to account for differently active specific Cu surfaces observed.

In contrast to our previous reports on the correlation of microstrain and activity of Cu/ZnO catalysts,[1,2] ^{63}Cu NMR spectroscopy studies on differently treated Cu/ZrO_2 catalysts yielded nearly symmetric NMR lines (Figure 4-13) independent on the treatment conditions. This is indicative of only minor amounts of microstrain in the copper phase in the Cu/ZrO_2 materials. Moreover, it seems that the varying amount of oxygen in the copper phase dependent on the treatment conditions has very little effect on the degree of strain detectable in the copper particles. The characteristic interaction between Cu and ZnO in the conventional Cu/ZnO catalysts (i.e. the epitaxial relationship between Cu and ZnO at the interface) is the most likely origin for the microstrain in the copper phase of these materials. Apparently, Cu on ZrO_2 exhibits a different metal support interaction which does not result in detectable strain in the copper particles.

Despite the absence of microstrain in the copper particles, analysis of the XAFS data of the activated Cu/ZrO_2 catalysts under MSR reaction conditions revealed that the Cu K edge spectra could not be simulated by assuming pure copper metal (Figure 4-5, Figure 4-10). A considerable amount of oxygen in the copper particles had to be assumed to obtain a satisfying fit of the corresponding theoretical XAFS function to the experimental spectra. The Cu/ZrO_2 catalyst reduced in hydrogen exhibited little initial catalytic activity. Under methanol steam reforming conditions, temporarily adding oxygen to the feed before or after the high temperature reduction resulted in an increased catalytic activity (Figure 4-10, Figure 4-11) accompanied by an increased amount of oxygen in the copper particles.

For Cu/ZnO catalysts it was also found that addition of oxygen results in an increase in copper crystallite size and, thus, a decrease in specific copper surface area.[3] After addition of oxygen, the Cu/ZnO catalysts re-reduced completely in the feed and an increased catalytic activity was obtained correlating with an increased degree of microstrain in the copper particles. In contrast to Cu/ZnO, the increased amount of oxygen remaining in the copper particles after oxygen addition to the feed is indicative of an incomplete re-reduction of Cu/ZrO_2. A comparable correlation

between activity and oxidation of copper has been reported for Cu/Al_2O_3 and Cu/ZnO catalysts, where the activity was suggested to result from a partial re-oxidation of copper metal to Cu_2O after a certain activation time in the MSR feed.[20] Chinchen et al.[21] observed similar results for $CuO/ZnO/Al_2O_3$ catalysts in the methanol synthesis reaction. Cheng et al.[9] correlated the MSR activity of copper on an oxygen ion conducting yttria-ceria-alumina support with the availability of sites for the adsorption of mobile oxygen and, hence, enhanced oxidation of Cu to Cu^+. For the catalyst investigated here such an interaction is not evident, nevertheless it is possible that oxygen stored at the surface of the ZrO_2 support stabilizes partially oxidized copper clusters or a copper oxide interface layer.

The lower reducibility of Cu/ZrO_2 and the small degree of microstrain in the copper particles strongly suggest a different metal support interaction between Cu and ZrO_2 compared to Cu and ZnO. Apparently, the defective microstructure of the Cu/ZrO_2 catalyst under reaction conditions considerably influences the catalytic activity and results in differently active specific copper surfaces depending on the treatment conditions. For the nanostructured Cu/ZrO_2 catalyst studied here it is proposed, that the incomplete re-reduction after temporary addition of oxygen to the feed, increases the effect of the oxidized copper bulk structure on the electronic structure of copper sites at the surface. Hence, the increase in reactivity observed after the addition of oxygen may be correlated to a change in the filling of the copper d-band and, resulting from that, changes in adsorption or dissociation energies. A comparable influence on the electronic Cu surface structure is ascribed to the microstrain in the more Cu/ZnO catalysts indicating that both effects may be complementary in modifying the catalytic activity of copper in methanol chemistry.

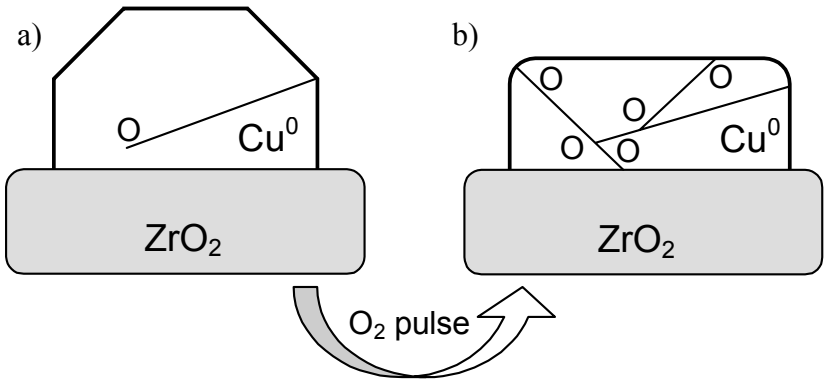

Figure 4-14 Schematic representation of a copper particle on a ZrO_2 support in a Cu/ZrO_2 catalyst (a) after initial reduction in hydrogen and (b) after temporary addition of oxygen to the methanol steam reforming feed. The increased catalytic activity after the oxygen pulse correlates with a transition from an ideal copper particle (a) to more disordered non-equilibrium copper particle containing an increased amount of oxygen that stabilizes the particularly active copper microstructure (b).

A schematic representation of a nanostructured copper particle on a ZrO_2 support in a Cu/ZrO_2 catalyst for the steam reforming of methanol is depicted in Figure 4-14: (a) after initial reduction in hydrogen and (b) after temporary addition of oxygen to the methanol steam reforming feed. The increased catalytic activity after the oxygen pulse correlates with a transition from an ideal copper particle (Figure 4-14a) to a more disordered non-equilibrium copper particle containing an increased amount of oxygen that results from an incomplete re-reduction after the addition of oxygen (Figure 4-14b). The oxygen in the copper particles stabilizes the particular copper microstructure, which exposes a modified surface that is more active in the steam reforming of methanol. Apparently, the role of oxygen in the Cu/ZrO_2 catalyst is related to the close interaction of copper and ZnO in the highly active Cu/ZnO catalyst.

4.4 Conclusion

In situ bulk structural investigations of a nanostructured Cu/ZrO_2 catalyst under methanol steam reforming conditions were performed to reveal structure-activity relationships. The major long-range ordered phase in Cu/ZrO_2 corresponds to tetragonal zirconium dioxide, with only minor amounts of monoclinic ZrO_2 present. Because no incorporation of copper in the ZrO_2 lattice was detectable, the stability of the t-ZrO_2 is attributed to the small crystallite size. Small and disordered CuO particles were identified as the main copper phase present in the precursors.

Reduction of the Cu/ZrO_2 catalyst in the feed or re-reduction after oxidation resulted in supported nanoparticles with an increased amount of oxygen in the copper particles. The increased activity of the Cu/ZrO_2 catalyst after oxidative treatment can be correlated to the increasing amount of oxygen in the copper particles. Furthermore, after extended time on stream and treatment at elevated temperatures (673 K), no significant sintering of the copper particles or deactivation of the catalysts was detected indicating a superior stability of the material. In contrast to conventional Cu/ZnO catalysts, only a minor degree of microstrain is detected in the active copper phase of Cu/ZrO_2 catalysts. The decreased reducibility of CuO/ZrO_2, the low degree of microstrain, and the correlation between the amount of oxygen remaining in the copper particles and catalytic activity indicate a different metal support interaction compared to Cu/ZnO catalysts. Similar to Cu/ZnO catalysts, however, the interaction between Cu and ZrO_2 stabilizes an active copper microstructure that strongly deviates from bulk copper metal.

4.5 References

[1] M.M. Günter, T. Ressler, B. Bems, C. Buscher, T. Genger, O. Hinrichsen, M. Muhler, R. Schlögl, Catal. Lett. **71** (2001) 37

[2] B.L. Kniep, T. Ressler, A. Rabis, F. Girgsdies, M. Baenitz, F. Steglich, R. Schlögl, Angew. Chem. **116** (2004) 114

[3] M.M. Günter, T. Ressler, R.E. Jentoft, B. Bems, J. Catal. **203** (2001) 133

[4] B.S. Clausen, L. Grabek, H. Topsoe, L.B. Hansen, P. Stoltze, J.K. Norskow, O.H. Nielsen, J. Catal. **141** (1993) 368

[5] A.V. Chadwick, I.J.F. Poplett, D.T.S. Maitland, M.E. Smith, Chem. Mater. **10** (1998) 864

[6] Y. Okamoto, H. Gotoh, H. Aritani, T. Tananka, S. Yoshida, J. Chem. Soc., Faraday Trans. **93** (1997) 3879

[7] R-x. Zhou, T-m. Yu, X-y. Jiang, F. Chen, X-m. Zheng, Appl. Surf. Sci. **148** (1999) 263

[8] M.G. Sanchez, J.L. Gazquez, J. Catal. **10**4 (1987) 120

[9] W-H. Cheng, I. Chen, J-s. Liou, S.-S. Lin, Top. Catal. **22** (2003) 225

[10] M.K. Dongare, V. Ramaswamy, C.S. Gopinath, A.V. Ramasamy, S. Scheurell, M. Brueckner, E. Kemnitz, J. Catal. **199** (2001) 209

[11] M.M. Cervera, M. Escobar, M.C. Caracche, P.C. Rivas, A.M. Rodriguez, Hyperfine Interact. **120/121** (1999) 469

[12] R.C. Garvie, J. Phys. Chem. **82** (1978) 218

[13] R.C. Garvie, J. Phys. Chem. **6**9 (1965) 1238

[14] T. Chraska, A.H. King, C.C. Berndt, Mater. Sci. Eng. A **286** (2000) 169

[15] Y. Wang, R.A. Caruso, J. Mater. Chem. **12** (2002) 1442

[16] L. Kundakovic, M. Flytzani-Stephanopoulos, Appl. Catal. **171** (1998) 13.

[17] R.O. Idem, N.N. Bakhshi, Indian J. Eng. Chem. Res. **33** (1994) 2065

[18] G.R. Apai, J.R. Monnier, M.J. Hanrahan, J. Chem. Soc., Chem. Com. **212** (1984) 212

[19] Y. Okamoto, K. Fukino, T. Imanaka, S. Teranishi, J. Phys. Chem. **87** (1983) 1747

[20] K. Klier, V. Chatikavanij, R.G. Herman, G.W. Simmons, J. Catal. **74** (1982) 343

[21] G.C. Chinchen, K.C. Waugh, J. Catal. **97** (1986) 280

5 The influence of preparation on structure and activity

5.1 Introduction

Diverse catalyst properties have been proposed to determine the catalytic activity of copper based materials. On the one hand, the positive effect of a large specific copper surface area has been established and confirmed oftentimes.[1,2,3] On the other hand, we reported on the correlation between microstructural defects in copper particles supported on zinc oxide and the catalytic performance of methanol synthesis and methanol steam reforming (MSR).[4,5] Other authors have proposed that the methanol synthesis activity of Cu/ZnO catalysts is influenced by the morphology and the structural disorder of the copper particles, or by incorporation of copper into ZnO.[6,7,8]

Once, the role of structural parameters of the active phase for catalysis has been identified, the way leads back to the question, how the synthesis method (e.g. co-precipitation, impregnation), the choice of the precursor material and the oftentimes numerous preparation steps (e.g. aging, washing, calcination) influence the final active catalyst. Recently, we presented the impact of precursor aging on the bulk microstructure and consequently on the methanol steam reforming activity for Cu/ZnO catalysts.[9] This work has shown, that certain preparation steps are important tools to stabilize catalytically relevant states. In the last time we investigated a novel binary Cu/ZrO_2 catalyst in the steam reforming of methanol (MSR) reaction. In comparison with a commercial $Cu/ZnO/Al_2O_3$ catalyst it was shown, that the novel zirconia supported catalyst is more active, produces less CO and is more stable during long time on stream.[10]

In this respect, the influence of the preparation technique and the choice of the precursors for copper and zirconium dioxide, on the bulk structure of the catalyst and hence on the catalytic activity is an important question. Here, we report on Cu/ZrO_2 nanostructured catalysts prepared by various precipitation and templating techniques and with different copper contents. Basing on our previous results, this study discusses the influence of the preparation on the general structure (morphologies, modifications, crystallinities, surface properties) of copper and zirconium dioxide and on microstructure-activity correlations for these different Cu/ZrO_2 catalysts.

5.2 Experimental

5.2.1 Catalysts

The investigated Cu/ZrO_2 catalysts can be divided into three groups.

First Cu/ZrO_2 nanopowders were synthesized via a precipitation method. The procedure for the sample *Nano-SA* refers to a so-called *short-aging* method, where both precursors (zirconium tetrapropylate and copper nitrate) were present during the precipitation. For the samples denoted as *Nano-LA-1* and *Nano-LA-2* a *long-aging* preparation was used. The calcination was carried out at 773 K for 12 h under air. This leads to a structure, where the support is mainly located in the center and the copper covers the surface of the particles.

Secondly, mesoporous zirconia was synthesized by a templating procedure, using the copolymer $EO_{20}PO_{70}EO_{20}$ (Polyethyleneglycol-Polypropyleneglycol, Pluronic P123, Aldrich) The introduction of CuO into the mesoporous ZrO_2 network was achieved via two methods. One was the chemisorption-hydrolysis or so called *post support formation* method (sample *Meso-post*). Alternatively the CuO was introduced before the support formed (sample *Meso-pre*).

Third, macroporous ZrO_2 was prepared from a polymer gel template.[11] The template was impregnated with a solution containing both precursors (sample *Macro*).

The characteristics of the catalysts are listed in Table 2-1.

5.2.2 Steam reforming of methanol in a three channel parallel reactor

The measurements of the catalytic activity for the MSR and investigation of the long-term stability were performed at atmospheric pressure and 523 K in a 3-channel tubular stainless steel reactor (10 mm i.d.), which is described in more detail in ([10,12]). The powdered catalysts were diluted with five times its weight of boron nitride (BN) and pressed at 200 bar three times each 5 minutes. The tablet was then crushed and sieved to obtain a defined particle size (0.71 – 1.0 mm). This ensured a plug-flow behaviour and reproducible conditions for all catalysts. The reactants, water, and methanol (from Roth) were introduced into the reactor in a molar ratio of 1 and at a liquid flow rate of 0.07 ml/min (by means of an HPLC pump). For oxidation/reduction treatments oxygen (50 ml/min) was added for 5 min to the reactant mixture. Helium (from Messer Griesheim) was used as a carrier gas. Unreacted water and methanol were separated from

the non-condensable product gases (CO_2, CO and H_2) by a series of cold traps. Gas chromatography was used to quantitatively analyze the remained reactants (methanol and water) and the products. From these data the methanol conversion and the CO production were determined and compared with an industrial $Cu/ZnO/Al_2O_3$ catalyst (from Südchemie, approximately 50 wt-% Cu).

5.3 Results

5.3.1 Catalysis tests in a three channel parallel reactor

5.3.1.1 Activation behavior

Except for *Nano-LA-1* and *Macro*[10], the activity of the catalysts is increasing during the first 70 hours of time on stream.

Figure 5-1 shows the conversion of methanol for catalyst *Nano-LA-1* and catalyst *Meso-pre* as a function of time on stream. Both catalysts clearly show different activation behavior. The initial activity of *Meso-pre* was significant lower than for *Nano-LA-1*, although the copper surface area of the both catalysts is almost the same ($A_{Meso\text{-}pre}$= 0,15; $A_{LA\text{-}1}$= 0,14 m^2/g_{cat}).

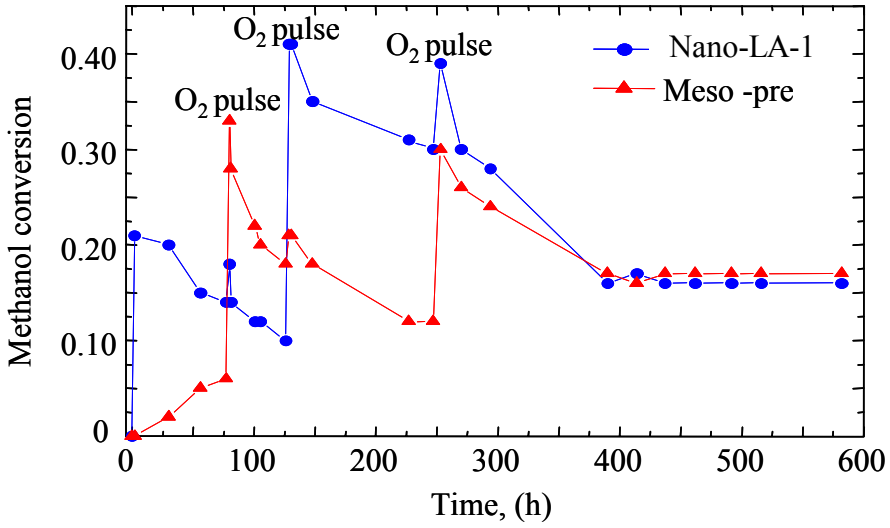

Figure 5-1 Conversion of methanol for Cu/ZrO_2 catalyst Meso-pre and Nano-LA-1 as a function of time on stream.

Whereas the activity of catalyst *Meso-pre* increased monotonically (from 0 to 6 %), the activity of catalyst *Nano-LA-1* decreased (from 21 % to 14 %). In order to activate the catalysts through the redox treatment, oxygen (50 ml/min, 5 min) was introduced to the feed.[10] After the first

addition of O_2, the activity of both catalysts increased shortly, but only the conversion from *Meso-pre* stayed at a higher level (higher also as *Nano-LA-1*) for a longer time. The second addition of oxygen caused a significant increase in the activity for sample *Nano-LA-1*. The third introduction of oxygen caused only minor changes for the activity of sample *Nano-LA-1*, whereas *Meso-pre* could be activated again significantly. The activity of the two catalysts decreased with time on stream and reached the same conversion of methanol, 125 h after the last addition of O_2. Afterwards, the activities of the two catalysts were found constant for about 200 h on stream.

Figure 5-2 shows the activation behavior of the samples *Nano-SA*, *Meso-post* and *Nano-LA-2*. The initial activity of the catalysts decreased in the order *Nano-SA* > *Nano-LA-2* > *Meso-post* and slowly increased during 200 h on stream. After constant conversions were reached, addition of oxygen to the feed resulted in a significant increase in activity. Although the catalysts slightly deactivated after the oxidation treatment, higher activities than before the oxygen addition were observed for *Nano-LA-2* and *Meso-post*. Conversely, oxidation treatment showed little influence on the methanol conversion of *Nano-SA*.

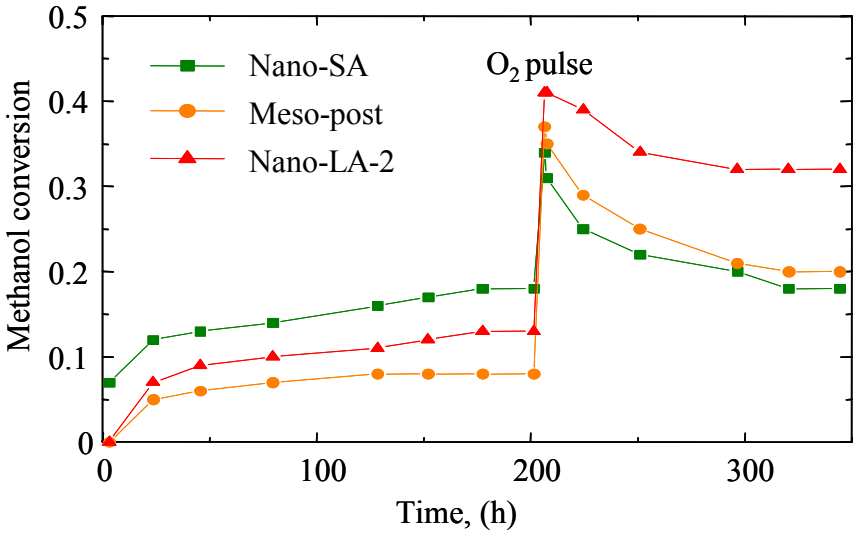

Figure 5-2 Conversion of methanol for catalyst Cu/ZrO_2 Nano-SA, Meso-post and Nano-LA-2 as a function of time on stream.

The study of the activation behavior of the catalyst *Macro* has been published recently.[10] For this catalyst a similar behavior was observed and it seems that the necessary time intervals between "successful" oxygen treatments increase continuously. The last oxygen addition, applied about 200 h after the previous (very effective) addition, resulted in no further improvement.

5.3.1.2 Specific copper surface area and activity

The specific copper surface area per gram copper was determined by N_2O decomposition on fresh and used catalysts (Table 5-1). The copper surface area of the used catalysts is higher than that of the fresh catalysts with the exception of *Meso-post*. The specific copper surface area per gram copper was determined by N_2O decomposition on fresh and used catalysts.

Table 5-1 Specific copper surface area of Cu/ZrO_2 catalysts determined by N_2O-decompostion for fresh and used catalysts.

	S_{Cu}, fresh		S_{Cu}, used		TOF*
Sample	(m^2/g_{cat})	(m^2/g_{Cu})	(m^2/g_{cat})	(m^2/g_{Cu})	(m^{-2})
Nano-SA	0.63	13.2	1.69	35.3	0.824
Nano-LA-1	0.14	2.8	1.79	36.1	0.732
Nano-LA-2	1.59	13.9	3.43	30	0.741
Meso-pre	0.15	2.9	1.26	24.5	1.106
Meso-post	0.77	25.4	0.77	25.4	1.915
Macro	0.18	2.1	0.71	8.4	2.654

* calculated on basis of S_{Cu} after reaction

The activity of the catalysts as a function of the copper surface area (measured at the end of the experiments, i.e. after approximately 350 to 600 h time on stream) is shown in Figure 5-3. No linear correlation between activity and copper surface area can be found.

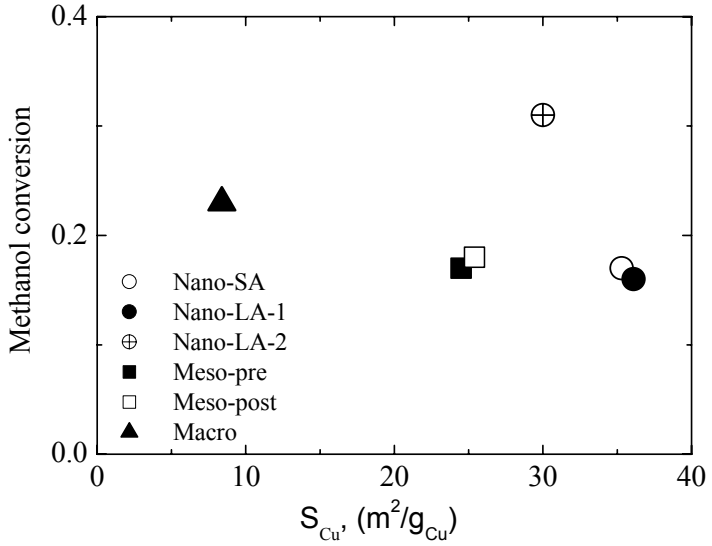

Figure 5-3 Activity of the Cu/ZrO_2 catalysts as a function of the copper surface area (measured at the end of the experiment).

5.3.1.3 CO formation

Selectivity and amount of CO produced are important issues concerning fuel cell application. CO formation was determined at different temperatures and methanol conversion and compared to a commercial $Cu/ZnO/Al_2O_3$ catalyst (Figure 5-4). As reported in our early work,[12] the CO concentration of the MSR process increases with the increase of the reaction temperature. The results reveal, that although the Cu/ZrO_2 catalysts were measured at a temperature higher than the reaction temperature (> 543 K), they produced less CO than the commercial $Cu/ZnO/Al_2O_3$ catalyst, even over a wide range of methanol conversion (from 0.45 to 0.94). The difference becomes significant at conversion higher than 0.5.

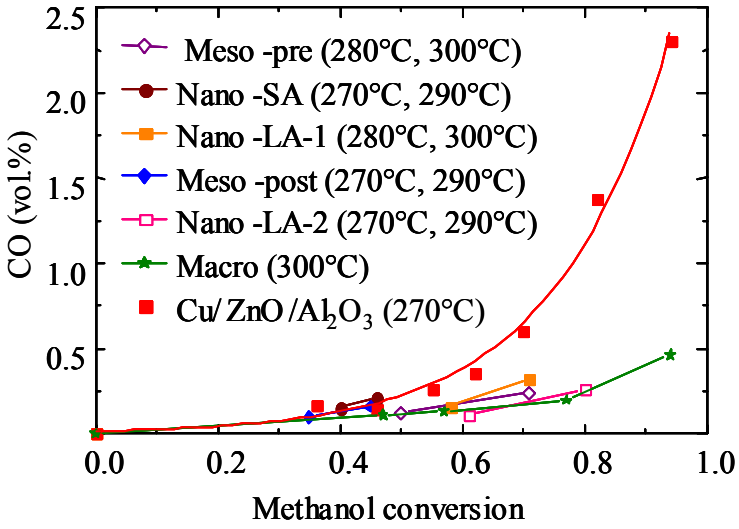

Figure 5-4 CO formation over Cu/ZrO_2 catalysts in comparison with a commercial $Cu/ZnO/Al_2O_3$ catalyst

5.3.2 XRD investigation of the precursors and the reduced material

From Figure 5-5 it can be seen, that the tetragonal modification of ZrO_2 is the dominant crystalline phase in all calcined samples. The XRD patterns of *Nano-LA-1* and *Macro* show minor contributions of monoclinic zirconia (~ 5-10 weight-%), similar to the nanostructured catalyst that we reported on in chapter 4. Apparently, the variation of the copper content in the *Nano-long-aging* preparation route influences the ratio of tetragonal to monoclinic zirconia modification. The sample with less copper (*Nano-LA-1*) contains a larger fraction of m-ZrO_2. Similar results were observed for the *Nano-SA* preparation route [chapter 6 and Ref. 13]. A small peak in the XRD pattern attributable to CuO can be seen for the samples *Nano-LA-2* and *Macro* with the highest copper contents (see *ins*et of Figure 5-5).

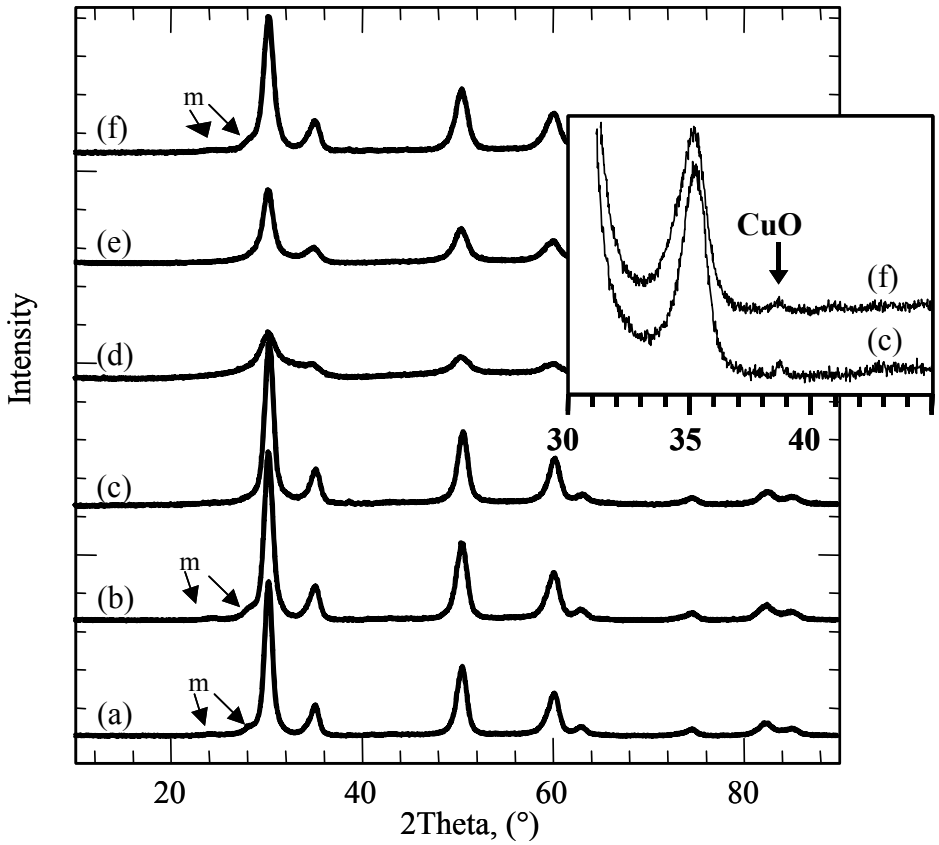

Figure 5-5 XRD patterns of calcined CuO/ZrO_2; (a) Nano-SA, (b) Nano-LA-1, (c) Nano-LA-2, (d) Meso-pre, (e) Meso-post, (f) Macro. Arrows mark small peaks of monoclinic zirconia (m). The inset shows the enlarged CuO peaks.

From the absolute XRD intensities, which should be roughly comparable between samples even without internal standard, it becomes apparent that the samples vary in crystallinity. Compared to the nanostructured samples, the mesoporous catalysts (Figure 5-5d,e) seem to contain a significant fraction of X-ray amorphous material (with domain sizes smaller than 20 Å). The crystallite size of the zirconia, calculated on the basis of the full width at half maximum of the ZrO_2 111 peak lies between 40-70 Å for the nanostructured and macroporous catalysts.

After the reduction of the precursor material in 2 vol-% H_2/He for 30 min, the Cu 111 peak was discernible in the XRD pattern of *Nano-LA-2* and *Macro* in addition to *Nano-SA*. Hence, changes of the copper crystallite size during the various treatments (see Table 3-1) can only be reliably determined for the samples *Nano-LA-2* and *Macro*, where the copper content is high enough to give significant high peaks in the XRD patterns. The overall changes lie in a range of 10 to 25 Å. *Nano-LA-2* was very sensitive to the applied conditions and an increase of the copper crystallite size of ~ 23 Å after temporary addition of oxygen and heating to 673 K in 2 vol-% H_2/He was observed.

5.3.3 Surface area determined with BET and N_2O decomposition

The BET surface areas of the CuO/ZrO_2 samples are listed in (Table 2-1). Except for *Nano-SA* (72 m^2/g) and *Macro* (67 m^2/g) the catalysts have surface areas higher then 100 m^2/g. Despite the same precursors and calcination conditions for all nanopowder samples, the *long-aging* preparation route results in larger surface areas then the *short-aging* preparation route. The impregnation of a calcined support (*Meso-post*) with a $[Cu(NH_3)_4]^{2+}$ solution resulted in the largest surface area. Complete isotherms were measured to evaluate the pore structure of the macroporous, mesoporous, and nanostructured catalysts. Analysis of the adsorption/desorption isotherms (type IV/H 3) for the nanopowders revealed a broad pore size distribution. The preparation route using a copolymer resulted in a fairly stable mesoporous network (type IV/H 4) with a narrow pore size distribution around 3 - 4 nm (Barrett-Joyner-Halenda analysis[14]) in addition to bulk ZrO_2 material. However, for the sample *Macro* it was found, that no stable macroporous network was generated during the preparation. The XRD measurements detected mainly crystalline ZrO_2 material in the nanopowders and the macroporous catalyst and support these results.

According to Table 3-1 the specific copper surface area was investigated after various reaction steps. After reduction in the feed and normalizing the specific copper surface area to the copper content, three groups can be distinguished for the Cu/ZrO_2 catalysts (Table 5-2). Small copper surface areas (~ 2 - 3 m^2/g_{Cu}) were detected for the samples *Meso-pre*, *Nano-LA-1* and *Macro,* although the macroporous sample has twice as much copper as the other two catalysts. The *Nano-SA* and the *Nano-LA-2* have six times larger copper surface areas (13 – 14 m^2/g_{Cu}), but again the *Nano-LA-2* consists of much more copper than the *Nano-SA*. The largest copper surface area is found with the *Meso-post* sample, that has the lowest copper content at all.

Table 5-2 Specific copper surface areas per gram copper (S_{Cu} (m^2/g_{Cu})) of the Cu/ZrO_2 catalysts after various reaction steps

Sample name	S_{Cu} (m^2/g_{Cu}) H_2red	S_{Cu} (m^2/g_{Cu}) feed red	S_{Cu} (m^2/g_{Cu}) 1. O_2 add	S_{Cu} (m^2/g_{Cu}) post $H_2$400	S_{Cu} (m^2/g_{Cu}) 2. O_2 add
Nano-SA	-	13.2	10.4	15.7	30.7
Nano-LA-1	-	2.8	-	-	-
Nano-LA-2	7.4	13.9	5.9	-	-
Meso-pre	-	2.9	9.3	-	-
Meso-post	10.2	25.4	29.7	63.7	66.6
Macro	-	2.1	3.6	1,3	1,7

The influence of the temporary addition of oxygen on the specific copper surface area during the steam reforming of methanol was also investigated. A significant increase in the surface area due to the temporary addition of oxygen was observable for the mesoporous samples, but only the sample denoted as *Meso-post* shows a clear positive correlation between the surface area and the H_2 production rate (Figure 5-6). However, the most active surfaces were found for the nanopowder samples *Nano-SA* and *Nano-LA-1*. The absolute activities that are correlated to the surface areas are different from the results of the EXAFS cell. This can be explained by the reactor designs with different volumes and flow conditions. Nevertheless we found that the catalysts denoted as *Nano-SA*, *Nano-LA-1* and *Meso-post* show the highest hydrogen production in both cells. For comparison an industrial catalyst is shown (Figure 5-6). Despite the highest surface area, it produces less hydrogen than *Meso-post*, *Nano-SA*, and *Nano-LA-1* in the steam reforming of methanol.

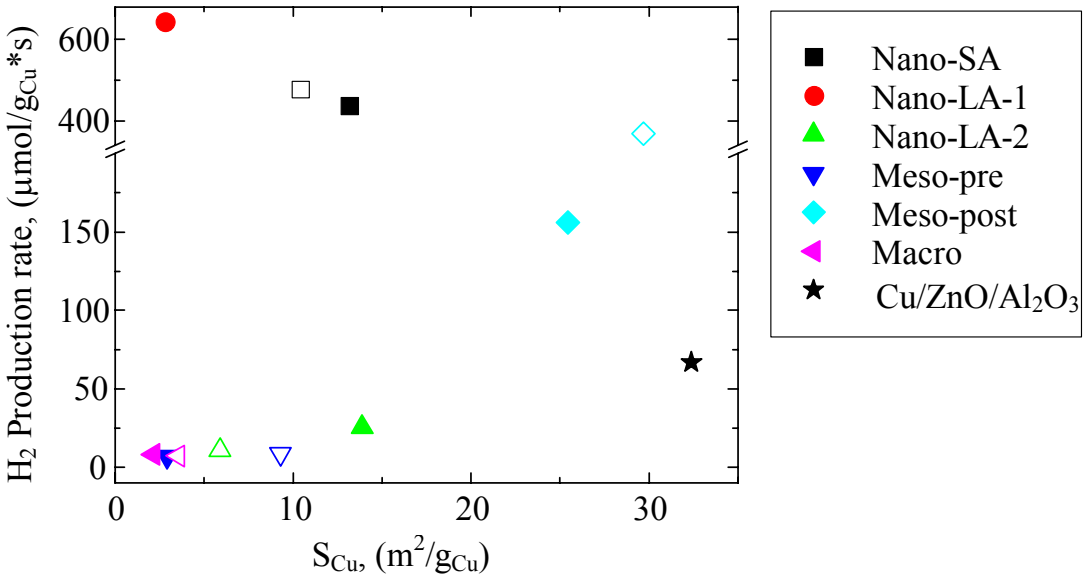

Figure 5-6 Surface areas of Cu/ZrO_2 catalysts after activation in the feed at 523 K, closed symbols: before O_2 addition; open symbols: after O_2 addition

5.3.4 X-ray absorption spectroscopy

5.3.4.1 Precursors

The Cu K edge XANES spectra of the precursor materials differ from that of a CuO reference (calcined malachite). From Figure 5-7 it can be seen, that the characteristic pre-edge at 8984 eV and the peaks directly after the absorption edge are less pronounced. Although, the k-range and the resolution in the FT($(\chi k)*k^3$) are restricted by the Hf L-edge (k = 2.3 – 10 $Å^{-1}$), a XAFS refinement of a CuO model structure to the experimental spectrum of the nanostructured CuO/ZrO_2 precursor confirmed copper oxide as the main copper phase present.[chapter 4.2.3]

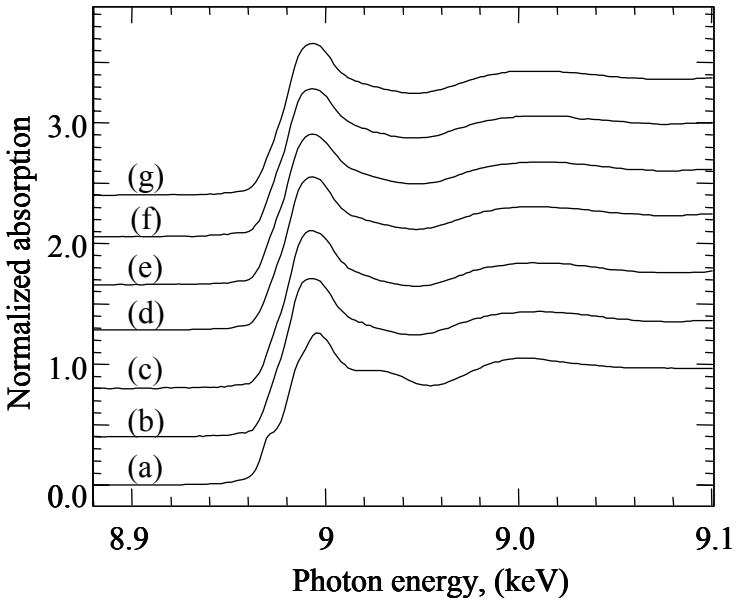

Figure 5-7 Cu K-edge XANES spectra of the precursor materials and the CuO reference (calcined malachite); (a) CuO reference, (b) Nano-SA, (c) Nano-LA-1, (d) Nano-LA-2, (e) Meso-pre, (f) Meso-post, (g) Macro

5.3.4.2 Reduction kinetics

A PC analysis of the time-resolved XANES spectra measured during reduction of the CuO/ZrO_2 precursors in 2 vol-% H_2 showed that three primary components (CuO, Cu metal and probably Cu_2O as an intermediate phase) are required to reconstruct the experimental data. The peak reduction temperatures of the precursors (corresponding to the maximum reduction rate, i.e. the inflection point of the sigmoidal trace) are given in Table 5-3. As shown previously,[chapter 4.2.4] for all catalysts reduction in 2 vol-% H_2 exhibited a lower on-set temperatures compared to the reduction in methanol and water.

Independent of the reduction conditions, the mesoporous samples required the highest reduction temperatures and in the case of *Meso-pre* the reduction continued after the maximum reduction temperature of 523 K was reached. The results are in agreement with TG/DSC experiments. It was also confirmed that for the reduction of *Macro* and *Nano-LA-2* two or more reduction steps were observed and continued at or were close to 523 K. Additionally, Table 5-3 contains the theoretical mass loss calculated for the complete reduction of CuO to Cu for each CuO/ZrO_2 precursor together with the corresponding mass loss measured.

Table 5-3 Temperature programmed reduction in 2 vol-% H_2/He (or in methanol and water, feed). Comparison of theoretical and experimental massloss, and peak reduction temperatures.

Sample	Massloss, (%) Theory 2 % H_2	Massloss, (%) Experiment (TG) 2 % H_2	Peak reduction Temperature (XAS) (K)	
			2 vol-% H_2/He	feed
Nano-SA	-1.21	-0.91	461	496
Nano-LA-1	-1.21	-.92	464	502
Nano-LA-2	-2.87	-2.05	447, 511	490
Meso-pre	-1.29	-1.08	503, 521	510
Meso-post	-0.76	-0.73	493	520
Macro	-2.13	-1.61	459, 523	505

5.3.4.3 Reduction in methanol and water and subsequent catalysis

From Figure 5-8 it becomes again apparent, that the preparation route influences the microstructure of the final catalysts. Shown are the FT(χ(k)*k^3) of the spectra directly reduced in the feed (methanol/water).

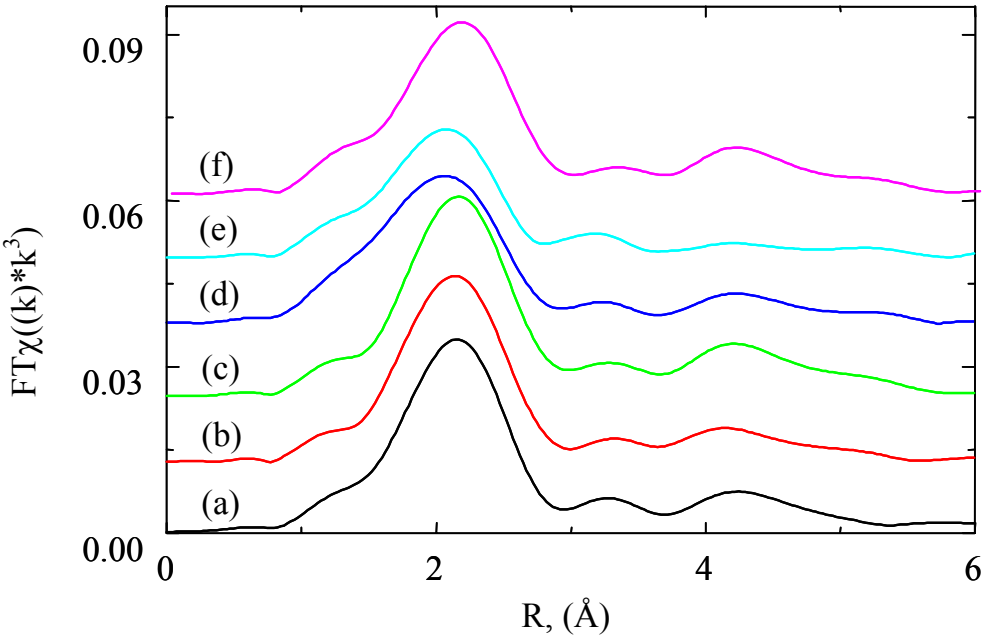

Figure 5-8 FT(χ(k)*k^3) of the Cu/ZrO_2 catalysts directly reduced in MeOH/H_2O; (a) Nano-SA, (b) Nano-LA-1, (c) Nano-LA-2, (d) Meso-pre, (e) Meso-post, (f) Macro

The position of the first Cu-Cu coordination shell of the mesoporous samples, denoted as *Meso-pre* and *Meso-post,* are slightly shifted to lower energies compared to the other four catalysts and also have the lowest amplitudes. As described in chapter 4.3.2 the analysis of the XAFS data measured under MSR reaction conditions revealed that the spectra could not be described by bulk copper metal. However, adding a Cu-O shell (first Cu-O distance in Cu_2O) to the Cu-Cu shells of copper metal sufficiently described the experimental XAFS spectra. Hence, the reduction of the catalysts in hydrogen or in the feed resulted in copper metal clusters exhibiting a varying amount of oxygen (Table 5-4). For the *Meso-post* the moderate agreement between experimental and refined theoretical FT(χ(k)*k^3) indicates that despite the calcinations, nitrate (or other precursor) species of the preparation are still present and additionally contribute to the spectra. This probably explains the comparatively high amount of remained oxygen for the meso- and macroporous samples.

Table 5-4 Chemical composition, characterization and initial methanol steam reforming activity data of Cu/ZrO_2 catalysts

Sample	Oxygen content, (%)				H_2 production rate, ($\mu mol/g_{Cu}*s$)			
	A	B	E	F	A	B	E	F
Nano-SA	30	47	34	41	39.8	59.7	39.8	64.6
Nano-LA-1	29	42	27	28	58.3	72.9	48.6	82.6
Nano-LA-2	27	43	30	41	23	10.4	8.4	12.5
Meso-pre	39	39	17	39	7.9	12.1	12.1	23.4
Meso-post	60	51	19	42	220	268	212.4	614
Macro	38	58	31	57	5.5	5.9	6.3	9.7

(A) after feed reduction, (B) after 1st O_2 addition, (E) after reduction in H_2 at 673 K and subsequent switching back to feed, (F) after 2nd O_2 addition (see also Table 3-1)

Except for the samples *Nano-LA-2 and Meso-post,* the catalytic performance for the Cu/ZrO_2 catalysts is characterized by a high initial activity that decreases rapidly within some minutes (Figure 5-9). After this first step the production increases again for the samples *Meso-pre* and *Macro*, stays almost constant for the sample *Nano-LA-2*, and even decreases slowly further for the samples *Nano-SA, Nano-LA-1* (Figure 5-9) and *Meso-post*.

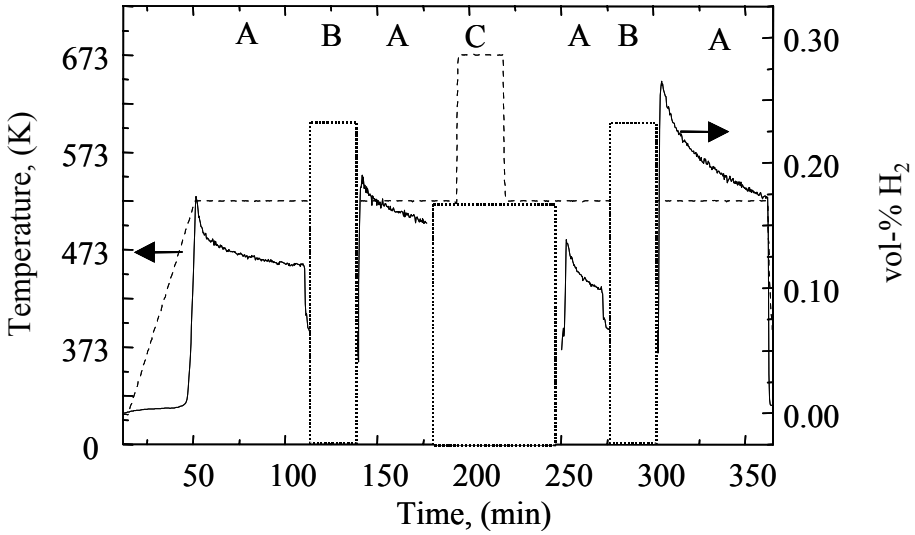

Figure 5-9 Evolution of the H_2 production over Cu/ZrO_2 during methanol steam reforming (A), oxygen pulses (B) and heating to 673 K in 2 vol-% H_2/He (C) of sample Nano-LA 1

In agreement with the described increased contribution of oxygen correlating with an enhanced MSR activity for the sample *Nano-SA* after a temporary addition of oxygen to the feed (chapter 4.2.5), similar results were observed for the samples discussed here. Figure 5-10a,b illustrates the evolution of the oxygen contribution (to copper metal) and the hydrogen production due to the different reaction steps applied (Table 3-1). Except for *Nano-LA-2* (decreasing activity) and *Meso-pre* and *Meso-post* (decreasing oxygen contribution) an increasing hydrogen production was found to coincide with an increasing oxygen contribution after the first temporary O_2 addition. The activities that are correlated to the surface areas are different from the results measured in the XAFS cell. This can be explained by the reactor designs with different volumes and flow conditions. Nevertheless, the catalysts denoted as *Nano-SA*, *Nano-LA-1* and *Meso-post* show the highest hydrogen production in both cells.

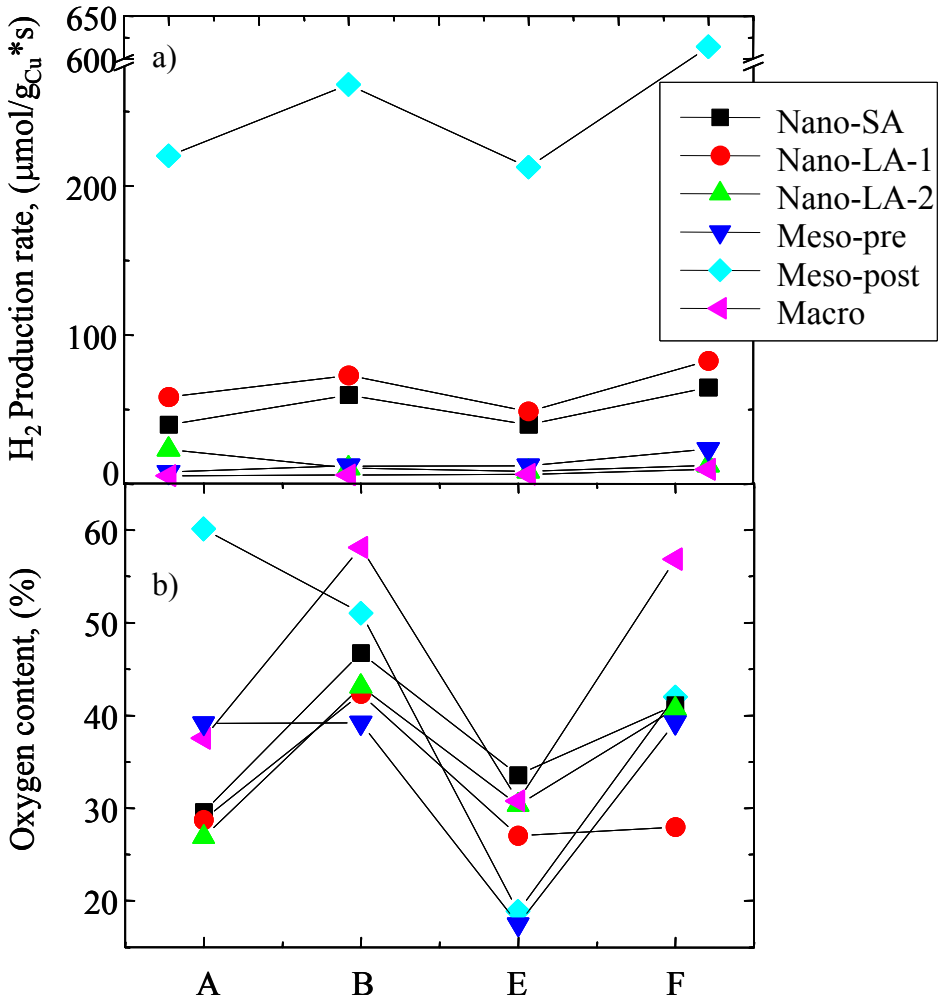

Figure 5-10 Evolution of the hydrogen activity (a) and oxygen contribution (b):during reaction, (A) after reduction in feed, (B) after 1. O_2 addition, (E) after heating to 673 K in 2 vol-% H_2/He, measured in feed, (F) after 2. O_2 addition

5.3.5 Stability during treatment in hydrogen at 673 K

The reduction at high temperatures (Table 3-1 revealed that except for *Nano-LA-2*, all catalysts are thermally stable and can be reduced under these conditions. After changing back to the MSR feed, the corresponding FT(χ(k)*k^3) exhibit again a pronounced contribution of an oxygen nearest neighbor, which indicates an oxidizing influence of the feed. Compared to the oxygen contribution prior to the high temperature treatment, only minor changes are detectable for the nanostructured samples, whereas a considerable decrease of the amount of oxygen was observed for the mesoporous and the macroporous samples (Figure 5-10a, b). Especially for the mesoporous samples ion current traces of m/e 30, 15, and 44 were observed during heating to 773 K for TG/DSC measurements.

For the catalysts *Nano-SA*, *Meso-post* and *Macro* the influence of the high temperature treatment on the copper surface area was investigated (Table 5-2). For all three catalysts the 2nd addition of oxygen to the feed resulted in increased activities, oxygen contributions (Figure 5-10, IV), and copper surface areas.

For the sample *Macro* the copper crystallite size was determined from the Cu 111 XRD line. Due to the treatment at 673 K, a slight increase from 46 to 60 Å was detected, whereas the 2nd oxygen led to a decrease of 9 Å. This could explain the overall smaller copper surface areas after the high temperature treatment.

Although no data about the copper surface area are available for sample *Nano-LA-2*, XRD results indicate a sintering effect due to the first oxygen addition and the subsequent high temperature treatment. The steam reforming and the 2nd oxygen addition lead to only minor changes in the crystallite size. This might explain the loss in activity after the first oxygen addition. Changes in the copper crystallite size should also be detectable in the Debye-Waller factors of the first Cu-Cu shell. In particular, for particles smaller than 70 - 80 Å, the reduced average number of nearest Cu neighbors results in a decreased amplitude of the FT(χ(k)*k^3).[15] However, for the nanostructured Cu/ZrO_2 catalysts the presence of an additional Cu-O shell and the limited data range render a reliable determination of crystallite size effects from an EXAFS analysis difficult.

5.3.6 Infrared spectroscopy – reduction/oxidation behavior

Figure 5-11 presents the IR spectra of CO adsorbed on the various catalysts after reduction in 2 vol-% H_2/He. Different band positions are observable. The band at ≈ 2185/2186 cm^{-1} is assigned to adsorption of CO on coordinatively unsaturated Zr^{4+} ions. For the catalysts Nano-LA-1, Nano-SA, and Meso-post and extended shoulder of the main peak at ≈ 2094 – 2109 cm^{-1} can be observed towards lower wavenumbers. An assignment of these bands based on their corresponding wavenumber is not unequivocally possible as the frequency regions for Cu^+-CO and Cu^0-CO are believed to overlap.[4] A good criterion to distinguish the copper oxidation states is the stability of the bands upon evacuation or purging.[4,16,17] Figure 5-12 demonstrates the stability of the adsorbed CO during evacuation. Band positions at higher wavenumbers (~ 2112 cm^{-1}) are characteristic for CO adsorbed after oxidation of the sample. These bands also appeared to be very stable upon evacuation. The corresponding copper species are therefore believed to be in an oxidized state (Cu^+-CO). After reduction in hydrogen and CO adsorption, the band intensity at 2093 cm^{-1} is rapidly decreasing upon lowering the pressure. However, a remained small band at 2100 cm^{-1} indicated, that additional to the unstable Cu^0-CO also a

fraction of Cu^+ species is present at the catalyst surface. Similar observations were made for all of the other catalysts. Furthermore, the formation of carbonate-species during CO adsorption was observed, which additionally indicates the presence of oxidized copper (that are reduced by CO at room temperature) states even after reduction in hydrogen. In contrast, experiments with Cu/ZnO (70 % copper) revealed no carbonate formation.

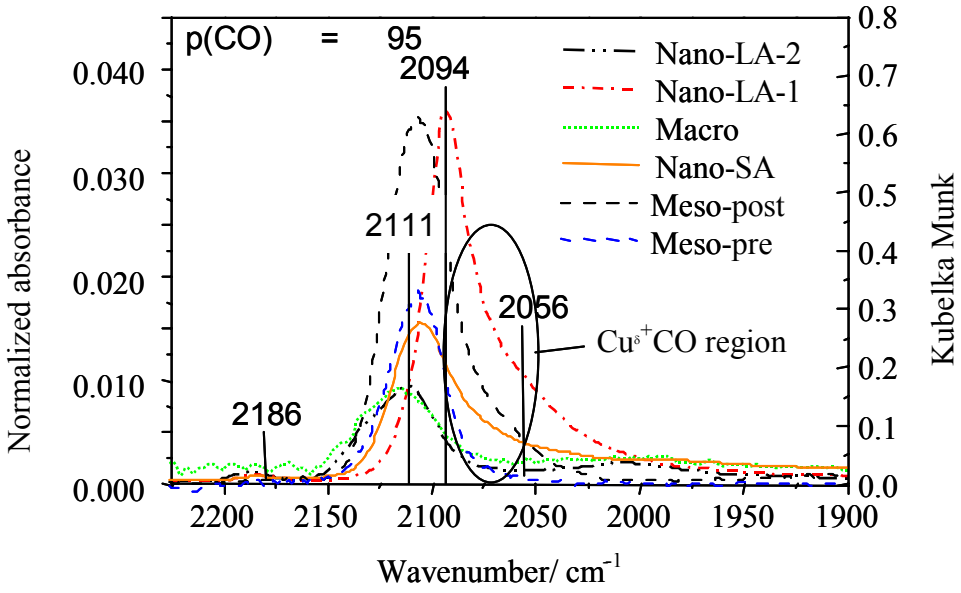

Figure 5-11 Infrared spectroscopy studies on room temperature CO adsorption on Cu/ZrO_2 catalysts. Solid lines: measurements in transmission cell, dashed lines: measurements in DRIFTS cell

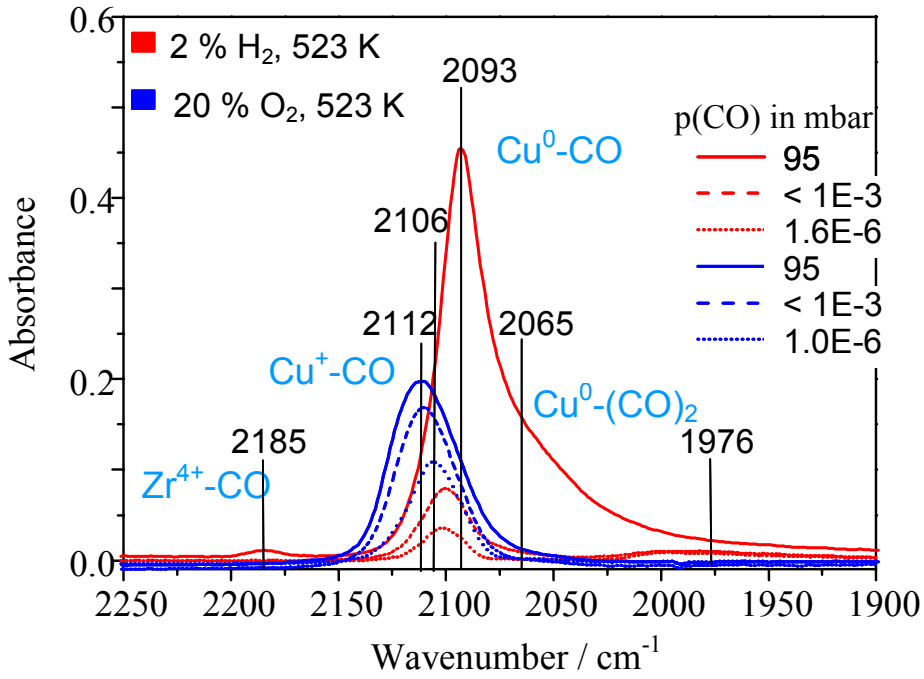

Figure 5-12 Difference FTIR spectra of CO adsorbed at room temperature on Nano-LA-2

5.3.7 TEM analysis

For TEM analysis samples of *Meso-pre* and *Macro* were collected directly after the reduction in the feed, after the high temperature treatment (673 K, 2 vol-% H_2) at 523 K, after switching back to MSR conditions, and finally after the 2nd O_2 addition. With this technique it was not possible to quantify the fraction of t- and m- ZrO_2, as the electron beam partly induces transformation. On the other hand, evidence for incomplete reduction of the copper crystallites was observed in both catalysts (Figure 5-13b). Furthermore it was found for both samples that the d-spacing in many copper crystallites differed from the ideal values and that many copper crystallites were present as multiple twins (MPT, Figure 5-13a). The copper, as well as the zirconia crystallites, is round shaped and the exposed facets were partly visible. The mean crystallite sizes are listed in Table 5-4. For the sample *Macro*, no significant differences could be observed due to the reaction conditions, except that after the reduction in hydrogen at 673 K sintering of some zirconia particles was observed.

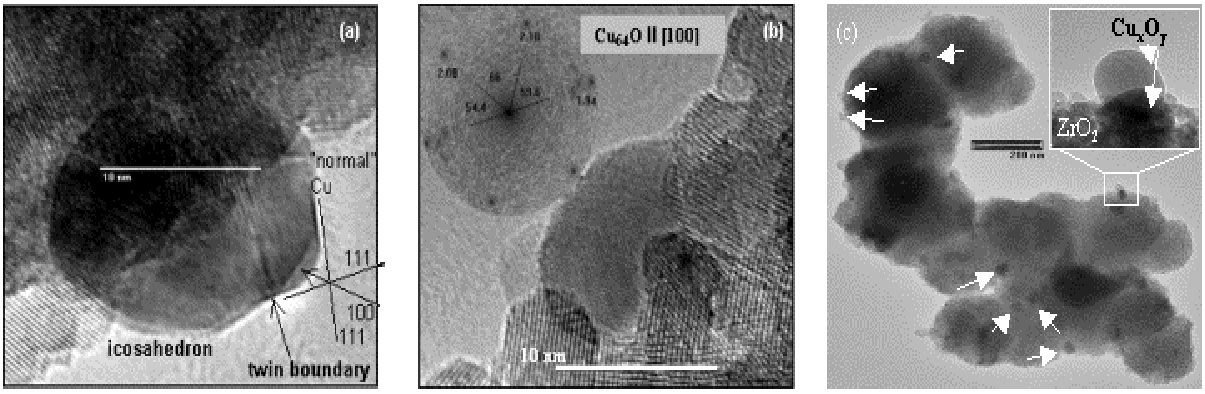

Figure 5-13 High resolution TEM image from sample Macro; (a) copper icosahedron (multiple twin) and (b) crystallite of $Cu_{64}O$ with corresponding power spectrum and sample Meso-pre (c), copper particles are marked with arrows

XRD pattern of the sample *Meso-pre* indicate, that a large fraction of ZrO_2 is at least X-ray amorphous. With TEM it was possible to show, that the catalyst consists of both, well-defined zirconia crystallites, and of material without a long-range order. Some of the larger zirconia particles are highly defective. Characteristic for this material are very large copper crystallites (40 nm), distributed in "clouds" of zirconia (Figure 5-13).

5.3.8 Nuclear magnetic resonance (NMR) spectroscopy

Analysis of the width and the profile of ^{63}Cu NMR lines of reduced copper particles permit qualitative conclusions concerning crystallite size and amount of disorder (e.g. microstrain). This was previously confirmed by our results on Cu/ZnO catalysts, where the existence of microstrain in the copper particles was additionally verified with XRD and XAS.[9]

Table 5-5 ^{63}Cu NMR measurements; ratio of the areas under the left and right side of the peak maximum (high/low); (* multiple peaks observable)

Sample	Feed red.	Post O_2 1	Post H_2 400°C	Feed 2	Post O_2 2
Nano-SA	1.19	1.01	1.01	1.33	1.13
Nano-LA-1	1.15	1.12	1.28	1.09	1.18
Meso-pre	1.1	1.07	1.09	1.05	1.02
Macro	1.25 *	1.05	1.27*	1.31	1.15

(b)

Figure 5-14 shows the ^{63}Cu NMR spectra of the samples *Macro*, *Nano-SA*, *Nano-LA-1* and *Meso-post* after reduction in methanol/water. It can be seen, that the NMR lines are only slightly asymmetrically broadened (Table 5-5) for most of the samples, except for *Macro*, where additional lines appear in the NMR spectrum. This low asymmetry of the ^{63}Cu NMR lines indicates a small degree of microstrain in the copper particles of the Cu/ZrO_2 catalysts studied. The presence of disordered copper crystallites in the sample *Macro* was confirmed by TEM measurements.

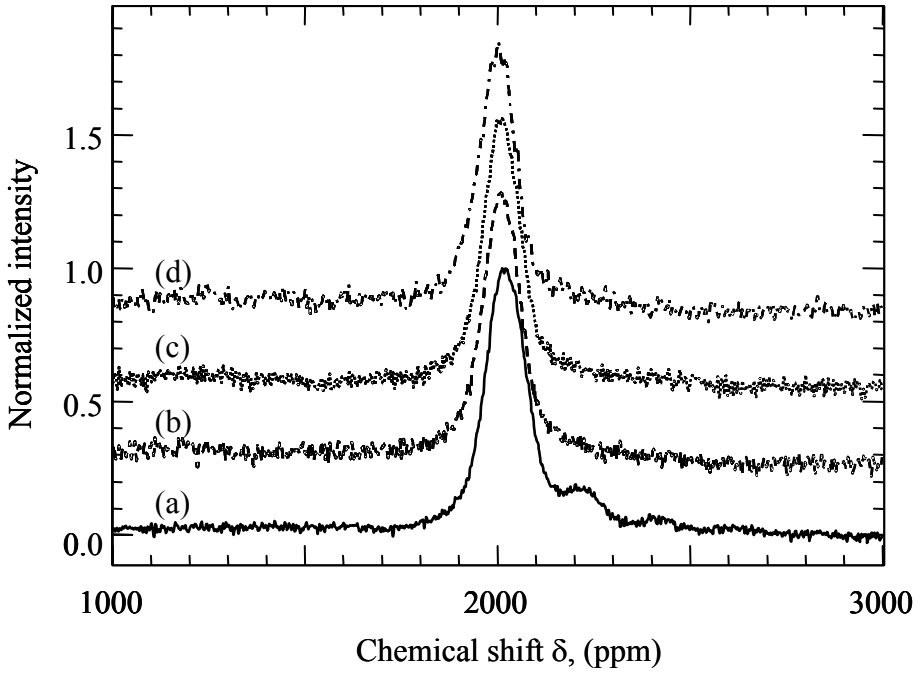

Figure 5-14 ^{63}Cu NMR measurements of sample Macro (a), Nano-SA (b), Nano-LA-1 (c), and Meso-post (d) after reduction in the feed.

5.4 Discussion

Recently, we reported on a macroporous Cu/ZrO_2 catalyst, with improved MSR activity, stability, and selectivity.[10] In chapter 4 it was shown for a nanostructured material, that these important properties are correlated with a modified copper bulk structure. Whether and how the partly complex preparations applied for the investigated Cu/ZrO_2 catalysts, are relevant for the catalytic performance of the materials is the subject of the present work.

5.4.1 Structure of CuO/ZrO_2 precursors

The analysis of the catalyst composition with XFA revealed, that only for the catalysts *Nano-LA-2* and *Meso-post* the amount of copper found in the catalysts is significantly lower than that used initially in the preparation. In the preparation of these systems, the support precursor was aged for 20 h or calcined, respectively, and subsequently the copper precursor was added to a preformed ZrO_2 network. Because of a weak interaction of the copper precursors with the zirconia support, a large amount of the copper precursors was washed away during the subsequent preparation steps.

The lack of a copper phase detectable in the XRD pattern can be due to the low copper content or the nanocrystallinity of the material. The evaluation of the Cu K edge FT(χ(k)*k^3) of the precursors revealed that the differences in the spectra of the CuO reference and the CuO/ZrO_2 precursors can be assigned to a high degree of structural disorder or small crystallite sizes as we have discussed previously.[10, and chapter 4.3.1] On the other hand, the evolution of ion currents of m/e = 44, 30, 15 (due to NO or ammonia) during temperature programmed drying (in a He flow, up to 523 K) and reduction (TG-DSC), indicate that remnants of the preparation (e.g. residuals of the copper nitrate precursors) are still present in the precursors after. The contribution of these species to the Cu K edge FT(χ(k)*k^3) could also explain the deviations from the FT(χ(k)*k^3) of the CuO reference.

From the Cu K edge XAS data no incorporation of Cu into the ZrO_2 lattice was detectable (complete reduction of Cu at 673 K, detection limit ≈ 1 wt. %) and a significant stabilization of t-ZrO_2 by Cu centers in ZrO_2 can be excluded in agreement with our previous results on nanostructured Cu/ZrO_2 catalysts.[chapter 4.3.1, 10] Accordingly, pure ZrO_2 prepared by the methods used here is also mainly present in the tetragonal modification.[13] With a diameter of about 7 nm the stabilization occurs probably by a lower surface energy (compared to the monoclinic zirconia) as it was discussed by several authors.[18,19,20]

Whether the modification of the zirconia directly modifies the catalytic performance or by stabilizing a certain active copper state is not consistently understood. For methanol chemistry on zirconia supported copper catalysts it is proposed, that the zirconia takes part actively in the reactions.[21] In such a case the zirconia modification would be crucial, as it has been shown, for the adsorption properties of OH groups[22] and CO or CO_2.[23,24,25] However, other work to this question has revealed, that copper provides the important sites for the methanol synthesis reaction mechanism (H_2/CO_2, 30 bar, 413 K).[26]

Although t-ZrO_2 constitutes the major phase in the CuO/ZrO_2 catalysts, an increasing contribution of the monoclinic ZrO_2 was observed with decreasing copper content for the *long-aging* preparation route (no variation in crystallite size of t-ZrO_2). It seems that the stabilization of tetragonal ZrO_2 is enhanced by the interaction with copper crystallites and lowering of the copper concentration therefore decreases this supporting effect. Comparing the BET surface areas of the Cu/ZrO_2 catalysts (Table 2-1) with those of co-precipitated Cu/ZnO catalysts[5] shows, that the aim to produce high surface area materials by the use of structure-directing agents or controlled hydrolysis/condensation has been achieved. Only the samples *Nano-SA* and *Macro* exhibit slightly lower BET surface areas of 72 m^2/g and 67 m^2/g, respectively. N_2 adsorption/desorption isotherms revealed that all catalysts contain varying amounts of mesoporous material. The duration of the intermediate aging step in the preparation of the nanopowder samples, where the zirconia precursor has time to slowly hydrolyze and condensate before the copper precursor solution is added, seems to have an important influence on the generation of a more extended porous ZrO_2 network. Hence, the *long-aging* preparation route should result in larger ZrO_2 particles than the *short-aging* preparation method. However, XRD measurements show that the final calcination at 773 K annihilates the differences in the crystallite size of ZrO_2.

The mainly amorphous character of ZrO_2 in *Meso-pre* and *Meso-post* (XRD and TEM after calcination) could be attributed to several parameters. Prior to the first calcination the samples were treated with hexamethyldisilizane to prevent crystallite growth.[27] This might explain the lower crystallinity of the samples and the stability of the tetragonal zirconia phase.[28] An influence of the structure-directing agent $EO_{20}PO_{70}EO_{20}$ is also possible, as very small ZrO_2 nanocrystallites have also been observed with TEM/XRD for samples prepared from $ZrCl_4$ using the same block-copolymer.[29,30] Furthermore, acetylacetonate could have hindered extensive long-range ordering during hydrolysis and condensation of the zirconia precursor (slow reactions because of the formation of stable intermediate complexes).[31] Finally, the calcination procedure must be taken into account, as this is known to determine the crystallinity and the porosity of the resulting materials.[32,33] Hence, lower calcination temperatures (723 K compared to 773 K for the other materials) could have suppressed the crystallization of the support. However, the aim to produce mesoporous materials, with copper particles located in the pores of the ZrO_2 network has probably not been achieved. TEM investigations of the catalyst *Meso-pre* showed that the copper phase is present mainly as large isolated crystallites on poorly crystalline zirconia particles. The absence of large pores in the ZrO_2 phase of the catalyst *Macro* may be caused by a

breakdown of the porous inorganic framework after removal of the template during calcination.[32]

5.4.2 Reduction of the CuO/ZrO_2 precursor

The on-set of reduction of the CuO/ZrO_2 precursors in methanol and water is shifted to high temperature compared to the reduction in hydrogen because of the oxidizing influence of water and carbon dioxide evolving (Table 5-3).[chapter 4.3.2,5,34] ,35] Nevertheless, among the catalysts investigated, *Meso-pre* and *Meso-post* exhibit the highest reduction temperatures in both procedures. As indicated by the low copper surface areas, the *pre-support formation* route, where the copper precursors reacted with the copolymer, resulted in poorly supported large copper crystallites and, hence, high reduction temperatures. This could also explain the slow increase in conversion under methanol steam reforming conditions. Conversely, the *post-support formation* route, where the pre-calcined ZrO_2 was impregnated with an aqueous solution of $[Cu(NH_3)_4]^{2+}$ yields small copper crystallites exhibiting a strong copper ZrO_2 support interaction. This may explain the high reduction temperature observed for this precursor. TEM investigations revealed, that the mesoporous materials are more compact and consist of smaller particles than the nanostructured and macroporous catalysts. Alternatively, the high reduction temperatures observed for the mesoporous samples may be caused by the treatment of the ZrO_2 precursor with hexamethyldisilazane. After calcination at 723 K in air the silicon dioxide formed may separate the copper particles and, hence, additionally hinder the reduction of the mesoporous CuO/ZrO_2 precursors.

The mass loss data measured during reduction of the CuO/ZrO_2 precursors (Table 5-3) indicate that independent of the preparation route, the theoretical mass loss corresponding to a complete reduction of CuO to Cu metal was not reached for the precursors studied. Although the copper phase may not be exclusively present as CuO in the precursors because of an incomplete calcination, it is reasonable to assume that the CuO phase was not completely reduced and that some oxygen remains in the copper particles. This is in agreement with the results from XAFS analysis (except for *Nano-LA-2*, where only copper metal was found after the reduction in 2 vol-% H_2). The observation of ion current traces for CO_2 (m/e = 44) and NO (m/e = 30) during the repeated treatment of sample *Nano-LA-2* in pure He prior to TG/DSC measurements (heating to 523 K) could result from the decomposition of nitrate or organic precursor compounds. Hence, the reduction of *Nano-LA-2* may not have started from the same precursor state in the XAS and TG experiments. In particular for *Nano-LA-2* it was observed, that the gas atmosphere (e.g.

humid, oxidizing) has a strong influence on the stability of the copper phase present. Reduction of the precursor without pretreatment in He ('wet' sample similar to XAS reduction conditions) resulted in a DSC signal with different reduction peaks (two instead of four peaks) compared to the reduction described above.

To further investigate the nature of the copper in the catalysts, the samples were investigated with IR spectroscopy using carbon monoxide as a probe molecule. However, Cu^{2+}-CO is difficult to detect at ambient temperatures, because of the low stability.[36,37,38] Authors also reported on the reducibility of Cu^{2+} by the ambient temperature contact with CO.[39] CO adsorption on the reduced (with 2 vol-% H_2/He at 523 K) materials revealed that the highly active catalysts (*Nano-INS*, *Nano-SBS-1* and *Meso-post*) have a certain amount of Cu^0 species (these reduced copper species are probably in an electron deficient state: $Cu^{\delta+}$-CO[40]) in addition to Cu^+-species at their surfaces. This observed type of copper maybe represents an important key to the active copper state under reaction conditions. In accordance to the results from TG and XAS experiments, Cu^+-species were observed after reduction in 2 vol-% H_2.

As it was discussed previously for the nanostructured sample *Nano-SA*, PC analysis of the in situ reduction (in 2 vol-% H_2 or feed) indicates, that the reduction proceeds via an intermediate Cu_2O. Nevertheless, multiple DSC peaks could also result from different crystallite sizes.[41] This is probably the case for sample *Nano-LA-2*, where 3 - 4 peaks can be observed during reduction in hydrogen. During the preparation of this material, the copper precursor was added to a long-aged ZrO_2 network. As the aging process probably resulted in larger agglomerates (of probably $Zr(OH)_4$ or some $(Zr_xO_yH_{z-1})Me_4N$ species),[31] the copper precursor species were poorly stabilized on the ZrO_2 support material. Therefore, calcination and reduction resulted in a broader crystallite size distribution.

5.4.3 Stability of Cu/ZrO_2 catalyst at 673 K in hydrogen

After treatment in 2 vol-% at 673 K, the Cu/ZrO_2 catalysts were completely reduced to Cu metal on ZrO_2. However, no significant sintering of the copper particles could be observed in the XAS and XRD data. This is a significant improvement over Cu/ZnO/Al_2O_3 catalysts, which are not stable upon heating to elevated temperatures in hydrogen and exhibit rapid sintering of the copper particles and deactivation. The Cu/ZrO_2 catalysts also exhibited a decreased activity after heating to 673 K in 2 vol-% H_2. However, most of the catalysts (except *Nano-LA-2*) could be entirely reactivated by a second temporary addition of oxygen to the feed at 523 K. After the

high temperature reduction and a subsequent addition of oxygen to the feed, the increased activity of the Cu/ZrO_2 catalysts *Nano-SA* and *Meso-post* is correlated to both an enlarged copper surface area and an increased amount of oxygen in the copper particles (Table 5-2, Figure 5-10). The decreasing TOF of the specific copper surface area, however, possibly indicates a deterioration of the important metal-support interaction.

5.4.4 Methanol steam reforming on a Cu/ZrO_2 catalyst

Chinchen et al.[42] proposed a linear correlation between the copper surface area of a catalyst and the activity for the methanol synthesis. However, Kurtz et al.[43] tested various $Cu/ZnO/Al_2O_3$ and found that this holds only in a first-order approximation for the methanol synthesis. As we discussed already for the *Nano-SA*, it has become evident, that additional microstructural parameters influence the catalytic activity. Nevertheless, the differences in the metal distribution, metal surface areas and the degree of interfacial contact between dispersed metal and zirconia are very important structural properties, in addition to the modification of the copper metal by remaining oxygen, that vary for the differently prepared copper/zirconia catalysts.

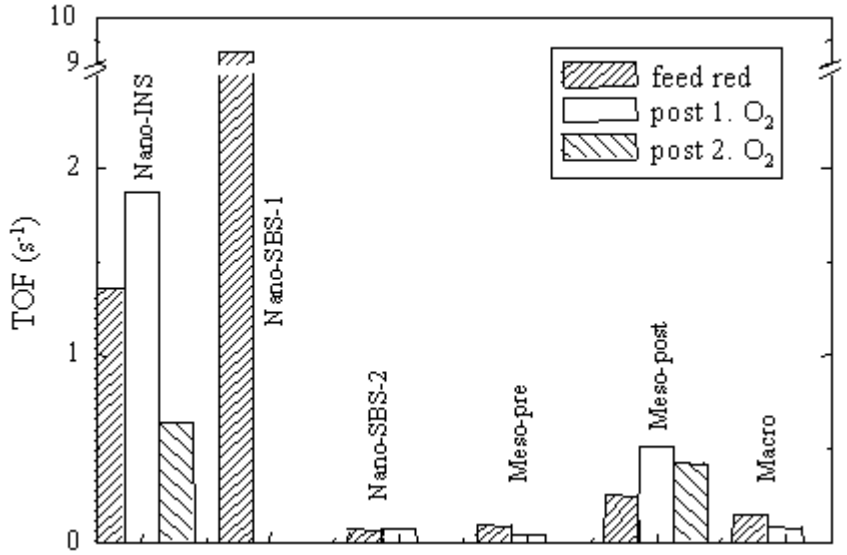

Figure 5-15 Turnover frequencies (based on specific copper surface area per gram copper) for various treatments of the Cu/ZrO_2 catalyst. (a) After initial reduction in methanol and water (feed), (b) after first oxygen addition, and (f) after heating to 673 K in 2 vol-% H_2, switching back to feed at 523 K, and the second addition of oxygen

The Cu/ZrO_2 catalysts investigated here also show no simple linear correlation between specific copper surface area and catalytic activity (Figure 5-3, Figure 5-6). The MSR experiments in the glass reactor (1 hour MSR with subsequent N_2O decomposition) revealed that, despite lower copper surface areas, the samples *Nano-SA* and *Nano-LA-1* are also highly active (Figure 5-6, Figure 5-15). This supports the assumption that a good metal-support interaction and the resulting amount of oxygen in the copper metal clusters upon reduction enhance the catalytic performance. Although a similar copper surface area has been determined for the sample *Nano-LA-2* the observed activity was lower (Figure 5-6, Figure 5-15). Due to the higher copper loading, part of the copper crystallites does not possess the beneficiary copper metal ZrO_2 support interaction. The sample *Nano-LA-1* shows a higher TOF than *Nano-SA* (Figure 5-15). As both samples have similar oxygen contents and a low degree of microstrain, the higher activity of the copper surface area of sample *Nano-LA-1* results probably from a more intense interaction with the support. For this sample the aqueous copper nitrate solution was added to a long-aged zirconia pre-amplifier with an already extended framework structure. Moreover, stabilization of formed metal colloids by TMAOH has been described in the literature.[44] Hence, differences in copper crystallite sizes (deduced from the copper surface area determination) and the activity of the copper particle surface may not only be the result of the poor stabilization by the support but also by the interaction of TMAOH with the metal precursor during the preparation. This may account for the differences in activity of *Nano-SA* and *Nano-LA-1*.

The *Meso-post* Cu/ZrO_2 catalysts, which possesses the lowest copper content and the least crystalline ZrO_2 phase, exhibits the highest specific copper surface area and BET surface area of all Cu/ZrO_2 catalysts described here (Table 2-1). This may result from impregnating the poorly crystalline zirconium dioxide (with high surface area) with the copper precursor yielding in a good metal-support interaction and separation of the copper particles. Despite the higher copper content, the *Meso-pre* Cu/ZrO_2 catalyst exhibits a lower copper surface area, also probably because of the preparation technique, where the copper precursor was mixed with the copolymer and already agglomerated before the modified $Zr(OC_3H_7)_4$ was added. Apparently, the specific copper surface area of the resulting Cu/ZrO_2 catalysts depends more on the preparation procedure employed than on the copper loading.

The catalyst *Macro* exhibits a significant amount of oxygen in the copper particles upon reduction (Figure 5-10), however, the low copper surface area results in a strongly reduced catalytic activity. Similar to *Meso-pre*, hydrolysis and condensation took place simultaneously for both precursors during the preparation. A study on differently prepared Cu/ZrO_2 catalysts[45] (prepared from $Cu(NO_3)_2$ and zirconia areogel) for methanol synthesis revealed, that despite

identical compositions, co-precipitated catalysts possessed smaller BET surface areas and less catalytic activity compared to catalysts prepared be impregnation or deposition-decomposition. Koeppel et al.[46] also investigated various copper-zirconia catalysts for methanol synthesis. By changing the copper precursor from copper acetate to copper nitrate (with zirconyl nitrate as zirconia precursor) they determined an increase in the TOF (CO_2) from 5.2 to 8.9 for co-precipitated materials.

On the other hand, it should be considered, that the oxygen contribution (determined with EXAFS) and/or copper clusters in remained precursor states could diminish the N_2O decomposition, and therefore make it difficult to interpret the data dependably. Infrared experiments, where CO adsorption bands ($CO\text{-}Cu^+/Cu^0$) were found at different wavenumbers (2025-2130 cm^{-1}) depending on the preparation, furthermore support the assumption, that the nature of the Cu surface atoms could alter the results for the copper surface area determination.

The question whether the degree of crystallization and /or the modification of zirconia has a direct or indirect influence on the copper surface area and the catalytic activity is not yet fully understood. As in this work many different preparation routes and copper contents were used, it is hard to derive a conclusive picture. In the literature there are examples were at least the zirconia crystallinity is found to play a significant role for the methanol synthesis. Koeppel et al.[46] reported on a decreasing activity through the transformation of amorphous into tetragonal zirconia (without changes in the specific copper surface area) and suppose, that this effect is due to the loss of interfacial area.
It was found for amorphous CuZr alloys[47] that although they evolved a porous high surface area during methanol synthesis reaction, the Zr-phase stayed almost X-ray amorphous. By comparing the TOF (CO_2/H_2 hydrogenation reaction) of catalysts, activated at different temperatures and with different gas mixtures, it becomes apparent, that the activation leading to the highest copper surface, results however in lower TOF. After investigation of several copper containing catalysts Bartley et al.[48] proposed, that only a small fraction of the copper (e.g. surface defects, particular surface facets etc.), rather than the total surface area may be important for the activity. These suggestions support the observations of a nonlinear relationship between activity.

5.4.4.1 Correlations between microstrain in copper particles and activity

Analysis of the width and the profile of ^{63}Cu NMR lines of reduced copper particles permit qualitative conclusions concerning crystallite size and amount of disorder (e.g. microstrain). This was previously confirmed by our results on Cu/ZnO catalysts, where the existence of microstrain in the copper particles was additionally verified with XRD and XAS.[4] From Figure 4-13 it can be concluded, that the profiles of the NMR signals are only slightly asymmetrically broadened. Hence, compared to Cu/ZnO catalysts microstrain appears to be less significant for stabilizing the microstructure of the active Cu/ZrO_2 catalysts. However, the various reaction steps do influence the chemical shift of the NMR lines (particularly for *Macro*) showing the instability of the non-ideal active copper structure. We proposed previously, that the incomplete re-reduction of the Cu/ZrO_2 catalysts after addition of oxygen modifies the electronic structure of copper sites at the surface and result in different adsorption or dissoziation energies, and, hence, catalytic activities.[49] The decreasing TOF of sample *Macro* after the temporary addition of oxygen to the feed may therefore be due to the loss of structural disorder observed in the NMR spectra.

5.4.5 Addition of oxygen to the MSR feed

Similar to Cu/ZnO catalysts,[9] the methanol steam reforming activity of most of the Cu/ZrO_2 catalysts studied here can be increased by a temporary addition of oxygen to the feed at 523 K (Figure 5-10). Except for the mesoporous catalysts, the improved MSR activity after the addition of oxygen to the feed can be correlated to an increase of the oxygen content in the copper catalysts (Figure 5-10). For the samples *Meso-pre* and *Meso-post* this is probably due to the presence of remnants from the preparation (e.g. nitrates), that are removed only during the treatment at 673 K in hydrogen.

The copper surface areas of the differently prepared Cu/ZrO_2 catalysts do not change uniformly with the temporary addition of oxygen. A significant increase in the specific surface area was observed only for the mesoporous samples. For the nanostructured catalysts similar or even increasing turn-over frequencies (despite decreasing copper surface areas) after the addition of oxygen indicate that the modification of the microstructure of the copper particles by the increasing oxygen contribution determines the catalytic activity. The decrease of the copper surface area (N_2O decomposition) of *Nano-LA-2* after the addition of oxygen addition was confirmed by an increasing crystallite sizes (~Δ14 Å, XRD), although the changes are smaller compared to Cu/ZnO catalysts.[5] An increasing TOF (Figure 5-15) after the oxygen addition was also determined for the sample *Meso-post*.

With respect to the MSR measurements in the three-channel reactor, the increase in activity observable after the addition of oxygen appears to depend on the duration of the preceding activation period. This may explain, why *Nano-LA-2* could be significantly activated by addition of oxygen after 200 h time on stream, whereas 1 h time on stream and subsequent addition of oxygen (e.g. in the XAS cell) resulted in no increase of activity. The study of the activation behavior of the catalyst *Macro* has been published recently.[10] For this catalyst it was observed that the necessary time intervals between "successful" oxygen treatments increase continuously. The last addition of oxygen at about 200 h after the previous effective additions resulted in no further improvement.

5.4.6 Correlation between preparation and catalytic performance

Calcination and reduction of the various precursor materials do not annihilate the structural differences in the precursors (“chemical memory”), and, hence, the different preparation routes employed result in differently active catalysts for the steam reforming of methanol. For comparison Cu/ZrO_2 catalysts have been prepared by impregnation of bulk ZrO_2 with an aqueous solution of copper nitrate. These materials possess a low BET and specific copper surface area. Catalysis tests revealed, that these catalysts exhibit a two times lower methanol conversion in the steam reforming of methanol compared to *Meso-post* Cu/ZrO_2 catalyst (with similar copper content).[50] According to the structure-activity relationship revealed for *Nano-SA*[chapter 4] the activity of the various Cu/ZrO_2 catalysts correlates with the deviation of the microstructure from the ideal structure of copper metal. This active “real structure” of the Cu/ZrO_2 catalysts described can be effectively tailored by choosing an appropriate preparation procedure.

For the samples prepared by precipitation, the succession of the preparation steps has a pronounced effect on the TOF. In the *long-aging* preparation route the zirconia precursor was given more time to condensate and the final ZrO_2 support seems to provide a larger area for metal-support interactions resulting in more active specific copper surfaces. From the comparison of the TOF of the mesoporous materials, it becomes apparent, that the *chemisorption-hydrolysis (post support formation)* preparation route leads to a more active catalyst surface. The higher copper surface area (and BET) and the resulting strong interaction between ZrO_2 support and copper metal are crucial parameter for a high methanol steam reforming activity.

Furthermore, in contrast to Cu/ZnO catalysts, good activity, selectivity, and stability can be achieved with Cu/ZrO_2 catalysts possessing a low copper concentration. For the *Nano*-catalysts the optimum concentration should be lower than approximately 20 mol-%. The deactivation behavior of sample *Nano-LA-2* (correlating with an increase in crystallite size and decrease in the copper surface area) is likely the result of the high copper loading and a reduced copper-support interaction. For the mesoporous Cu/ZrO_2 catalysts, where hydrolysis and condensation take place simultaneously (*Meso-pre*), a concentration even lower than 10 mol-% needs to be chosen to avoid the formation of large copper crystallites. The results described indicate that the controlled preparation of nanostructured zirconium dioxide particles followed by an introduction of the copper precursor significantly enhances the methanol steam reforming activity of the nanostructured, mesoporous, and macroporous Cu/ZrO_2 catalysts.

5.5 Conclusion

In situ bulk structural investigations of differently prepared Cu/ZrO_2 catalysts under MSR conditions were performed to reveal the effects of the preparation of the catalytic performance. For all catalysts the major proportion on all components corresponds to tetragonal zirconium dioxide. Depending on preparation and copper concentration, small varying amounts of monoclinic ZrO_2 are present. Only with a copper loading of more than 15 mol-% copper oxide was detectable with XRD. XAS identified very small and/or highly disordered CuO particles as the main copper phase present in the precursors.

The properties of the final Cu/ZrO_2 catalysts strongly depend on the preparation conditions. Calcination and reduction of the various precursor materials do not annihilate the structural differences in the precursors (“chemical memory”), and, hence, the different preparation routes employed result in differently active catalysts for the steam reforming of methanol. The catalysts obtained exhibited a high stability at 673 K and under changing reaction conditions over a long time on stream. At conversions higher than 50 %, the Cu/ZrO_2 catalysts are more selective and produce less CO than a conventional $Cu/ZnO/Al_2O_3$ catalyst. The microstructure of the copper phase in the activated catalysts strongly deviates from that of ideal copper metal. The enhanced catalytic activity after a temporary oxidation/reduction treatment correlates with an increasing amount of oxygen in the copper particles. In order to ensure a good metal support interaction and, hence, good catalytic performance, a copper concentration in the materials of less than ~ 15 % had to be chosen. Possibly because of reduced metal support interaction, co-precipitation

routes resulted in large copper particles and inferior catalytic properties. Conversely, impregnation of a pre-formed ZrO_2 support resulted in small Cu particles, and a superior activation behavior and catalytic performance.

5.6 References

[1] G.C. Chinchen, K.C. Waugh, D.A. Whan, Appl. Cat. **25** (1986) 101

[2] M.M. Günter, T. Ressler, B. Bems, C. Büscher, T. Genger, O. Hinrichsen, M. Muhler, R. Schlögl, Catal. Lett. **71** (2001) 37

[3] Kurtz, M., Wilmer, H., Genger, T., Hinrichsen, O., Muhler, M., Cat. Lett. **86**, 77 (2003)

[4] Kniep, B.L., Ressler, T., Rabis A., Girgsdies, F., Baenitz, M., Steglich, F., Schlögl R., Angew. Chem. **116**, 114 (2004)

[5] Günter, M.M., Ressler, T., Jentoft, R.E., Bems, B., J. Cat. **203**, 133 (2001)

[6] Hansen, P.L., Wagner, J.B., Helveg, S., Rostrup-Nielsen, J.R., Clausen, B.S., Topsøe, H., Science **295**, 2053 (2002)

[7] Bulko, J.B., Herman, R.G., Klier, K., Simmons, G.W., Journ. Phys. Chem. **83**, 3118 (1979)

[8] Clausen, B.S., Schiøtz, J., Gråbæk, L., Ovesen, C.V., Jacobsen, K.W., Nørskov, J. K. Topsøe, H., Top. in Catal. **1**, 367 (1994)

[9] B.L. Kniep, T. Ressler, A. Rabis, F. Girgsdies, M. Baenitz, F. Steglich, R. Schlögl, Angew. Chem. **116** (2004) 114

[10] Purnama, H., Girgsdies, F., Ressler, T., Schattka, J.H., Caruso, R.A., Schomäcker, R., Schlögl, R., Cat. Let. **94**, 61 (2004)

[11] Schattka, J.H., Shchukin, D.G., Jia, J., Antonietti, M., Caruso, R.A., Chem. Mater. **14**, 5103 (2002)

[12] H. Purnama, T. Ressler, R.E. Jentoft, H. Soerijanto, R. Schlögl, R. Schomäcker, Appl. Cat. A –General **259** (2004). 83

[13] Y. Wang,, R.A. Caruso, J. Mater. Chem. **12** (2002) 1442

[14] E. P. Barrett, L.G. Joyner, P.P. Halenda, J. Am. Chem. Soc. **73** (1951) 373

[15] Clausen, B.S., Grabek, L. Topsoe, H. Hansen, L.B. Stoltze, P. Norskow, J.K. Nielsen, O.H., J. Cat. **141**, 368 (1993)

[16] K. Hadjiivanov, T. Venkov, H. Knözinger, Catal. Lett. **75** (2001) 55

[17] F. Boccuzzi, A. Chiorino, M. Manzoli, D. Andreeva, T. Tabakova, L. Ilieva, V. Iadakiev, Catal. Today **75** (2002) 169

[18] R.C. Garvie, J. Phys. Chem. **82** (1978) 218

[19] R.C. Garvie, J. Phys. Chem. **69** (1965) 1238

[20] T. Chraska, A.H. King, C.C. Berndt, Mater. Sci. Eng. A **286** (2000) 169

[21] Jung, K.-D., Bell, A.T., J. Catal. **193**, 207 (2000)

[22] Jacob, K.-H., Knözinger, E., Beníer, S., J. Mater. Chem. **3**, 651 (1993)

[23] Jung, K.T., Bell, A.T., Catal. Lett. **80** (2002) 63

[24] Jung, K.T., Bell, A.T., J. Mol. Catal. A: **163** (2000) 27

[25] Prokovski, K., Jung, K.T., Bell, A.T., Langmuir, **17** (2001) 4297

[26] S. Bailey, G.F. Froment, J.W. Snoeck, K.C. Waugh, Catal. Lett. **30** (1995) 99

[27] Wu, N.-L., Wang, S.-Y., Rusakova, I.A., Science **285**, 1375 (1999)

[28] Wu, N.-L., Wu, R.-F., S.-Y., Rusakova, J. Mater. Res. **16**, 666 (2001)

[29] P. Yang, D. Zhao, D.I. Margolese, B.F. Chmelka, G.D. Stucky, Nature **396** (1998) 152

[30] P. Yang, D. Zhao, D.I. Margolese, B.F. Chmelka, G.D. Stucky, Chem. Mater. **11** (1999) 2813

[31] A. Chemseddine, T. Moritz, Eur. J. Inorg. Chem. 1999, 235

[32] F. Schüth, Handbook of porous solids, ed. by F. Schüth, K.S.W. Sing, J. Weitkamp, Vol. 1, 622 pp., Wiley & sons, New York 2002

[33] G.J. de A.A. Soler-Illia, C. Sanchez, B. Lebeau, J. Patarin, Chem. Rev. **102** (2002) 4093

[34] Idem, R.O., Bakhshi, N.N., Ind. Eng. Chem. Res. **33**, 2065 (1994)

[35] R.O. Idem, N.N. Bakhshi, Indian J. Eng. Chem. Res. **33** (1994) 2065

[36] K. Hadjiivanov, H. Knözinger, Phys. Chem. Chem. Phys. **3** (2001) 1132

[37] A. Dandekar, M.A. Vannice, J. Catal. **178** (1998) 621

[38] K.I. Hadjiivanov, G.N. Vayssilov, Advances in Catalysis 47, ed. B.C. Gates, H. Knözinger, Academic Press, San Diego 2002

[39] C. Morterra, E. Giamello, G. Cerrato, G. Centi, S. Perathoner, J. Catal. **17**9 (1998) 111

[40] A.N. Pestryakov, A.A. Davydov, Kin. Catal. **37** (1996) 859

[41] Kundakovic, L., Flytzani-Stephanopoulos, M., Appl. Cat. **171**, 13 (1998)

[42] Chinchen, G.C., Waugh, K.C., J. Catal. **97**, 280 (1986)

[43] Kurtz, M., Wilmer, H., Genger, T., Hinrichsen, O., Muhler, M., Cat. Lett. **86**, 77 (2003)

[44] M.T. Reetz, W. Helbig, S.A. Quaiser, U. Stimming, N. Breuer, R. Vogel, Science **267** (1995) 367

[45] Liu, J., Shi, J., He, D., Z, Q., Wu, X., Liang, Y., Zhu, Q., Appl. Catal. A: **218**, 113 (2001)

[46] R.A. Koeppel, A. Baiker, Appl. Catal. A: **84** (1992) 77

[47] Gasser, D., Baiker, A., Appl. Cat. **48**, 279 (1989)

[48] Bartley, G.J.J., Burch, R., Appl. Cat. **43**, 141 (1988)

[49] S. Sakong, A. Groß, Surf. Science **525** (2003) 107

[50] Personal communications with Dr. A. E. Ihmels and Prof. Dr. R. Schomäcker, Technical University Berlin, Germany

6 Nanostructured catalysts: influence of the copper content on the catalytic performance

6.1 Introduction

Studies have shown, that the Cu concentration is one important parameter for the properties of supported copper catalysts for the methanol synthesis and MSR.[1,2,] Günter et al.[1] for example compared co-precipitated Cu/ZnO materials for the methanol synthesis reaction. The highest methanol production was found for catalysts with 70 to 40 mol-% Cu. They reported, that the copper surface area and microstructural strain/disorder in Cu are controlled by the copper concentration and that a combination of these parameters determines the activity.

The results of the nanostructured *long-aging* precipitated catalysts *Nano-LA-1* and *Nano-LA-2* also show a significant influence of the copper concentration on the catalytic performance. There it was found, that the copper crystallites in the material with the higher copper content are very sensitive and easily agglomerate under changing reaction conditions and higher temperatures.

To study the influence of the copper concentration on the correlation between bulk properties and activity for the *short-aging* precipitation route applied here, samples with 5 and 2.5 atom-% copper (see also Table 6-2) denoted as *Nano-SA-5* and *Nano-SA-2.5*, respectively were prepared and investigated.

For the catalyst preparation the amount of Cu and Zr were adjusted to yield catalysts with 5 mol-% Cu and 95 mol-% Zr (*Nano-SA-5*) and 2.5 mol-% Cu and 97.5 mol-% Zr, respectively for *Nano-SA-2.5* (with respect to the metal content). XFA (X-ray fluorescence analysis), performed on a Seiko Instrument (SEA 2010) revealed that the materials obtained contained 6.1 and 2.2 mol-% (*Nano-SA-5 and Nano-SA-2.5*).

6.2 Results

6.2.1 XRD investigation of the catalyst precursors

From Figure 6-1 it can be seen, that similar to the *long-aging* preparation route, the monoclinic zirconium dioxide (m-ZrO_2) modification becomes more pronounced with decreasing copper content (*Nano-SA-5*: 6.1 atom-%*, Nano-SA-2.5*: 2.2 atom-%*)*. Nevertheless, the tetragonal zirconia (t-ZrO_2) is the dominant modification. The crystallite size of the tetragonal zirconia was determined from the t-ZrO_2 111 peak and is highest for the sample *Nano-SA-5* (84 Å), whereas

there is no significant differences between *Nano-SA* and *Nano-SA-2.5* (68 and 75 Å, respectively).

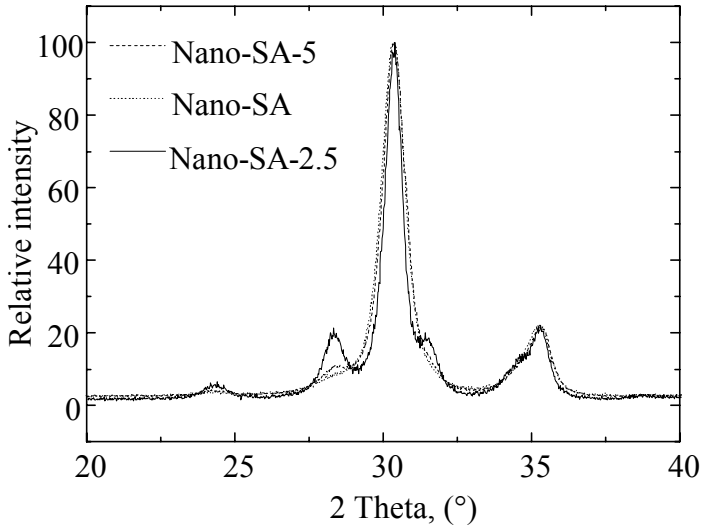

Figure 6-1 XRD investigation of the precursors: (dashed) Nano-SA-5, (dotted) Nano-SA, (full) Nano-SA-2.5

6.2.2 Surface area determined with N_2O decomposition (RFC)

The specific copper surface area has been determined after various reaction steps (see Table 3-1). For *Nano-SA* we already described, that before the reduction at 673 K in hydrogen, the specific copper surface area was almost constant, whereas after this treatment the increase in activity correlated with an increase in the specific copper surface area. The lower copper concentration in *Nano-SA-5* compared with *Nano-SA*, seems not to have a great influence (Table 6-1). However, a further decrease of the copper content (*Nano-SA-2.5*) results in a strong enlargement of the copper surface area. For *Nano-SA-5* similar ratios of S_{Cu}pre/S_{Cu}post (i.e. before and after the oxygen addition) were measured before and after the high temperature treatment, whereas a significant increase of the copper surface area was observed after the 2nd oxygen addition for sample *Nano-SA-2.5* (as for *Nano-SA*).

Table 6-1 Specific copper surface areas after various reaction steps

Sample	S_{BET} (m^2/g)	S_{Cu} (m^2/g_{Cu}) Feed red	S_{Cu} (m^2/g_{Cu}) 1. O_2 add.	S_{Cu} (m^2/g_{Cu}) post $H_2$400	S_{Cu} (m^2/g_{Cu}) 2. O_2 add.
Nano-SA	72	13.2	10.4	15.7	30.7
Nano-SA-5	66	15.8	30.8	15.3	27
Nano-SA-2.5	54	42.6	53.3	42.9	63.8

Nevertheless, in all cases an increase in the MSR activity was observed after the temporary addition of oxygen to the feed (Figure 6-2). The highest activities were found for *Nano-SA-2.5* with the highest copper surface areas.

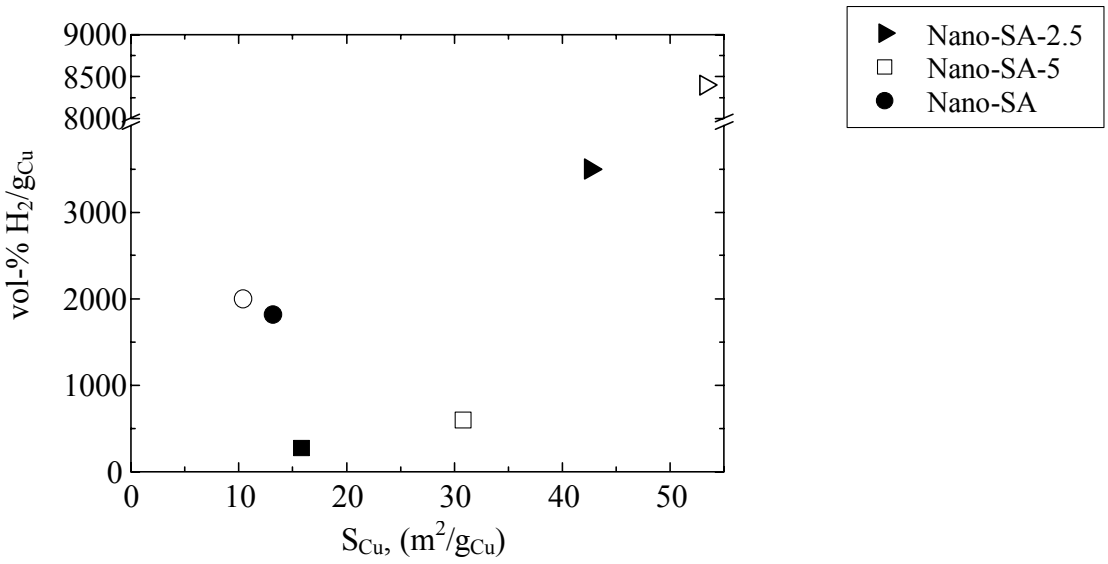

Figure 6-2 Correlation between copper surface area and activity before (closed symbols) and after (open symbols) the temporary addition of O_2 to the feed

6.2.3 X-ray absorption spectroscopy

6.2.3.1 Reduction of the CuO/ZrO_2

Figure 6-3 shows the evolution of the abstract concentration of copper during reduction in methanol/water for the precipitated samples. Similar to the results from the determination of the copper surface area, a grouping of the catalysts can be observed. *Nano-SA* and *Nano-SA-5* reduce at temperatures about 490 K, whereas the copper in *Nano-SA-2.5* needs significant higher temperatures (see Table 6-2).

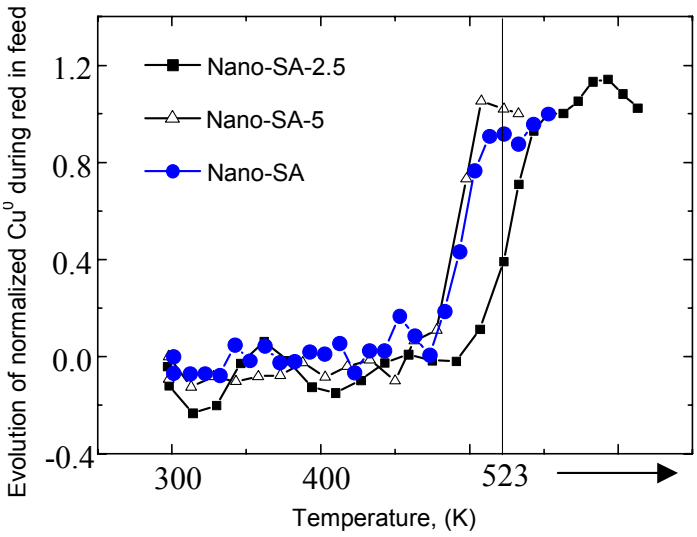

Figure 6-3 Evolution of the abstract concentration of copper during reduction in methanol and water

The reduction in 2 vol-% hydrogen was investigated with TG-DSC/MS after the samples were dried in He two times at 523 K. Only a weak DSC signal could be observed due to the low copper concentration of *Nano-SA-2.5*. Figure 6-4 shows the normalized evolution of the mass loss during the temperature-programmed reduction in hydrogen. From this graph it is possible to describe the temporal progression of the weight loss. All three catalysts start to loose weight already at low temperatures of approximately 330 K. Simultaneously, the evolution of water was detected with a mass spectrometer. The release of water in this first step of reduction was slower, the higher the copper concentration was. However, from 415 K on the reduction of the copper in *Nano-SA* proceeded faster, than for *Nano-SA-5* and *Nano-SA-2.5*.

Table 6-2 Characterization of Cu/ZrO_2 catalyst precursor and after reduction

Sample	Copper content (atom-%)	Massloss, (%) Theory	Massloss, (%) Experiment (2 vol-% H_2)	Peak reduction Temperature (**feed**), (K)
Nano-SA	8.9	-1.21	-0.91	493
Nano-SA-5	6.1	-0.81	-0.6	489
Nano-SA-2.5	2.2	-0.29	-0.26	523

The reduction of copper started at higher temperatures for Nano-SA-2.5, than for the other two catalysts. The determination of the exact onset temperature is however, complicated by the absence of clear-cut steps in the mass loss and DSC signal, but lies approximately at 430 K. Table 6-2 lists the calculated theoretical and the experimentally determined mass loss due to the reduction of copper oxide in hydrogen. None of the samples was totally reduced, which is in agreement with results from EXAFS investigations.

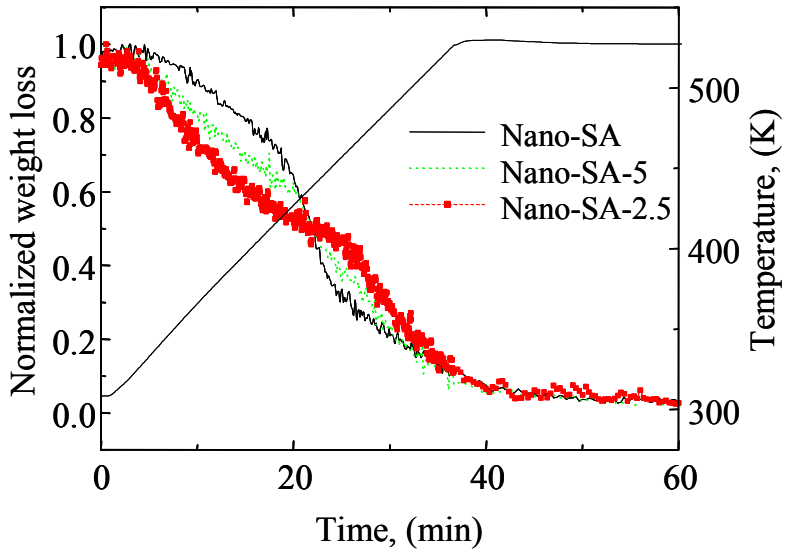

Figure 6-4 Evolution of the mass loss during temperature programmed reduction in 2 vol-% H_2/He

6.2.3.2 Reduction in methanol and water and subsequent catalysis

Figure 6-5 shows the FT(χ(k)*k^3) of the catalysts *Nano-SA* after reduction in the feed. Because of the low copper concentration in sample (and high amount of ZrO_2) *Nano-SA-2.5* the X-ray

absorption signal was insufficient to obtain good resolution (signal to noise ratio) of the spectra. In Figure 6-5a, the FT(χ(k)*k^3) of *Nano-SA* and *Nano-SA-5* are shown. Both FT(χ(k)*k^3) look very similar, except for the reduced amplitude of the first Cu-Cu distance for sample *Nano-SA-5*. Analysis of the corresponding pseudo radial distribution functions with experimentally determined phases and amplitudes of the first shell of Cu metal revealed the actual coordination number for the first Cu-Cu distance. Following the relations proposed by Clausen et al.[3] the crystallite size was estimated. The reduced amplitude for Nano-SA-5 can therefore be correlated to copper clusters smaller than 15 Å.

On the other hand, significant differences can be observed between the Cu K edge XANES spectra of *Nano-SA-5* and *Nano-SA-2.5* (Figure 6-5b). In comparison with copper metal (chapter 4.2.3.1) the characteristic doublet in the post-edge region (8.99 – 9.0 keV) of the XANES spectra is less resolved for *Nano-SA-5* and the edge features of *Nano-SA-2.5* resemble rather that of CuO, than that of Cu metal.

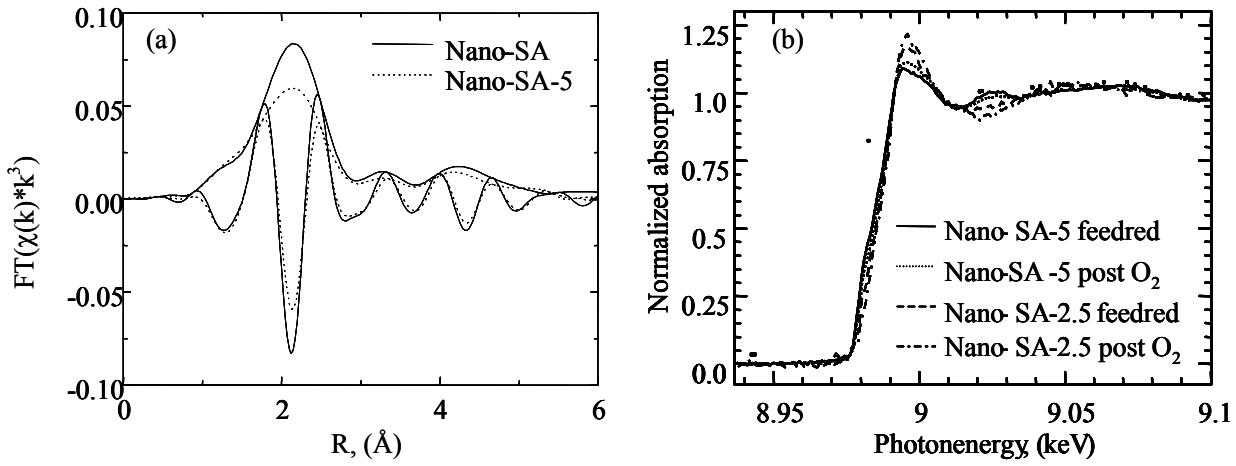

Figure 6-5 (a) FT(χ(k)*k^3) of Cu/ZrO_2 catalysts after reduction in methanol and water at 523 K, (b) Cu K edge XANES of Nano-SA-5 and Nano-SA-2.5 after reduction in feed and after temporary addition of oxygen to the feed (both at 523 K)

After the temporary addition of oxygen to the feed, the copper of *Nano-SA-2.5* is even more oxidized, as indicated by the XANES spectrum (Figure 6-5b, *Nano-SA-2.5* post O_2). These observations indicate, that after reduction in methanol and water the catalysts are still in a partially oxidized state. For *Nano-SA-5* more oxygen was determined from the analysis of the corresponding FT(χ(k)*k^3) in addition to copper metal Figure 6-5a).

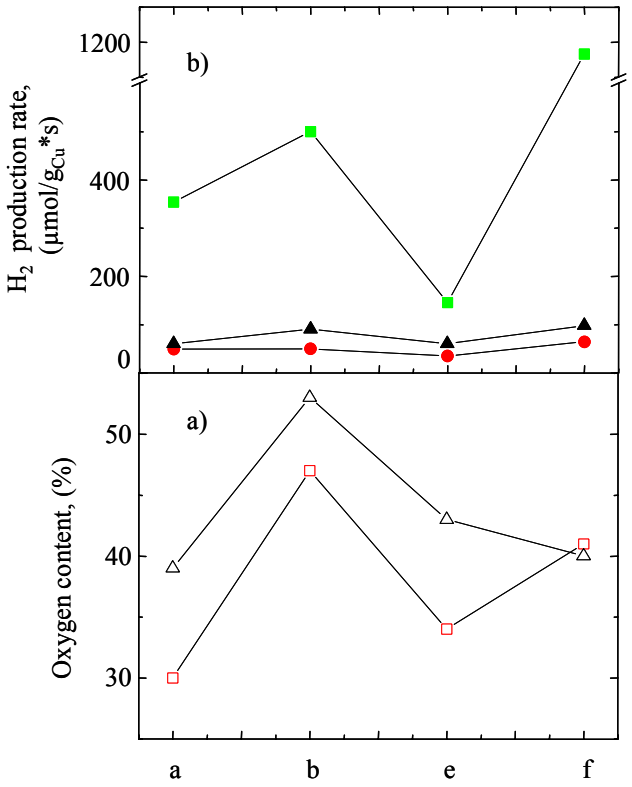

Figure 6-6 (a) Oxygen contribution to the copper metal, (b) hydrogen production rate of samples Nano-SA (circle), Nano-SA-5 (triangle) and Nano-SA-2.5 (square) after various reaction treatments (Table 3-1)

Nevertheless, all three catalysts are active as shown in Figure 6-6b and an arrangement in groups can be observed. Despite the incomplete reduction of the copper oxide, the sample with the lowest copper concentration (*Nano-SA-2.5*) revealed the highest hydrogen production rate, whereas the other two catalysts show very similar activities. For all catalysts an increase in activity can be observed after the temporary addition of oxygen that correlates with an incomplete re-reduction. The corresponding oxygen contributions (Figure 6-6a indicate, that an increased amount of oxygen remained in the samples.

6.2.3.3 Thermal stability

Similar to the other reported Cu/ZrO_2 catalysts, the thermal stability was tested by heating the samples to 673 K in 2 vol-% H_2/He. After cooling down to 523 K in hydrogen a spectrum was recorded. The refinement of the structure of copper metal to the related experimental

FT(χ(k)*k^3) revealed, that full reduction was achieved for *Nano-SA* due to this reaction step, whereas a Cu-O shell was still detectable for *Nano-SA-5* and *Nano-SA-2.5*.

After this treatment, the conditions were changed back to the steam reforming of methanol. As it can be seen from Figure 6-6b, the corresponding activities were similar or less than after initial reduction of the catalysts in the feed. From the analysis of the XAFS FT(χ(k)*k^3) measured under MSR conditions, a contribution of oxygen was found for all three catalysts. Furthermore, a considerable increase in activity could be achieved by a second temporary oxygen addition to the feed. Especially the hydrogen production of *Nano-SA-2.5* was improved by the factor of 6 (Figure 6-6). This treatment resulted in an increase of the oxygen contribution for *Nano-SA*, whereas a depletion of oxygen was determined from the FT(χ(k)*k^3) of *Nano-SA-5* . However, these contents are similar to the beginning of the experiment.

The corresponding copper surface areas are listed in Table 6-1. For *Nano-SA* and *Nano-SA-2.5* the partial oxidation in the feed and subsequent incomplete re-reduction (both after 673 K) resulted in an increased copper surface area, whereas no significant changes could be detected for *Nano-SA-5* in comparison with earlier stages of the reaction.

6.2.4 Infrared spectroscopy after reduction in 2 vol-% H_2/He

To further investigate the nature of the copper in the catalysts, the samples were investigated with IR spectroscopy using carbon monoxide as a probe molecule. Figure 6-7 shows the room temperature adsorption of CO on the different Cu/ZrO_2 samples after reduction in 2 vol-% H_2 at 523 K. Again an arrangement in groups is observable, like for the reduction kinetics and also the activity data.

The band at ≈ 2179 cm^{-1} is assigned to adsorption of CO on coordinatively unsaturated Zr^{4+} ions. A distinct band at 2093 cm^{-1} was detected with sample *Nano-SA-2.5*. All bands show extended shoulders towards lower wavenumbers. An assignment of the bands based on their corresponding wavenumber is not unequivocally possible as the frequency regions for Cu^+-CO and Cu^0-CO are believed to overlap.[4] A good criterion to distinguish the copper oxidation states is the stability of the bands upon evacuation or purging.[4,5,6] For all three catalysts a decreasing band intensity was observed during evacuation and therefore, these weakly adsorbed CO species arise most likely from adsorption on reduced Cu in different environments.

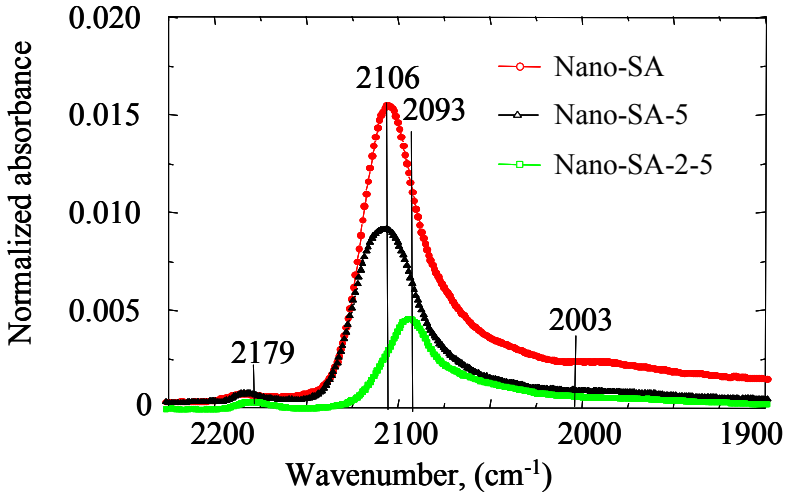

Figure 6-7 Variation of the infrared spectra of CO adsorbed (p(CO) = 95 mbar) on Cu/ZrO_2 catalysts

The investigations demonstrate that a number of different surface sites are available on zirconia supported Cu catalysts. The results show that a tuning of the electronic nature of the Cu species can be achieved through variation of the copper content (and/or the copper surface area). The obtained results can however not be directly applied to describe the states of the catalysts under MSR conditions. Nevertheless, they indicate, that probably certain adsorption sites are responsible for a good catalytic performance.

6.3 Discussion

6.3.1 Structure of the CuO/ZrO_2 precursor

In chapter 4.3 the stability of the tetragonal ZrO_2 has been discussed to generate from the lower surface area of the tetragonal ZrO_2 crystallites, as no incorporation of copper into the ZrO_2 lattice was detectable by XRD or EXAFS. Reference samples, that were prepared via the same precipitation method but without copper, also have only minor contribution of the monoclinic modification.[7] However, the comparison of two equal samples, that have been prepared at different times, revealed, that the samples can not be perfectly reproduced. An idea would be, that the stabilization of the tetragonal modification is partly enhanced through the contact with copper crystallites, and the lowering of the copper concentration therefore decreases this supporting effect. The mutual influence between copper and zirconia is also reflected by the diminished reducibility of the copper oxide that has been observed with different techniques.

All three catalysts have similar low S_{BET}, which probably can be traced to the *in situ* precipitation technique, as was discussed in chapter 5.4. The decreasing trend of the S_{BET} with decreasing copper concentration indicates, that a significant contribution to the overall surface area comes from the copper oxide particles.

6.3.2 Reduction of the CuO/ZrO_2 precursor

The reduction behavior of the precipitated CuO/ZrO_2 precursor was investigated in diluted hydrogen or methanol/water with TG/DSC and XAS. Simultaneously the gas phase composition was monitored with a mass spectrometer. A weight loss at low temperatures (< 440 K) that correlates with the evolution of water (despite a preceding drying step), was observed for all *in situ* precipitated samples, for *Nano-LA-1*, and for *Macro* (Figure 6-8). Moreover, a faster release of the corresponding water was recorded with decreasing copper content and increasing contribution of monoclinic zirconia in the case of the *in situ* precipitated samples. The reference (*Macro-reference*) shows a similar behavior.

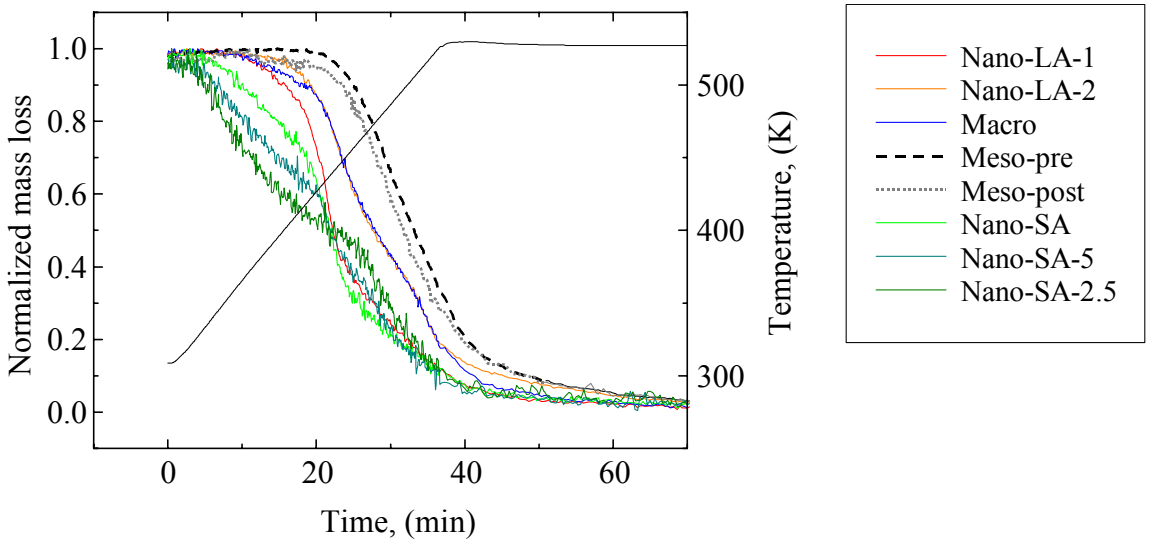

Figure 6-8 Normalized mass loss of CuO/ZrO_2 catalysts and reference during reduction in 2 vol-% H_2/He

From XRD measurements it is known, that monoclinic ZrO_2 is the major modification in this reference (prepared like the sample *Macro*). Therefore, the results indicate a connection between the presence of the monoclinic zirconia phase and the adsorbed hydroxyl groups that are released at relatively low temperatures. Jung and Bell[8] have investigated monoclinic and tetragonal ZrO_2

with infrared spectroscopy and found a higher concentration of OH groups on monoclinic zirconia. However, in this report they did not investigate the corresponding stabilities. Nevertheless, their result might support the observation of an increasing amount of released water (at low temperatures up to 440 K) correlating with an increasing contribution of monoclinic zirconia. The fact, that such pronounced water evolution is not observable for the mesoporous structured catalysts, cannot reliably be assigned to the absence of monoclinic zirconia because of the broad XRD peaks. On the other hand, these catalysts were treated with HMDS in order to diminish adsorbed hydroxyl groups and probably therefore, do not show such behavior.

The observation, that the sample with the lowest copper content (*Nano-SA-2.5*) needs the highest reduction (in methanol and water) temperatures among the precipitated catalysts resembles the behavior of the mesoporous materials. Both, a very large specific copper surface area (Table 6-1) and XAFS analysis indicate a very small copper crystallite size for the *Nano-SA-2.5*. According to the discussion in chapter 5.4, highly dispersed copper clusters can reduce at higher temperatures than "normal" small copper clusters.
Despite the statement of TG measurements, that the copper oxide in Nano-SA-2-5 is almost fully reduced, XAFS investigation still detect the contribution of oxides in the sample. However, the determination of the mass loss from TG experiments is complicated by the absence of clear-cut steps, as well as a distinct DSC signal. Moreover, the continuous mass loss during heating to 673 K indicates, that additional species partly contribute to the overall weight reduction.
The observed IR bands with their low stability during evacuation and their assignment to Cu^0-CO species is not in disagreement with the EXAFS results. They rather underline the idea of copper metal with some oxygen contribution as active catalyst for MSR.

6.3.3 Correlation between catalyst surface and activity

Figure 6-2 indicates, that there is no linear correlation between the copper surface area and the activity. Despite the higher copper surface areas of *Nano-SA-5* compared to *Nano-SA* the catalyst is not more active. As discussed in chapter 4 (1 paper) the results support the observations the metal support interaction, significantly influence the catalytic activity.

The comparison of the bands observed with IR spectroscopy for the differently loaded catalysts strongly indicates, that the copper concentration influences the nature of the copper species

present at the surface. Shen et al.[9] investigated the effect of the preparation on the surface structure of co-precipitated Cu/ZnO catalysts. After reducing the catalysts in 3 vol-% H_2 at 523 K they studied the adsorption of carbon monoxide. By decreasing the copper concentration they observed the formation of a band at lower wave numbers
(2090 cm^{-1}) in addition to a band at 2100 cm^{-1}, which is also present for unsupported copper. Furthermore, they determined an increasing specific copper surface area up to a ratio of Cu/Zn 50/50. Although, they worked with a different support, their observations are similar to the effects, found for the zirconia-supported catalysts reported here. They did not assign the different bands to different oxidation states of copper. Referring to the work of Pritchard et al.[10 they discussed the band positions in the context of different copper surface sites (i.e. facets, steps, defects). On the other hand, they did not consider a potential effect of the crystallite size (i.e. copper surface area) and the consequent influence of the support (perhaps through an electronic interaction with very small crystallites). In the mentioned work of Pritchard and co-workers[10] materials with 5 and 10 % copper on silica were also investigated by room temperature adsorption of CO after reduction in flowing hydrogen. The decrease in the copper concentration likewise resulted in a shift of the corresponding band to lower wave numbers (from 2120 to 2113 cm^{-1} from 5 to 10 % copper, respectively). Furthermore, they also observed low-frequency shoulders, especially for the sample with the higher copper concentration.
Based on the comparison of results from various characterizations, other authors also discussed the observed copper-CO species with respect to different surface sites.[11,12]
Taking the results from our determination of the specific copper surface area into account, the observation of a band shifted to lower wave numbers (2093 cm^{-1}), with increasing copper surface area, indicates, that the copper oxide in the catalysts is well reducible and that possibly different copper surface sites or copper differently interacting with the support (also indicated by the copper surface area) is responsible for the observed band shift. It cannot be excluded, that the detected species forms not before the reaction with carbon monoxide. However, these reduced copper species are likely in an electron deficient state[13]; probably due to the low copper content and crystallite size. Such a band position (< 2100 cm^{-1}) would correspond to CO adsorption on close packed high index planes like Cu (110)[10,11,12].
One remaining question concerns a possible relationship between monoclinic ZrO_2 and the detected incomplete/retarded reduction of copper oxide. Remained oxygen has been observed mainly in those catalysts, where a certain portion of m-zirconia exists. It has been shown, that the adsorption properties (e.g. of CO) are very different, depending on the modification, i.e. the crystallite structure (chapter 5.4.1). Whereas, mainly Zr^{4+}-ions are present in the tetragonal

lattice, the monoclinic structure also contains Zr^{3+}-ions.[14,15] This means, that there are tetracoordinated O^{2-} in tetragonal zirconia and tri- and tetracoordinated oxygen ions in the monoclinic phase. Therefore, an interaction between nanostructured copper crystallites and monoclinic zirconia might exist, that changes the properties of the metal oxide (e.g. reducibility). Zhao et al.[16] correlated the observation of two TPR peaks for monolayer CuO supported on monoclinic zirconia to the according interface centres, i.e. the high temperature peak (~ 510 K) corresponds to the reduction of CuO in the environment of tricoordinated O^{2-}.

Jung and Bell[17] investigated copper on both supports under methanol synthesis conditions. They found a higher activity for the catalyst with the m-ZrO_2, whereby the copper crystallite sizes and dispersion were similar for both materials. They discussed the results in terms of a direct participation of the support, however they did not concern the oxidation state of copper.

6.4 Conclusion

Bulk structural and surface investigations were performed to investigate the correlation between copper concentration and properties of nanostructured catalysts, prepared by *short-aging* precipitation of zirconium propylate and copper nitrate.

Conspicuous during analysis of the results was the grouping of the catalysts, as the sample with the lowest copper content showed more pronounced properties and catalysis.

Nevertheless, for all copper concentrations the established correlation between the amount of remaining oxygen and catalytic activity was confirmed.

Tetragonal ZrO_2 is the major long-range ordered phase in the materials, although an increase in the monoclinic fraction was detected with decreasing copper concentration.

A drastic increase of the onset temperature of reduction (in methanol and water) was observed by decreasing the copper concentration to ~ 2 atom-%. The reduction process even continued during the isothermal step at 523 K, indicating a possibly incomplete reduction. Indeed, an increasing contribution of remaining oxygen was found from XANES analysis in the sequence of *Nano-SA* < *Nano-SA-5* < *Nano-SA-2.5*. On the other hand, a significant larger copper surface area and hydrogen production was observed for the lowest copper content.

Infrared spectroscopy with CO adsorption at room temperature revealed, that the nature of the detectable copper species also changes by decreasing the copper concentration.

6.5 References

[1] M.M. Günter, T. Ressler, B. Bems, C. Büscher, T. Genger, O. Hinrichsen, M. Muhler, R. Schlögl, Catal. Lett. **71** (2001) 37

[2] M.M. Günter, T. Ressler, R.E. Jentoft, B. Bems, J. Catal. **203** (2001) 133

[3] B.S. Clausen, L. Gråbæk, H. Topsøe, L.B. Hansen, P. Stoltze, J.K. Nørskov, O.H. Nielsen, J. Catal. **141** (1993) 368

[4] K. Hadjiivanov, H. Knözinger, Phys. Chem. Chem. Phys. **3** (2001) 1132

[5] K. Hadjiivanov, T. Venkov, H. Knözinger, Catal. Lett. **75** (2001) 55

[6] F. Boccuzzi, A. Chiorino, M. Manzoli, D. Andreeva, T. Tabakova, L. Ilieva, V. Iadakiev, Catal. Today **75** (2002) 169

[7] Y. Wang, R.A. Caruso, J. Mater. Chem. **12** (2002) 1442

[8] K.T. Jung, A.T. Bell, J. Mol. Catal. A: **163** (2000) 27

[9] G.-C. Shen, S.-i. Fujita, S. Matsumoto, N. Takezawa, J. Mol. Catal. A **124** (1997) 123

[10] J. Pritchard, T. Catterick, R.K. Gupta, Surf. Sci. **53** (1975) 1

[11] A.R. Balkenende, C.J. van der Grift, E.A. Meulenkamp, J.W. Geus, Appl. Surf. Sci. **68** (1993) 161

[12] F. Boccuzzi, G. Ghiotti, A. Chiorino, Surf. Sci. **156** (1985) 933

[13] A.N. Pestryakov, A.A. Davydov, Kin. Catal. **37** (1996) 859

[14] G. Teufer, Acta Cryst. **15** (1962) 1187

[15] K.-H. Jacob, E. Knözinger, S. Benfer, J. Mater. Chem. **3** (1993) 651

[16] Y. Zhao, K. Tao, H.L. Wan, Catal. Comm. **5** (2004) 249

[17] K.T. Jung, A.T. Bell, Catal. Lett. **80** (2002) 63

7 A next step: Investigation of the correlation between catalytic performance and surface properties of $Cu/ZrO_2/CeO_2$ catalysts for the steam reforming of methanol

The investigation of the reaction mechanism and the kinetic analysis were undertaken by Dr. Agnés Mastalir in the group of Prof. Schomäcker at the Technical University in Berlin.

7.1 Introduction

$Ce_xZr_{1-x}O_2$ mixed oxides are widely used in current automotive three-way catalysts, to regulate the oxygen partial pressure by storing/releasing O_2 due to the Ce^{3+}/Ce^{4+} redox couple.[1] Furthermore it has been found, that ZrO_2 and CeO_2, either as support materials or promoters generally improve the catalytic performance of copper-based catalysts. Materials with this mixed oxide exhibit higher thermal stability, surface areas, and catalytic activity compared to a CeO_2 support alone.[2,3] Moreover, it was shown, that the reducibility of CuO increased with different supports in the order of $ZrO_2 < CeO_2 < CeO_2$-ZrO_2.[3] Depending on the composition (ratio of CeO_2/ZrO_2), the crystallite size, and the temperature several Ce-Zr phases can occur under ambient conditions. Besides a monoclinic, also metastable tetragonal and cubic solid-solutions have been observed.[1and references therein] This in turn might be the reason for the ongoing debate about the optimal $Ce_xZr_{1-x}O_2$ composition, in terms of redox and textural stability, as even the tuning of the synthesis at a single composition can have remarkable influence on the textural and chemical properties.[4] The comparison of co-precipitated and impregnated copper-ceria catalysts presented by Liu et al.[5], has shown, that despite the same composition, co-precipitated copper (from aqueous solutions of $Cu(NO_3)_2$ and $Ce(NO_3)_3$) is more dispersed on the support and reveals higher conversion of methanol (for the steam reforming of methanol) than copper, that is introduced after the support has formed. Despite they do not show direct evidence for copper in a Cu^+ state under reaction conditions, the idea of an interaction of Ce and Cu in form of the following redox equilibrium, could be taken into consideration, especially for samples, where all precursors precipitate simultaneously.

$Ce^{4+} + Cu \rightarrow Ce^{3+} + Cu^+$

In consequence, the synthesis method plays an important role in preparing well-defined, homogenous and reproducible materials.

In the present study, $Cu/ZrO_2/CeO_2$ catalysts were prepared by impregnating a highly porous organic template with a sol of the corresponding metal hydroxides. The definite size of the template beads enables the direct use of the catalyst in a fixed bed reactor (no clogging), without intensive preparation (e.g. pressing, grinding, sieving).

7.2 Experimental

7.2.1 Preparation

The ternary CZC (Ce/Zr/Cu) catalysts were synthesized by a combination of co-precipitation and templating technique. First metal sols were prepared by mixing $(NH_4)_2Ce(NO_3)_6$, $ZrO(NO_3)_2 \cdot H_2O$ and $Cu(NO_3)_2 \cdot 2.5\ H_2O$ (all Aldrich products of > 99 % purity), dissolved in 40 ml of distilled water and revealing a total metal content of $5 \cdot 10^{-3}$ mol. After the co-precipitation of the corresponding metal hydroxides by addition of NaOH (at pH > 10), the precipitate was washed with distilled water until a pH = 7 was obtained and finally suspended in 5 ml distilled water. Depending on the sample composition a certain amount of HNO_3 (90 %) was added to the suspension. 1.5 ml of the wet beads (XAD-16 non-functionalized polystyrene beads, Sigma, specific surface area of 800 $m^2\ g^{-1}$) were mixed with 0.005 mol of the metal sol and then heated to 333 K for 2 days. After drying for one day, repeated washing and further drying, the samples were first heated in N_2 (100 ml/min) and then calcined in air at 773 K. A SEM picture (Scanning electron micrograph) of CZC5 is given in Figure 7-1. More experimental details can be found in [6,7].

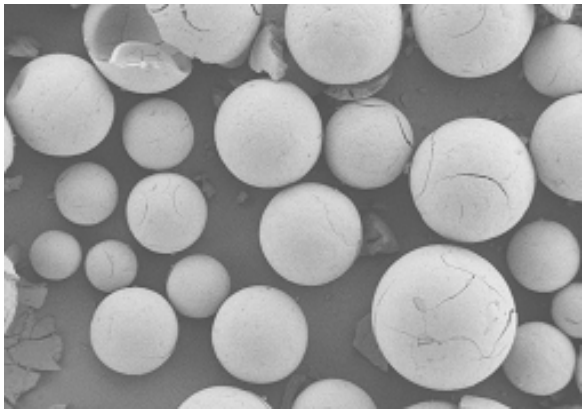

Figure 7-1 Scanning electron micrograph of a $Cu/ZrO_2/CeO_2$ catalyst (CZC5) after calcinations

The composition of the catalysts was determined with X-ray fluorescence analysis (Seiko Instrument, SEA 2010). The amount of Cu detected was in good agreement with the expected value, and so was the ratio ZrO_2:CeO_2 of 1:1 (see also Table 7-1).

7.2.2 Catalytic test reaction

The experiments were performed in a fixed bed tubular reactor with three channels (see also chapter 5.2.2).

The copper surface area was determined with N_2O decomposition after reduction in a mixture of methanol/water (2:1) (see chapter 3.3). Where possible, copper crystallite sizes were calculated from the FWHM of the Cu (111) XRD peak (chapter 3.1).

7.3 Results and Discussion

The characteristic data of the CZC samples are listed in Table 7-1. By the usage of a polymer template it was possible to synthesize catalysts with high BET surface areas, which has also been found for the Cu/ZrO_2 catalysts in this study.

Table 7-1 Characterization of CZC samples

Sample	Cu [atom-%]	Zr [atom-%]	Ce [atom-%]	S_{BET} [m^2g^{-1}]	S_{Cu} [$m^2g^{-1}_{cat}$]	S_{Cu} [$m^2g^{-1}_{Cu}$]	copper metal crystallite size [Å]
CZC5	4.4	44.6	510	96	0.9	51.4	--
CZC15	12.1	44.3	43.6	102	1.8	25.8	--
CZC25	23.9	37.6	38.5	94	1.8	12.3	12.4
CZC35	31.0	32.7	36.3	83	1.5	7.6	15.3

Except for CZC5, similar copper surface areas per gram catalyst were found, irrespective of the copper content. However, the highest specific copper surface area per gram copper was obtained for CZC5. Similar observations have been made for the series of nanostructured catalysts (*Nano-SA),* where the decrease of the copper content also resulted in an increase of the copper surface area. For copper catalysts supported on yttria-doped ceria/alumina Cheng et al.[8] also achieved an increase of the specific copper surface area, by decreasing the copper loading from 20 to 5 wt-%.

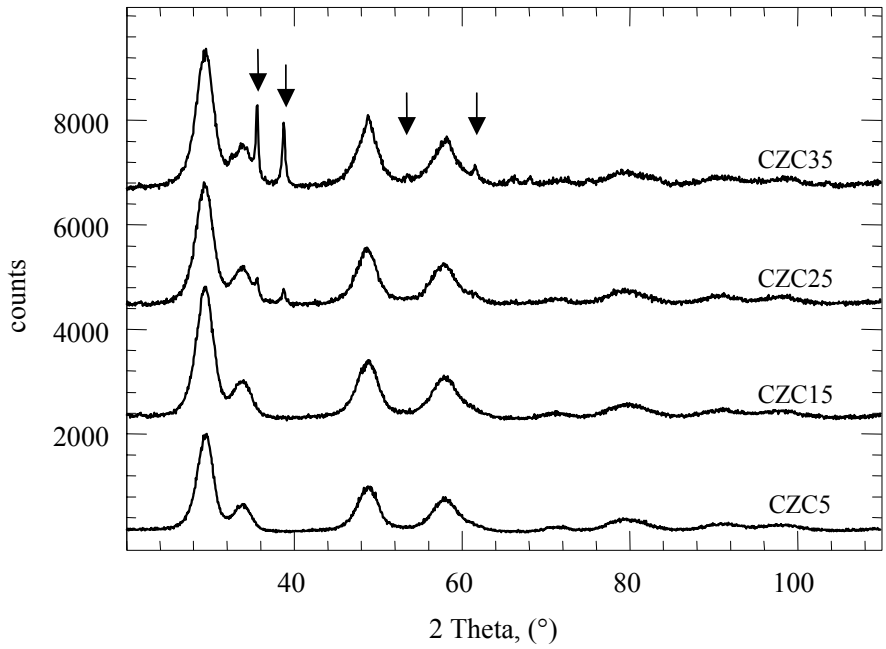

Figure 7-2 X-ray diffraction pattern of CZC catalysts (arrows indicate CuO phase)

For CZC5 and CZC15 no copper phase was detected with XRD (Figure 7-2). This can be due to the low copper content, but probably also because of the small crystallite sizes. An evalutation of the XRD pattern of the CZC catalysts is difficult, because of the broad peaks. Therefore, it was not possible to distinguish, whether zirconia and ceria are present as separate or mixed $Ce_{1-x}Zr_xO_2$ phases.

From long-time experiments[7] it was found, that during the first 5 days, the catalysts CZC15 and CZC25 deactivate significantly. After a period of 5 days, the conversion approached a constant value, except for CZC5. Nevertheless, the catalyst CZC5 revealed the highest conversion. A positive correlation between the specific copper surface area and the activity was only found for CZC5 and CZC15. On the other hand, CZC5 produced significantly more CO. For the catalysts with a copper content higher than 5 wt-% comparable CO levels were detected.

Activity tests with different particle sizes revealed no significant influences of mass transport limitations on the conversion and therefore, a reliable kinetic model, taking into account three reactions (MSR, methanol decomposition, and reverse water gas shift), was proposed. Kinetic parameters were determined, by fitting the experimental results to the model. The main process contributing to the production of CO is the reverse water gas shift (RWGS) reaction, which has also been found for Cu/ZrO_2[9] and $Cu/ZnO/Al_2O_3$[10] catalysts. Experiments further revealed, that with increasing temperature (to 573 K) more CO is formed and moreover, deactivation occurs. Sintering is one of the reasons, leading to the deactivation of a catalyst, especially at working temperatures above the Huttig temperature (1/3 $T_{melting}$; for Cu: 450 K).[11] In consequence, temperatures between 523 K and 543 K are most suitable for a productive steam reforming of methanol.

The analysis of the activation energies of the included reactions revealed a linear correlation with the copper content. For all three processes the increase of the copper loading resulted in a decrease of the activation energy.

All these results confirm, that besides the specific copper surface area, other parameters like the dispersion, crystallite size but also microstructural effects contribute to the catalytic performance.

7.4 Conclusion

The novel $Cu/ZrO_2/CeO_2$ catalysts were investigated for the methanol steam reforming. The co-precipitation from the aqueous solution of the corresponding nitrates and the usage of a highly porous template resulted in a catalyst material with a large surface area. During long-term experiments the conversion of catalysts with a copper loading exceeding 5 % stabilized after an initial period of deactivation. No linear correlation between the copper surface area and the conversion could be found, indicating, that other bulk/surface properties also determine the catalytic performance. Furthermore, it was found, that an increase of the copper content from 5 to 15 % positively influenced the stability and the suppression of the CO formation. The strong influence of the copper concentration was also confirmed, by the systematic decrease of the activation energy of each individual reaction (MSR, MD, RWGS) with increasing copper loading. Despite the low complexity of the preparation (only one parameter was changed), the variation of the copper content evidently takes effect on the microstructure, and hence on the active Cu surface, thus affecting the catalysis over the CZC catalysts.

7.5 References

[1] J. Kašpar, P. Fornasiero, M. Graziani, Catal. Today **50** (1999) 285

[2] J. Kašpar, P. Fornasiero, G. Calducci, R. Di Monte, N. Hockey, V. Sergo, Inorg. Chim. Acta **349** (2003) 217

[3] P. Ratnasamy, D Srinivas, C.V.V. Satyanarayana, P. Manikandan, R.S. Senthil Kumaran, M. Sachin, V.N. Shetti, J. Catal. **221** (2004) 455

[4] J. Kašpar, R. Di Monte, P. Fornasiero, M. Graziani, H. Bradshaw, C. Norman, Top. Catal. **16/1**7 (2001) 83

[5] Y. Liu, T. Hayakawa, K. Suzuki, S. Hamakawa, T. Tsunoda, T. Ishii, M. Kumagai, Appl. Catal. A: **223** (2002) 137

[6] A. Deshpande, N. Pinna, P. Beato, M. Antonietti, M. Niederberger, Chem. Mater. **16** (2004) 2599

[7] A. Mastalir, B. Frank, A. Szizybalski, H. Soerijanto, A. Deshpande, M. Niederberger, R. Schomäcker, R. Schlögl, T. Ressler, J. Catal. **230** (2005) 464

[8] W.-H. Cheng, I. Chen, J.-S. Liou, S.-S. Lin, Top. Catal. **22** (2003) 225

[9] H. Purnama, F. Girgsdies, T. Ressler, J.H. Schattka, R.A. Caruso, R. Schomäcker, R. Schlögl, Catal. Lett. **94** (2004) 61

[10] H. Purnama, T. Ressler, R.E. Jenoft, H. Soerijanto, R. Schlögl, R. Schomäcker, Appl, Catal. A: **259** (2004) 83

[11] M.S. Spencer, Nature **323** (1986) 685

8 Summary and Perspectives

The object of the present thesis is the investigation of the correlation between bulk and surface properties of binary Cu/ZrO_2 catalysts and their activity in the steam reforming of methanol. In order to find a good catalyst and to understand the influence of the catalyst preparation on the catalytic performance, different preparation routes were chosen. Three major synthesis methods were applied. While maintaining zirconium tetrapropylat as the ZrO_2 precursor, diverse inorganic and organic copper precursors were added; either simultaneously or after the formation of the support material. Furthermore, two different structure-directing agents were used, in order to obtain catalysts with large surface areas.

Besides thermo gravimetry (TG-DSC), nuclear magnetic resonance (NMR), and transmission electron microscopy (TEM), experiments with the complementary methods X-ray absorption spectroscopy (XAS) and X-ray diffraction (XRD) have been performed to characterize the microstructure of the catalysts. To describe the corresponding catalyst surface, nitrogen adsorption (BET), N_2O decomposition (RFC), and infrared spectroscopy (with probe molecule CO) have been applied. This broad spectrum of analytical methods enables the comprehensive investigation of the solid-state chemical processes occurring during reduction and under working conditions. Especially the complementary information from XRD, XAS, and NMR allowed a description of both, the long-range order of zirconia, as well as the short-range order of copper and zirconia. Following the proposed structure-activity correlations of Cu/ZnO catalysts, this thesis presents the attempt to prepare zirconia supported copper catalysts and to evaluate the role of the real structure of the active phase for the steam reforming of methanol. At first, the changes of the bulk and surface properties of a nanostructured catalyst during the reduction and under reaction conditions were investigated in chapter 4. The influence of the preparation on the established structure-activity correlations is discussed in chapter 5. Whereas several parameters have been changed during the preparation of the catalysts presented in chapter 5, the effect of the variation of the copper concentration has been studied in detail in chapter 6. Finally, chapter 7 reports on the structure and catalytic performance of ternary $Cu/ZrO_2/CeO_2$ catalysts.

In situ investigation of structure-activity relationships

In a first approach, the nanostructured catalyst *Nano-SA* was investigated after calcination at 773 K, during reduction and the steam reforming of methanol. The determination of the long-range order with X-ray diffraction revealed, that the ZrO_2 is well crystallized and mainly present

in the tetragonal modification. Due to the low copper concentration and the small crystallite size, no copper oxide phase was detected. After reduction in 2 vol-% hydrogen a small peak attributable to Cu metal appears. From the FWHM of this peak and according to the Scherrer formula, a copper crystallite size of ~ 20 Å was calculated. However, the concept of line profile analysis in order to reveal further information about the nature (e.g. strain) of the copper in the precursor and in the working catalysts was not feasible. Therefore, X-ray absorption spectroscopy was applied and although, the information depths of this method is restricted, too, CuO was concluded as the major copper phase present in the catalyst after calcination. The changes of the microstructure during reduction in either hydrogen, or methanol/water were monitored with TG-DSC and XAS. Due to the absence of suitable references for a standard principle component analysis, the formation of copper metal was described by the development of the "abstract concentrations". In agreement with Cu/ZnO catalysts, the course of these concentration curves indicated the existence of an intermediate phase during the heating from room temperature to 523 K, independent of the reducing agent (i.e. hydrogen or feed).

A modified analysis procedure to determine the specific copper surface area has been successfully applied. The N_2O decomposition was performed after various reaction steps, revealing, that the temporary addition of oxygen to the feed resulted in a decreased, but more active copper surface. Evidently, other parameters influence the catalytic activity, besides the surface properties. Reduction and catalysis have also been investigated with XAS. The most decisive result is the existence of an oxygen-copper distance in addition to the metal-metal distances in Cu^0, in both hydrogen and methanol/water atmosphere at 523 K. This oxygen contribution can be quantified, which enhances the comparison between different reaction steps. Such an incomplete reduction, as concluded from the remaining oxygen, was also indicated by the too low weight loss observed with TG. On the other hand, a shift of the reduction to higher temperatures was observed for the direct activation in the feed, probably due to the oxidizing influence of water and CO_2. Accordingly, more remained oxygen was determined form the corresponding Cu-O shell. After temporarily adding oxygen to the feed, an incomplete re-reduction results in an increased contribution of oxygen, which however correlates with an increase in activity.

A further important question concerned the stability of the material. Therefore, the catalyst was reduced in 2 vol-% H_2 at 673 K. These severe conditions lead to full reduction of the copper oxide, corresponding with the loss of activity during subsequent catalysis. Reactivation was achieved via a second temporary addition of oxygen, evidencing the thermal stability of the Cu/ZrO_2 catalyst.

Information about the microstructure was given by NMR measurements after the various reaction steps. In contrast to conventional Cu/ZnO catalysts, small variations of the asymmetric line broadening indicate, that besides the remaining oxygen, only a minor degree of microstrain in copper can be imagined to influence the active copper surface of Cu/ZrO_2 catalysts and thus, enhance the catalytic performance. Together with the decreased reducibility of CuO/ZrO_2 these observations indicate a different metal support interaction compared to Cu/ZnO catalysts, although the interaction between Cu and ZrO_2 again stabilizes an active copper microstructure that strongly deviates from bulk copper metal.

The influence of preparation on structure and activity

The aimed preparation of an active phase requires a fundamental knowledge about the relationship between bulk/surface properties of the catalyst and the catalytic performance (i.e. activity, selectivity, and stability). Based on the description that the role of ZrO_2 as a support goes beyond the promotion of the structural stabilization, the influence of the preparation on the microstructure and activity was studied in chapter 5. Structural data were supplemented with the results of long-term experiments, and the analysis of the CO production.

Pretreatments like calcination and reduction of the various precursor materials do not annihilate the structural differences in the precursors (“chemical memory”), and hence lead to differently active catalysts for the steam reforming of methanol.

Investigation of the long-range order with XRD revealed, that in contrast to the nanostructured and macroporous samples, the degree of crystallization for the mesoporous catalysts is lower. On the other hand, large BET surface areas were found especially for these mesoporous samples and the comparison with other samples indicated, that rather the preparation method and the usage of a block copolymer as structure-directing agent, than the copper content are important parameters for the generation of a large surface area. A similar picture arises by comparing the specific copper surface areas, as the highest value was determined for the mesoporous sample with the lowest copper concentration (*Meso-post*). However, a copper concentration as high as 20 mol-% lead to a nanostructured catalyst with a low copper surface area, low activity and which turned out to be very susceptible against sintering of the copper particles.

The low crystallinity of the support material in the mesoporous catalysts probably results in a strong interaction with the metal and, hence partly explains the difficult reducibility (expressed in the higher peak reduction temperatures) of the copper oxide in these materials. On the other

hand, the role of hexamethyldisilazane beyond the elimination of adsorbed hydroxyl groups has to be clarified in this context, too.

The stabilization of oxygen in copper metal and the correlation between the oxygen amount and activity could be recovered with all catalysts, irrespective of the preparation. The same is valid for the observation of microstructural strain with NMR. Especially, the synthesis from copper acetylacetonate resulted in an asymmetric line profile, comparable to those from Cu/ZnO catalysts.[1] Further confirmation for the presence of microstructural defects and oxygen in copper have been provided by transmission electron microscopy and IR spectroscpy.
Summarizing all these results, it becomes evident, that: (i) the sequential formation of the components results in catalysts with higher surface areas, partly higher specific copper surface areas, and higher activity
(ii) the copper concentration is an important parameter for the preparation)
(iii) the highest copper surface area and activity were determined for a mesoporous catalyst with the lowest copper loading, using a porous template, and where the copper precursor (from copper nitrate) was added after the zirconia compound had formed.

Nanostructured catalysts: influence of the copper content on the catalytic performance

The former experiments indicated, that one crucial parameter during the preparation is the copper concentration. An increase of the loading higher than 15 mol-% has been shown, to form sensitive copper crystallites, that easily agglomerate and therefore abet the deactivation of the catalyst. On the other hand, the sample with lower copper contents revealed very good catalytic performances. Following these results, nanostructured catalysts with approximately 5 and 2.5 mol-% Cu have been prepared via the co-precipitation route. Concerning the long-range order zirconia (copper phases were not detected with XRD), an increasing contribution of the monoclinic ZrO_2 modification was observed with decreasing copper loading. To which extent this evolution influences the catalysis is not yet fully understood.
Throughout the results of all characterization methods, a grouping of the catalysts can be observed. The decrease of the copper concentration to ~ 2.5 mol-% had a more pronounced effect on the structure and the activity of the catalysts, than the decrease from 9 to 5 mol-%. Similar specific copper surface areas were determined for *Nano-SA* and *Nano-SA-5*, whereas a

significantly higher surface area was found for *Nano-SA-2.5*. The peak reduction temperature was strongly shifted to higher temperatures for *Nano-SA-2.5* and the process even continued at isothermal 523 K. Even, heating in 2 vol-% H_2 to 673 K did not result in complete reduction of the copper oxide for *Nano-SA-5* and *Nano-SA-2.5*, indicating a strong interaction with the support. The analysis of the short-range order revealed an increasing amount of remained oxygen in sample with decreasing copper content. Simultaneously, a pronounced improvement of the hydrogen production was detected for *Nano-SA-2.5*. Several experiments with infrared spectroscopy have been performed to investigate the nature of the catalyst surface. Reducing and oxidizing atmospheres were used to distinguish between CO adsorbed on Cu^0, $Cu^{\delta+}$, and Cu^+. For the *Nano-SA-2.5* a shift of the detected band to lower wavenumbers indicated the presence of Cu^+-species besides reduced copper species ($Cu^{\delta+}$-CO species, electron deficient two-dimensional copper clusters) at the surface (after the reduction in 2 vol-% H_2).

A next step: Investigation of the correlation between catalytic performance and surface properties of $Cu/ZrO_2/CeO_2$ catalysts for the steam reforming of methanol

In chapter 7 the chemical complexity was increased by the introduction of CeO_2 into the Cu/ZrO_2 catalysts. Maintaining one preparation method, samples were prepared by only varying the copper concentration. In a first approach, activity tests were performed and information about the critical CO formation were obtained. Data from long-term experiments and investigations of the reaction kinetics were supplemented by results from the determination of the copper surface area. A classification, concerning the copper surface area and activity, as it was observed for the nanostructured catalysts, was not found for the ceria containing materials. A stabilization of the conversion and a lower production of CO was noticed for the catalysts exceeding 5 % Cu. Moreover a systematic decrease of the activation energy of each individual reaction (MSR, MD, RWGS) with increasing copper content supports the observations, that additionally to the copper surface area, differences in the microstructure of the catalysts contribute to the hydrogen production of these catalysts. Further studies are needed to describe the bulk properties of the system. As XRD alone can give only limited information about the long-range ordered structure of the components, other techniques as for example Raman spectroscopy or X-ray absorption spectroscopy are suitable to obtain more details about the bulk microstructure of the components.

It has been shown in this thesis that the increase in activity correlates with a modification of the copper bulk structure. Thereby, zirconia as a support plays a major role, as it stabilizes oxygen in copper metal and to a lesser extent, introduces microstrain into the copper crystallites. According to this, an increase in activity was observed after the temporary addition of oxygen to the feed and the following incomplete re-reduction of the oxidized copper. Therefore, experimental evidence was given, that the catalytic performance depends not only on the copper surface area, but also on the copper loading, the bulk microstructure, and the nature of the species exposed at the surface.

Similar observations have been reported for the Cu/ZnO system during methanol synthesis and steam reforming of methanol. The combination of the beneficial properties of ZnO and ZrO_2 as supports would give a promising system for the methanol chemistry.[2,3,4,5,6]

Perspectives

In order to understand the particular effects of the variety of applied preparation techniques, detailed analysis of the individual preparation steps, of the influence of the various precursors and solvents, and of the copper concentration on the microstructural arrangements of Cu and ZrO_2 under working conditions should be undertaken. Especially the solid-state interaction between zirconia and copper is still an open question. Electron spin resonance experiments that investigate the contact region between metal/metal oxide and support can give first ideas to this subject. For example Liu et al.[7] describe the incorporation of Cu^{2+} ions into surface vacant sites of t-ZrO_2. For low copper loadings this would most probably influence the reduction behavior of copper oxide.

The knowledge about the processes occurring during the formation of the precursors and during all subsequent activation procedures will contribute to the comprehension.

Besides the investigations of the catalyst properties, a detailed description of the processes taking place during the N_2O decomposition would promote the reliability of the determined copper surface areas. For example infrared spectroscopy could provide interesting information.

Acknowledgement

The authors are grateful to the ZEIT-Foundation, Hamburg, Germany, for financial support. The *Hamburger Synchrotronstrahlungslabor*, HASYLAB, is acknowledged for providing beamtime for this work.

8.1 References

[1] B. Kniep, T. Ressler, A. Rabis, F. Girgsdies, M. Baenitz, F. Steglich, R. Schlögl, Angew. Chem. **116** (2004) 114

[2] Y.-W. Suh, S.-H. Moon, H.-K. Rhee, Catal. Today **63** (2000) 447

[3] P.H. Matter, D.J.Braden, U.S. Ozkan, J. Catal. **223** (2004) 340

[4] J.P. Breen, J.R.H. Ross, Catal. Today **51** (1999) 521

[5] J. Agrell, H. Birgersson, M. Boutonnet, I. Melián-Cabrera, R.M. Navarro, J.L.G. Fierro, J. Catal. **219** (2003) 389

[6] Y. Ma, Q. Sun, D. Wu, W.-H. Fan, Y.-L. Zhang, J.-F. Deng, Appl. Catal. A: General **171** (1998) 45

[7] Z. Liu, W. Ji, L. Dong, Y. Chen, J. Catal. **172** (1997) 243

9 Figures

10 Tables

11 Appendix

Curriculum Vitae

Alexandra Szizybalski
Date of Birth: 16.01.1978 in Havelberg
Nationality: german

School

1984 – 91	Hermann – Matern - Oberschule Klietz
1991 – 93	Bismarck - Gymnasium Schönhausen
1993 – 96	Diesterweg - Gymnasium Tangermünde

University

10/96 – 12/2000	Studies of Mineralogy at the University Potsdam Major subjects: Petrology and Geochemistry
01/01 – 10/01	Diplomathesis at the Institut fo Geoscience at the University Potsdam: Mineralogy and structure of bladder stones Degree: Diplom – Mineralogin

Promotion

11/01	Zirconium dioxide supported Copper Catalysts for the Methanol Steam Reforming; Fritz – Haber – Institute of the Max – Planck – Society, Department of Inorganic Chemistry under Prof. Dr. R. Schlögl, Group Geometric Structure under supervision of Dr. habil T. Ressler

Publications

1 Steam reforming of methanol over $Cu/ZrO_2/CeO_2$ catalysts: a kinetic study,

A. Mastalir, B. Frank, A. Szizybalski, H. Soerijanto, A.S. Deshpande, M. Niederberger, R. Schomäcker, R. Schlögl, T. Ressler, J. Catal. 230 (2005) 464

2 In situ investigations of structure-activity relationships of binary Cu/ZrO_2 catalyst for the steam reforming of methanol

A. Szizybalski, F. Girgsdies, A. Rabis, Y. Wang, M. Niederberger, T. Ressler, eingereicht bei J. Catal.

3 Binary Cu/ZrO_2 catalysts for steam reforming of methanol: The influence of preparation on structure and activity

A. Szizybalski, F. Girgsdies, R. Jentoft, I. Kassatkin, R. Schlögl, T. Ressler, Y. Wang, J.-H. Schattka, M. Niederberger, A. Rabis, in Bearbeitung

Poster

4 Cu/ZrO_2 Catalysts for Methanol Steam Reforming

F. Girgsdies, H. Purnama, A. Szizybalski, T. Ressler, J.H. Schattka, Y. Wang, R.A. Caruso35. Jahrestreffen Deutscher Katalytiker, Weimar, März 2002

5 Cu/ZrO_2 Catalysts for Methanol Steam Reforming

F. Girgsdies, H. Purnama, A. Szizybalski, T. Ressler, J.H. Schattka, Y. Wang, R.A. CarusoHasylab Nutzertreffen, Hamburg, Januar 2003

6 In situ structural characterization of Cu/ZrO_2 catalysts for Methanol Steam Reforming

A. Szizybalski, F. Girgsdies, T. Ressler, R. Schlögl, J.H. Schattka, Y. Wang, R.A. Caruso, M. Antonietti

36. Jahrestreffen Deutscher Katalytiker, Weimar, März 2003

7 Structure-Activity Correlations for Cu/ZrO_2 catalysts in the Methanol Steam Reforming

A. Szizybalski, F. Girgsdies, T. Ressler, R. Schlögl, J.H. Schattka, Y. Wang, R.A. Caruso, M. Antonietti

XAFS 12 Konferenz, Malmö (Schweden), Juni 2003

8 Copper based catalysts for steam reforming of methanol

A. Szizybalski, B.L. Kniep, F. Girgsdies, R.E. Jentoft, B. Bems, M. Schur, R. Schlögl, T. Ressler, J.H. Schattka, Y. Wang, R.A. Caruso, M. Antonietti, M. Niederberger

Hasylab Nutzertreffen, Hamburg, Januar 2004

9 Cu/ZrO_2 Catalysts for Methanol Steam Reforming: Structure – Activity Correlations

A. Szizybalski, F. Girgsdies, R. Schlögl, T. Ressler, J.H. Schattka, Y. Wang, R.A. Caruso, M. Antonietti, M. Niederberger

37. Jahrestreffen Deutscher Katalytiker, Weimar, März 2004

10 Cu/ZrO_2 Catalysts for Methanol Steam Reforming: Structure – Activity Correlations

A. Szizybalski, F. Girgsdies, R. Schlögl, T. Ressler, J.H. Schattka, Y. Wang, R.A. Caruso, M. Antonietti, M. Niederberger

13. International Congress on Catalysis, Paris (Frankreich), Juli 2004